# The Influence of the Agulhas Current on two South African Extreme Weather Events

Sarah April White

*Ocean Climate Research Group, Department of Oceanography*

*University of Cape Town, Rondebosch, South Africa*



Dissertation submitted to the Faculty of Science, University of Cape Town, in fulfillment of the requirements for the Master of Science degree

November 2000

# ABSTRACT

Surface station, satellite and NCEP re-analysis data are used to examine the evolution of two severe storms that occurred over the eastern coastal regions during South Africa's summer season 1998/99. The storms in November and December were both accompanied by heavy rainfall in two widely separated locations. The storm in December proved to be more severe as it resulted in flooding while tornadoes were reported in the Umtata and Hogsback regions of the Eastern Cape. Both storms appeared to result from interaction between a continental heat low, advection of warm moist air around an anticyclone in the South-west Indian Ocean and an approaching midlevel westerly trough. NCEP derived moisture flux diagrams and back trajectories of air parcels constructed from ECMWF data suggest that the Agulhas Current region was a major source of low level moisture for both storms. TRMM satellite imagery captured heavy rainfall above the high sea surface temperatures of the Agulhas Current. TRMM measurements of rainfall and latent heat in the atmosphere show that the high sea surface temperatures of the Agulhas Current modified the mesoscale environment above the current. To what extent the mesoscale environment above the Agulhas Current modified the synoptic situations over land could be answered using regional modeling and more frequent radiosonde data.

*Acknowledgements.* I thank Eumetsat for providing the Meteosat images as well as data. Thanks to the South African Weather Bureau for providing data and support to this project. The OI SST was provided by the NOAA-CIRES Climate Diagnostics Center, Boulder, Colorado, from their web site at http://www.cdc.noaa.gov. I wish to thank Bill Teng for answering my many questions, the Distributed Active Archive Center at the Goddard Space Flight Center for producing and distributing the data and the TRMM Science Data and Information System for providing the original data from which these products originate (see http://daac.gsfc.nasa.gov/). I want to thank Remote Sensing System for providing the SST TMI TRMM data at http://www.ssmi.com/. My thanks goes out to the National Center for Environmental Prediction (NCEP) and the National Center for Atmospheric Research (NCAR) for providing data on the internet http://www.cdc.noaa.gov/ and http://wesley.wwb.noaa.gov; to the ECMWF (Operational Analyses and Re-analyses) for supplying the data and to the BADC for providing the internet based trajectory service at http://www.badc.rl.ac.uk/data/ecmwf. I personally thank Isabelle Jobard for giving me special attention concerning the TRMM satellite and algorithms. To Fleur Couvreux, whom I will never forget, thank you for the mental support and computer skills in the very beginning when I needed it most. Thanks goes out to Dr Henry Mulenga and Dr Chris Reason for their meteorological expertise. Thank you to Leslie Stageman and Lesley Elley for helping me with my stay and making it more pleasant. To my surrogate parents away from home, Paul Hanekom and Penny Krohn, I never would have managed without your friendship and advice. To Ewa Stachlewska, my polish physicist friend, thank you for helping me understand the mathematical explanation of vorticity. Thank you to Mark Majodina, Jeremy Main, Chris Jack, Raymond Roman, Salwyn Bergman and Isabelle Ansorge for always helping me in a

kind and efficient way. I thank Professor G. Brundrit for our many interesting discussions about surf and weather and for welcoming me so warmly into the department. I thank my advisor Dr Mathieu Rouault most graciously, for despite our many battles he always kept my best interests in mind. I want to give my utmost gratitude to Professor J. R. E. Lutjeharms for giving me this priceless opportunity and the guidance I needed to accomplish the task. I especially recognize the WRC for the project "The influence of the ocean on South African rainfall" and the CNRS/NRF for the project "Satellite remote sensing of rainfall and convective systems" as part which this investigation was funded.

## PUBLICATIONS FROM THIS DISSERTATION

Rouault, M., I. Jobard, S. A. White and J. R. E. Lutjeharms (2000). Monitoring rainfall over South Africa and adjacent oceans using the TRMM satellite. *South African Journal of Science*, submitted.

Rouault, M., S. A. White, C. J. C. Reason and J. R. E. Lutjeharms (2000). Influence of the Agulhas Current on a South African Extreme Weather Event. *Weather and Forecasting*, submitted.

## ABSTRACTS BASED ON THIS RESEARCH

White, S. A., F. Couvreux and M. Rouault (1999). Satellite Remote Sensing of Rainfall over the Ocean. South Africa Marine Science Symposium, Wilderness, South Africa.

## POSTER BASED ON THIS RESEARCH

Rouault, M., F. Couvreux, S. A. White, M. Desbois and L. Jobard (1999). TRMM measurements of extreme weather during the South African 98/99 rainy season, TRMM Global Precipitation Mission Meeting, October 25-29, 1999. University of Maryland.

## TALKS GIVEN, BASED ON THIS RESEARCH

Rouault, M, F. Couvreux, S. A. White, M. Desbois, L. Jobard, M. Majodina and F. Stuart (1999). Meteosat and TRMM measurements of extreme weather during the South African 98/99 rainy season: A South African French Cooperative project. 15th Annual South African Society for Atmospheric Science Conference, Richards Bay, South Africa.

White, S. A., F. Couvreux, M. Rouault (1999). Satellite remote sensing of rainfall over the ocean. South Africa Marine Science Symposium 2000, Wilderness, South Africa.

White, S. A. and M. Rouault (1999). Rainfall measurement over the ocean using the TRMM satellite. University of Cape Town, Department of Environmental and Geographical Studies.

White, S. A. and M. Rouault (2000). Comparing the Agulhas Current influence on two storm events. University of Cape Town, Department of Oceanography.

# CONTENTS

# 1. INTRODUCTION

The dynamic nature of southern Africa's surrounding oceans and atmosphere creates an environment conducive to extreme weather. Since most of South Africa's population is living in precarious conditions, the consequences of such floods are often devastating to both people and property [Bang 1988]. The oceanic influence on the atmospheric circulation has been shown to affect the subcontinent's weather [Lindesay and Jury 1991; Jury et al. 1990; Walker and Lindesay 1989; Reason 1998 and Reason and Mulenga 1999]. The atmospheric conditions often result in heavy rainfall, which can lead to flooding [Triegaardt et al. 1991]. This thesis is aimed at making a modest contribution towards a deeper understanding of this oceanic influence on heavy rainfall events over southern Africa.

*OCEANIC SETTING*

Located at the southern tip of the African continent, South Africa is bounded by two distinct ocean current regimes: the Agulhas Current system along the east and south coasts and the Benguela Current system along the west coast. To the south of the continent, the Southern Ocean is bordered by the Subtropical Convergence near 38°- 42° S (Figure 1.1).

The warm Agulhas Current, which forms the most intense western boundary current of the southern hemisphere, completes the South Indian Ocean subtropical gyre as

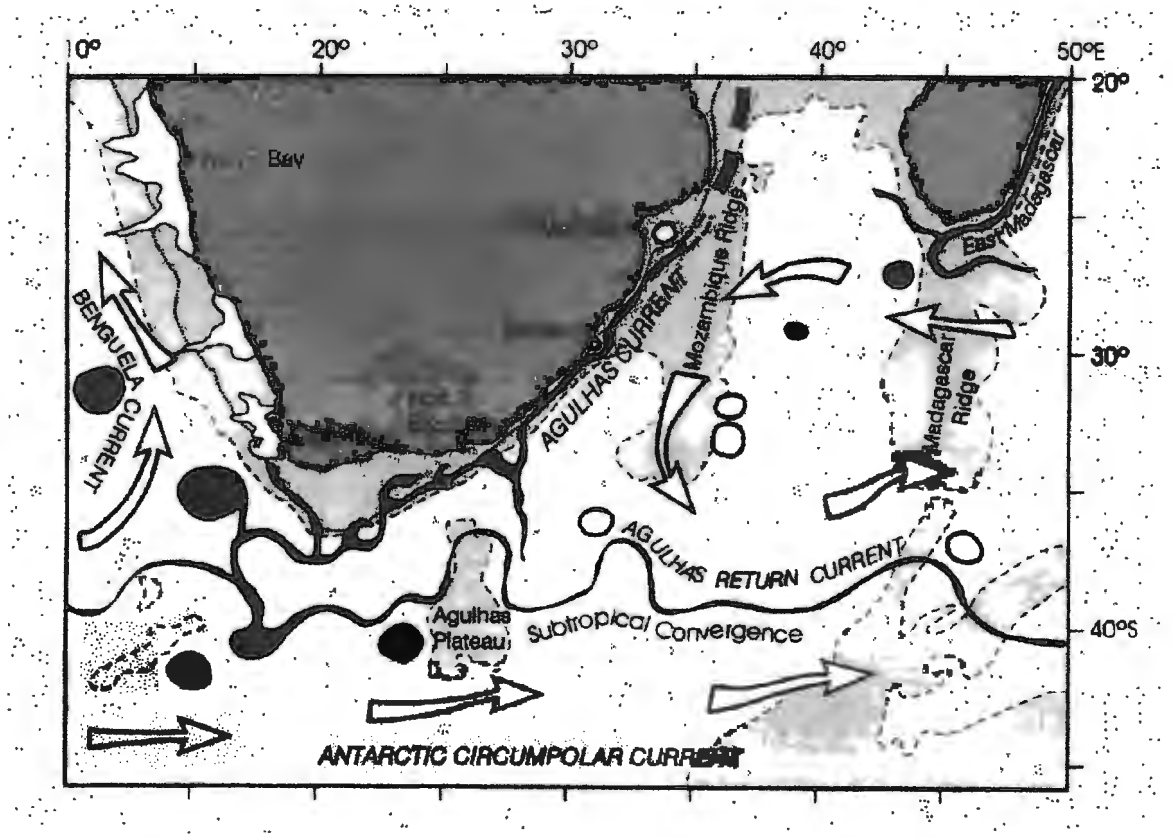


**Figure 1.1.** Schematic representation of the ocean circulation surrounding southern Africa [Lutjeharms in press]. The large arrows demarcate the general oceanic flow; the Agulhas Current is black with rings shedding off as black circles. The dotted line is the bathymetry demarking features such as the continental shelf, plateau and ridge systems. The white areas on South Africa's west coast close to shore are regions of upwelling.

its waters flow south-westward along the east coast of southern Africa. Its source regions have formerly been identified as the westward surface drift of the South Equatorial Current, the East Madagascar Current, and the Mozambique Current [Harris 1972; Lutjeharms et al. 1981a-b]. However, recent research is uncovering inadequacies in this simplistic model. Even though the core width of the Agulhas Current is relatively narrow, approximately 100 km [Pearce 1977], a large portion of the South-west Indian Ocean is influenced by what may be termed as the Greater Agulhas Current and the resulting recirculation region south-east of the subcontinent [Gründlingh 1978].

The Agulhas Current can also influence a significant portion of the ocean area south of the African continent encompassing the Agulhas Retroflection Region (ARR). It

is here that a large part of the Agulhas Current turns anticyclonically and starts flowing eastward near 18°- 20° E, 40° S. This results in a return current of Agulhas waters back into the South-west Indian Ocean [Lutjeharms and van Ballegooyen 1988a]. Warm Agulhas water can also extend considerable distances into the South-east Atlantic Ocean via Agulhas Rings that are shed at the retroflection loop [Lutjeharms 1981a-b] or as anomalous westward intrusions [Lutjeharms and van Ballegooyen 1988a]. The spatial extent of this warm water zone south of Africa is highly variable depending on the dynamics of the Agulhas Current system.

South of the subcontinent near 40°- 42° S, warm Agulhas waters encounter cold Subantarctic water at the Subtropical Convergence, where sea surface temperature (SST) gradients in excess of 10° C/100 km can result [Lutjeharms and Valentine 1984]. West of southern Africa from 15° to 35° S, cold, wind-driven, upwelled waters border the coastline and contribute to the waters in the northward flow of the Benguela Current system, the eastern boundary current of the South Atlantic subtropical gyre.

The existence of pronounced SST variability within both the Agulhas and Benguela Current systems was first demonstrated by Streten [1981]. Particular attention has since been paid to the region south of the subcontinent, where the existence of large interannual SST variability near 40° S and 20° E has been attributed to Agulhas Current influences [Gillooly and Walker 1984]. Walker and Lindesay [1989] have studied the relationship between SST anomalies surrounding Southern Africa and the development of major rain-bearing weather systems. Extratropical cyclones which developed over positive SST anomalies were considered. Their analysis suggests that early recognition of above normal SSTs in key areas may facilitate predicting severe rain-bearing potential of low

pressure systems. The retroflection region proved to be a key area where anomalously high SSTs were ideal for cyclogenesis.

High SSTs in the South-west Indian Ocean have also been shown to contribute to the intensity of cyclones responsible for flood producing rainfall [Lindesay and Jury 1991; Jury et al. 1990]. These studies examined flood rains which occurred only when SSTs in most of the South-west Indian Ocean were above normal during the month surrounding the event. Atmospheric general circulation model studies (e. g. Reason 1998; Reason and Mulenga 1999) support the idea that increased latent heat fluxes off warmer than average areas in the South-west Indian Ocean contribute towards increased rainfall over eastern South Africa.

The link between above normal SSTs and heavy rainfall events has therefore been established in past research. The logical progression from here to a better understanding of the role of the Agulhas Current in extreme rainfall events is to consider only those events which occurred during times of high SSTs in the Agulhas Current region. This type of consideration would most likely isolate those events influenced by the Agulhas Current. At this point it is important to understand the characteristic rainfall patterns and atmospheric conditions which govern southern Africa to compare with the anomalous conditions during extreme events.

*RAINFALL*

Heavy rains and floods occur more regularly over South Africa than is generally believed. These are often accompanied by the loss of life and extensive damage. Irregular variations in rainfall which lead to excessive rains and drought are of great concern to

farmers because South Africa is semi-arid with rapidly increasing demands for water [Harrison 1984]. Extreme events pose a threat to crop yield, water supplies, soil erosion, fisheries, etc. [as quoted by Jury and Majodina 1997]. The majority of these floods or heavy rains seem to occur in the KwaZulu-Natal province as well as the Eastern Cape province [Van Heerden 1988] (Figure 1.2).

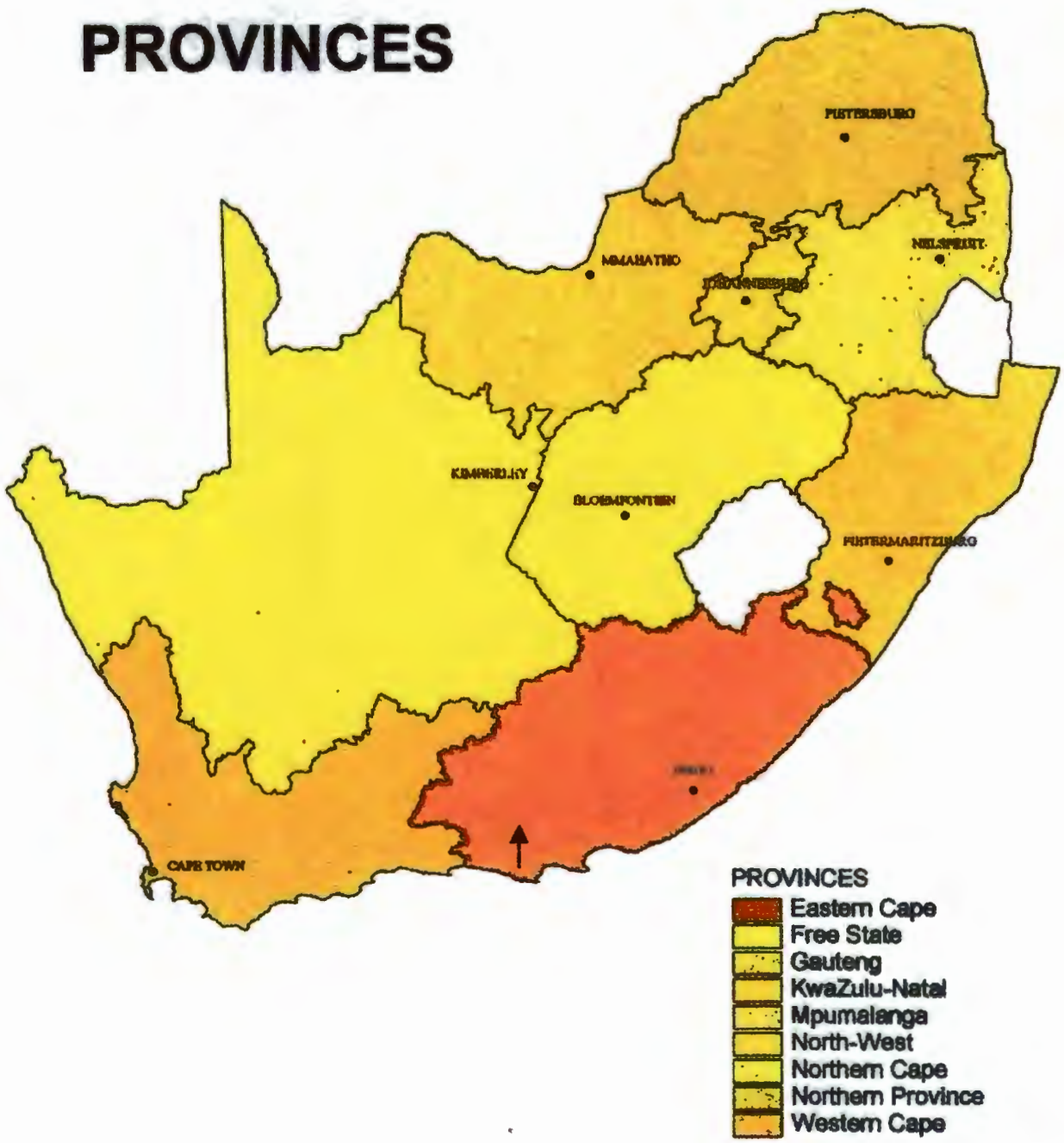


**Figure 1.2.** The provinces of South Africa are shown above.

The Kwazulu-Natal province encompasses the north-east quadrant of South Africa. This region receives the bulk of its annual rainfall during the summer months. North-east South Africa experienced one of its wettest summers in recorded history between the months December 1995 and January 1996 [De Coning et al. 1998]. The Eastern Cape southern coast receives significant rainfall throughout the year [Keen and Tyson 1973].

A generalized synoptic classification of significant summer rain-bearing disturbances over South Africa has been developed by Harrison [1984]. Cloud bands connecting a synoptic scale disturbance in the tropical easterlies with one in the mid-latitudes south of South Africa (so-called tropical-temperate trough) have been shown to be the major contributors to rainfall over the summer rainfall area of the country. Other important rain bearing systems include tropical and subtropical cyclones. Cut-off lows are another atmospheric system which account for many of the flood-producing rains observed over South Africa. The Laingsburg floods of 1981 and the Natal flood disaster of 1987 both resulted from a cut-off low [Triegaardt et al. 1988; Estie 1981].

Cut-off lows are a more intense form of a westerly trough, with a cold core which starts as a trough in the upper westerlies and deepens into a closed circulation extending downward to the surface [Preston-Whyte and Tyson 1988]. Cut-off lows are baroclinic low pressure systems that have a pool cool of air overlaying the surface low. Cyclonic vorticity in the air motion is apparent at all heights above the low pressure center. The slope of the low pressure core is tilted towards the upper cold air. Thus it slopes usually to the west with increasing height.

*ATMOSPHERIC SETTING*

Since most of the heavy rainfall events occur in the Kwazulu-Natal and Eastern Cape province during the summer rainfall season, it is important to consider the mean atmospheric setting during those months. Once the mean conditions are understood, then a comparison with the atmospheric setting during extreme events can be made.

The main atmospheric features during summer shown in Figure 1.3a, are a subtropical anticyclone at 30° S, 5° W in the Atlantic Ocean linked by a ridge a few degrees south of the continent to the anticyclone at 35° S, 85° E in the Indian Ocean [Van Heerden and Taljaard 1998]. There are easterly trade winds in the Indian Ocean between the subtropical ridge and the Intertropical Convergence Zone (ITCZ). A north-east monsoon current crosses the equator and spreads into East Africa and southward to the ITCZ. South to south-east trades between the Atlantic Ocean anticyclone and the continent recurve to become the south-west monsoon. The Interocean Convergence Zone (IOCZ) confluence stretches along about 15° S from eastern Zambia to southern Angola. Easterly trades over Zimbabwe and northern South Africa, recurve anticyclonically southward over Botswana and Namibia. The westerly air flow over the extreme south-western plateau of South Africa splits to become either southerly or westerly over the plateau.

Above the Atlantic Ocean, the core of the subtropical anticyclone is displaced in winter only 3 degrees to 4 degrees northward and about 5 degrees westward from its position in the summer season (Figure 1.3b). The pressure change is greater along the coast than at the core, and the zonal pressure gradient weakens substantially as does the southerly flow. The characteristic fresh south-easterlies over the south-west coast in summer shifts to predominant north-westerlies in winter.

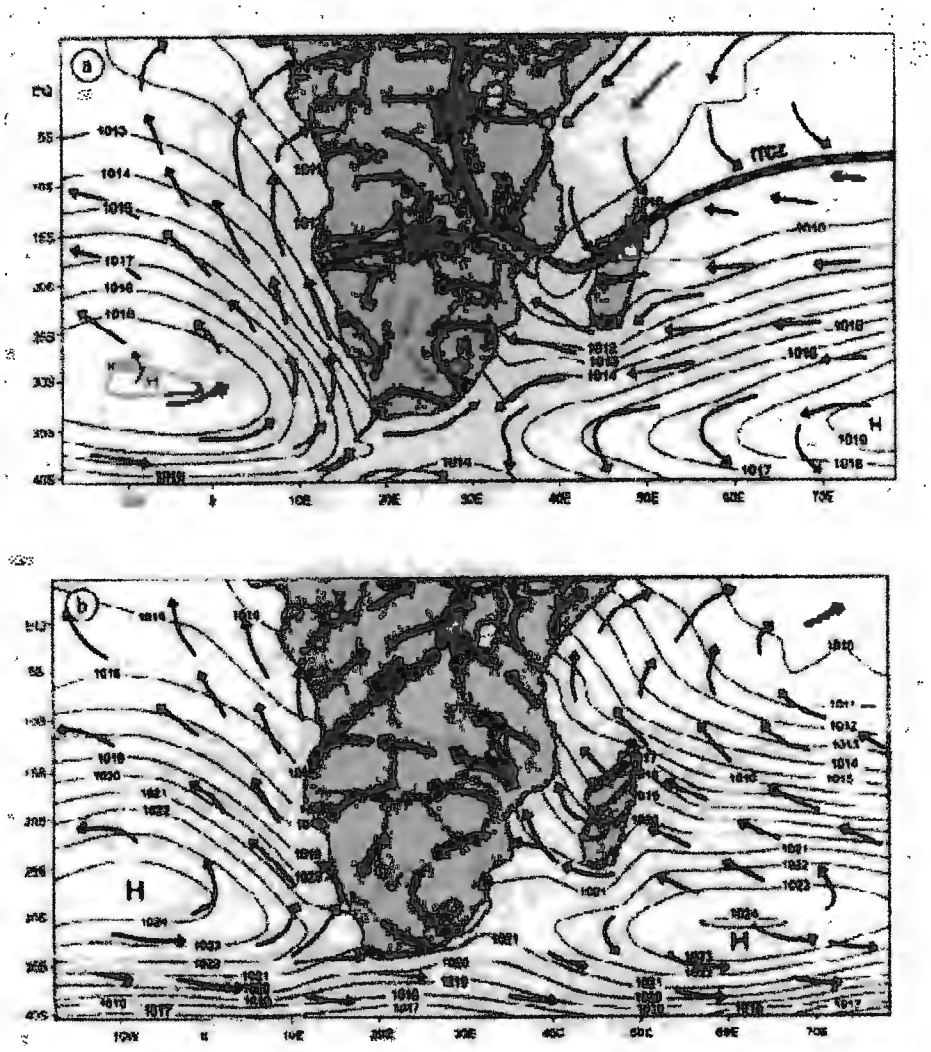


**Figure 1.3.** Mean SLP (hPa) based on daily analyses by the European Centre for Medium Range Weather Forecasting (ECMWF) for the eight years 1985-1992 for (a) summer (DJF) and (b) winter (JJA). Thick solid lines in summer represent the Intertropical Convergence Zone and Interocean Convergence Zone. The broken thick line in winter is the mean boundary between the dry continental south-east trade winds and the moist south-west monsoon air [Van Heerden and Taljaard 1998].

Above the Indian Ocean there is a more dramatic seasonal difference between summer and winter. In winter the anticyclone undergoes a westward shift of 25 degrees and a northward shift of 5 degrees. As the ITCZ shifts north of the equator in winter, the north-east monsoon is replaced by a south-westerly monsoon. The core of the predominant anticyclonic surface flow over South Africa remains almost in the same position over the

east coast as in summer, but with the strong pressure rise of 10 hPa. The circulation over two thirds of the southern African plateau reverses to the steady south-easterly to easterly trade wind flow.

Geopotential height figures during summer at 850/700 hPa (Figure 1.4a) over the continent show that the Atlantic and Indian Ocean anticyclones are much weaker at the 700 hPa level. The 500/700 hPa level shows the Atlantic anticyclone has weakened and a subtropical ridge axis at 500 hPa has shifted 10 degrees equatorward (Figure 1.4b). At 200 hPa an anticyclone between 15° and 20° S is predominant. The increase in temperature during summer months is found to be greater along the east coast than the west coast [Karoly and Vincent 1998]. Near the equator however, the temperature is approximately 2° C greater along the east coast than the west coast. At 30° S, it is 8° C greater in both summer and winter. This profound difference of surface air temperature along the east and west coasts is not maintained aloft. Taljaard [1996] has shown that on the east coast there is a much deeper layer of fairly warm maritime air than on the west coast in summer.

Taljaard [1955] has drawn attention to the marked stability of the atmosphere over most parts of South Africa and surrounding oceans in both summer and winter. This has a relationship to the low values of rainfall over most of South Africa. An increase in temperatures in the Indian Ocean and a predominant easterly onshore component flow of

(a)

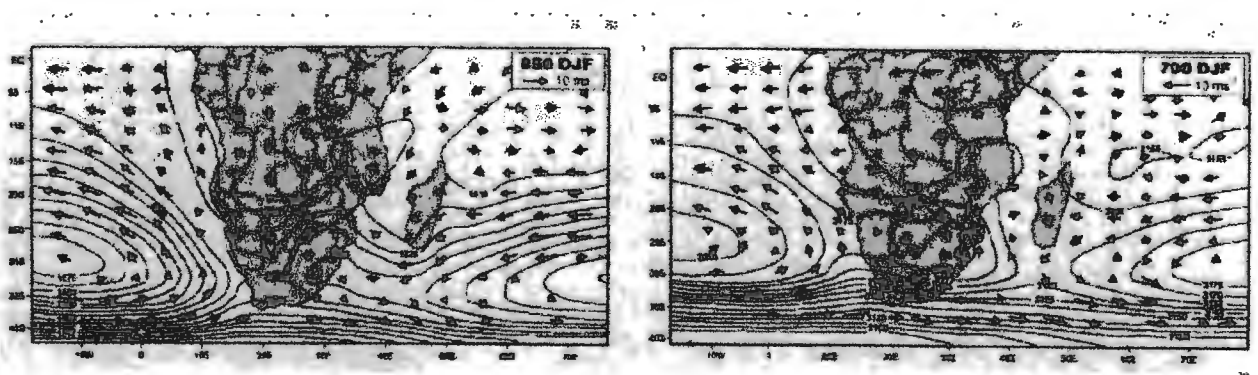

(b)

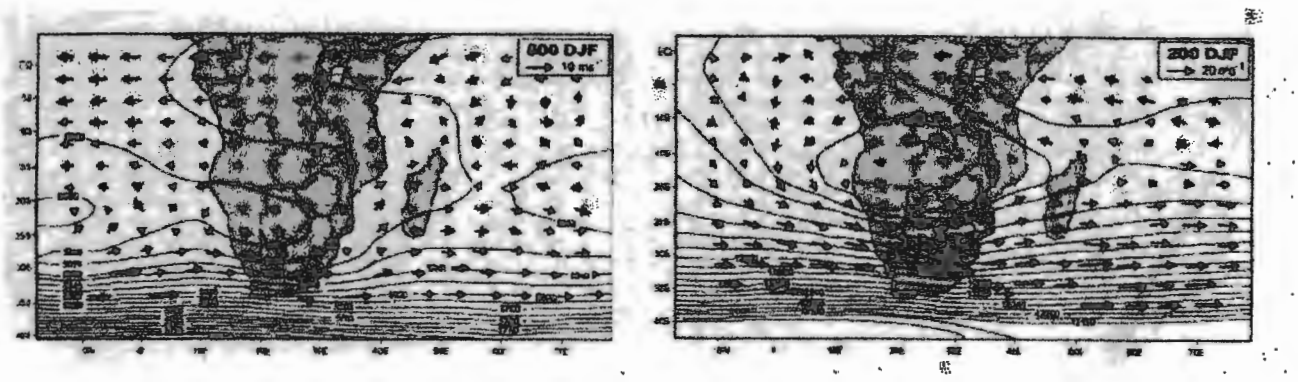


**Figure 1.4.** Mean contours of geopotential height (gpm), derived from daily European Centre for Medium Range Weather Forecasting (ECMWF) analyses (1985-1992) for (a) 850, 700 and (b) 500, and 200 hPa levels for summer (DJF) [Van Heerden and Taljaard 1998].

air masses between the equator and 30° S, create more favorable conditions for rainfall. In the northern parts of South Africa the air becomes humid and unstable in summer preceding upper troughs.

During wet summer months there are positive surface pressure anomalies over the central interior of subtropical Africa, particularly to the south-west, south, or south-east of the continent (Figure 1.5a). The sea level pressure is usually highest along 40° S. The upper air geopotential heights are below normal over western and central South Africa (Figure 1.5b). The presence of slow moving anticyclones along 40° S leads to the influx of moist maritime air from the Indian Ocean to the eastern regions. Moist tropical air can be advected as far north as the Zaire basin or Tanzania southward to 30° S. At 500 hPa, large anomalies indicate frequent occurrences of troughs or cut-off lows. It is important to note that Figure 1.5 refers to one year of data which implies this situation is only a generalization.

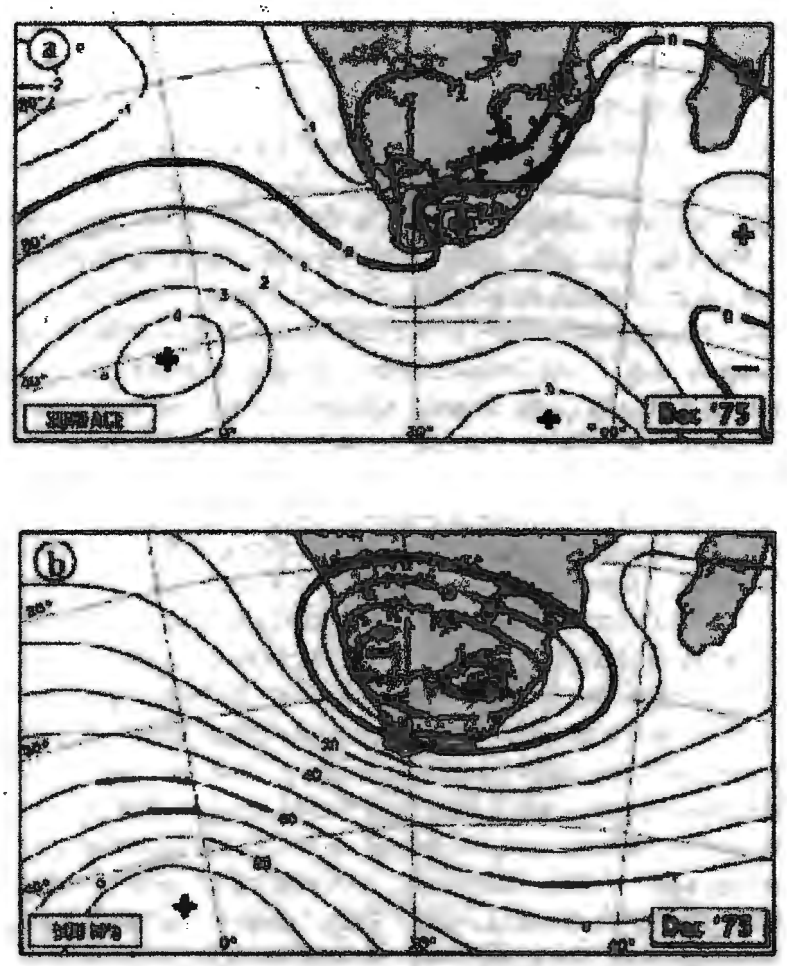


**Figure 1.5.** Anomalies of (a) surface pressure (hPa) and (b) 500 hPa geopotential height (gpm) during the very wet December 1975 [Taljaard 1987].

The features found during the wet period and identified by Triegaardt and Landman [1995] have shown a longwave upper ridge (Rossby wave number 3 or 4) south-west, south, and south-east of Africa. The strength of upper westerlies decreases at 30° to 40° S and positive surface pressure anomalies are present south-west, south, or south-east of South Africa. A cut-off low over South Africa is often characteristic. When a large

amplitude upper trough is present over the west coast, divergent upper circulation downwind of the trough causes large-scale upward motion and rainfall, provided the surface circulation is favorable for the advection of moisture.

Heavy rainfall events studied in the past have shown similarities and differences to the circulation features of the wet period mentioned above. De Coning et al. [1998] have suggested that heavy rains in northern South Africa are influenced by the strong low-level lifting provided as the northerly flow carries a moist tropical plume over the northern slopes of the mountain escarpment. The mountain escarpment provides the upward motion and the tropical air supplies the moisture. The mountain escarpment is a significant feature in the topography of southern Africa (Figure 1.6).

Crimp and Mason (1999) have pointed out that adjustments in circulation patterns as well as the timing and contribution of moisture from different source regions are important in influencing the duration and intensity of extreme events. Their study has identified the Indian Ocean to the east and south-east of South Africa as the moisture source region for one extreme precipitation event. Lindesay and Jury (1991) have similarly shown that an anticyclone over the South-west Indian Ocean and Mozambique Channel contributed to the synoptic-scale forcing of flood-producing rainfall over central South Africa. The ridging anticyclone in the South-west Indian Ocean provided the mechanism to supply moisture from the east.

James and Anderson [1984] have shown that the transfer of water vapour to tropical and midlatitude regions serves to enhance the rate of growth and intensity of baroclinic systems. Two areas have been identified in their study as possible moisture sources for rainfall over South Africa: the Indian Ocean with water vapour being advected

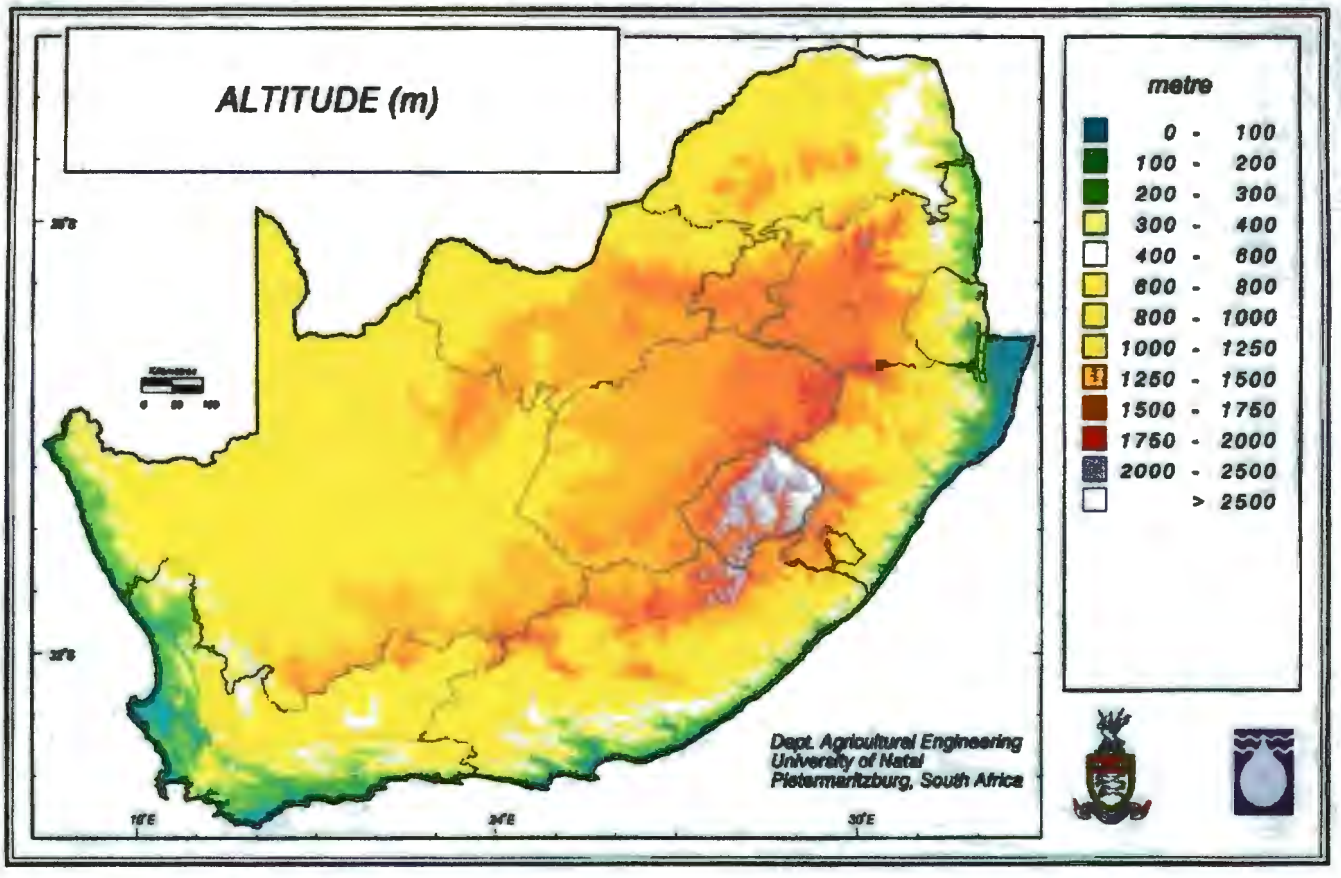


**Figure 1.6.** The altitude of South Africa.

over the continent around the South Indian Ocean anticyclone and the southward extent of the ITCZ. Considerable uncertainty therefore still exists over which source regions are dominant for individual heavy rainfall events.

This introduction has provided the scientific background so that a review of past research concerning the link between southern Africa's surrounding oceans and atmosphere can now be given. This review is undertaken to identify the scientific 'gaps' in current knowledge. It is from this reference point that a list of unanswered questions can be then drawn.

# 2. PREVIOUS RESEARCH

Over the past few years increasing recognition has been given to the importance of sea surface temperature (SST) changes in regulating the atmospheric circulation and rainfall over southern Africa [Walker and Lindsay 1989; Reason and Mulenga 1999]. It has been suggested that significant deviations in the general circulation from South Africa's climatological patterns are generated by large-scale, persistent SST anomalies [Tennant 1996]. These features may therefore contribute to the incapacitating droughts and devastating floods which plague the tropical and subtropical regions of southern Africa.

There have been many investigations on the effect of tropical SST anomalies on the atmospheric circulation around the globe [Webster 1981; Rocha and Simmonds 1997; Tyson et al. 1993; Fenessay and Shukla 1988]. Most global climate research [e. g. Foreman 1990; Cattle and Gordon 1990] and air-sea interaction studies [Charnock and Businger 1991; Webster and Lukas 1992] have tended toward treating the ocean and atmosphere as a coupled system. A theory explaining the main mechanism involved in this link between ocean and atmosphere was put forth by Wallace and Hobbs [1977]. The enhancement of upward air motions in the region of a warm anomaly and thus an increase in rainfall is attributed to the enhanced diabatic heating in the area of the anomaly, which causes condensation and the subsequent release of latent heat. The result is a convergence zone characterized by heavy precipitation. This mechanism is commonly referred to as Conditional Instability of the Second Kind (CISK).

Simulations conducted by Webster [1981] have shown that there was a different climatic response to positive SST anomalies placed at different latitudes. The most striking result was the diminishing magnitude of the total diabatic heating and vertical velocity as the SST anomalies were placed progressively poleward. Webster has shown that at the low latitudes there was a diabatic limit in response to the SST anomaly, whereas at mid-latitudes there was an advective limit. This is because at mid-latitudes there is cold air advection from the poles, whereas at low latitudes the air temperature is relatively homogeneous.

For a positive SST anomaly, the vertical velocity develops in the vicinity of the initial heating if the thermal advection above the sea surface is small. This means that at higher latitudes, where cold air from the poles is rapidly advected across positive SST anomalies, the initial upward motion which is tied to the anomaly forces the vertical advection of this cold air. Webster [1981] has suggested that at mid-latitudes, only when cold air advection is less (i. e. summer when air temperatures are higher) will a significant climatic response arise in midlatitudes to positive SST anomalies. Therefore, in the mid-latitude regions, summer is the season most likely to be affected by positive SST anomalies.

The CISK mechanism depends on the air-sea interaction which takes place immediately above the sea surface, i.e. within the region of the marine atmospheric boundary layer (MABL). This region responds to surface forcings on the time scale on the order of an hour or less [Stull 1988]. Investigations of the climatological response to air-sea interaction near South Africa have been undertaken by a number of authors [Mey and Walker 1990; Walker 1990; Jury and Levy 1993; Jury et al. 1993; Reason 1998; Reason

and Mulenga 1999]. Air-sea interaction research has also emphasized the importance of the small scale meteorological effects [Jury and Courtney 1991; Jury 1993; Jury 1994; Jury and Walker 1988]. These studies have focused on the way in which the warm water of the Agulhas Current affect South Africa's climate and weather.

The Agulhas Current is a dynamic system with different regions of the current affecting the atmospheric circulation in different ways. The Agulhas Retroflection Region (ARR) is distinctive in terms of its climatological impact as fluxes of heat of up to 200-225 $W/m^2$ to the atmosphere have been observed to occur here throughout the year [Walker and Mey 1988]. Meteorological observations from an aircraft survey in the ARR have shown the MABL to be significantly modified due to a SST front of 6° C at the edge of the Agulhas Current [Jury and Walker 1988]. Mey and Walker [1990] have calculated an occasional oceanic heat loss of 828 $W/m^2$ over the ARR. Such a high flux may enhance cyclogenesis in the region of frontal uplift. Mason et al. [1994] have used computer simulations that suggest that as SSTs in the Agulhas Current region increase, the sea surface temperature gradients strengthen which encourage cyclogenesis.

More recently, the first dedicated air-sea interaction research cruise, the Agulhas Current Air Sea Exchange Experiment (ACASEX) of autumn 1995, gathered evidence of significant latent heat fluxes in the area of the Agulhas Current [Rouault et al. 1995]. Most of the measurements showed that the core of the Agulhas Current, about 80 km wide, transferred about 5 times as much water vapour to the atmosphere as the surrounding water [Rouault et al. 2000]. A maximum latent heat flux of up to 600 $W/m^2$ was measured during the cruise. The marine boundary layer was found to be generally unstable above the current, stable above the inshore cold water and near neutral offshore. For the westerly and

easterly wind cases observed, the mean specific humidity and potential temperature of the boundary layer increased significantly with a concomitant boundary layer deepening over the current. In the presence of alongshore winds an atmospheric moisture and thermal front developed over the inshore SST front [Lee-Thorp et al. 1998a]. Other high fluxes have been measured above the current during various cruises made at different times of the year [Rouault et al. 1998]. Modification of the atmosphere by the high Agulhas Current SST has been observed through cloud lines aligned with the warm water edge [Lutjeharms et al. 1986, Lutjeharms and Rouault 2000]. During the ACASEX cruise [Lee-Thorp et al. 1998b] a transition in cumulus was observed above the Agulhas Current during a period of anticyclonic ridging. Clear conditions over the shelf were replaced by active, coupled cumuli above the current and partly cloudy conditions above the seaward border.

Many statistical links have been made between the locally high SSTs of the Agulhas Current system and the summer climate of the subcontinent [Walker 1990; Jury et al. 1993; Mason 1995; Reason and Mulenga 1999]. One such study focused on the influence of the Agulhas Current on summer rainfall along the south-east coast of the subcontinent [Jury et al. 1993]. Jury et al. have shown that strong correlation exists between the adjacent coastal rainfall and SSTs as well as distance of the current core offshore. Rainfall was found to decrease in a north-east/south-west gradient in conjunction with a north-east/south-west decline of maximum SSTs within the core of the current. These results indicate the influence of the proximity and temperature of the warm Agulhas Current on the local rainfall. Jury et al. [1993] have proposed two potential mechanisms which may produce alongshore variation in rainfall. These are, modification of onshore moving air by surface heat fluxes and the interaction between transient weather systems

and the embedded mesoscale circulation over the Agulhas Current.

South Africa is positioned within the subtropical belt of high pressure which results in an arid to semi-arid climate with most moisture that contributes to precipitation imported from source regions elsewhere [D'Abreton and Tyson 1996]. The moisture content of the air plays an important role in determining the thermal stability of the atmosphere and is a crucial factor in the precipitation process. The two major source regions of moisture established thus far are the tropics (coming from the north) and the Agulhas Current (coming from the east) [D'Abreton and Tyson 1995].

Atmospheric moisture studies in South Africa have been undertaken by D'Abreton and Lindsay [1993] and D'Abreton and Tyson [1995]. Analyses conducted by D'Abreton and Tyson [1995] have revealed that transport to the south-west from the tropical Indian Ocean is the most important source for water vapour during a wet January over South Africa. Often during the wet mid-summer month of January, conditions are characterized by enhanced northerly meridional flow, in contrast to dry conditions when westerly zonal flow is the predominant circulation characteristic [D'Abreton and Lindsay 1993].

D'Abreton and Tyson [1996] have studied water vapour transport over the interior regions of the country for rain days and no-rain days to determine the major moisture contributor at the 700 hPa level. It has been show in previous research that the 700 hPa level is the level of greatest importance for moisture transport during rain events over the summer rainfall region of the South African plateau [D'Abreton and Tyson 1995]. Backward moisture trajectories in D'Abreton and Tyson's [1996] research have shown that on rain days, moisture transport at 700 hPa is characterized by easterly-component flow

from the tropical Indian Ocean north of Madagascar (Figure 2.1a). No-rain days are characterized by a south-westerly moisture transport from the South Atlantic Ocean to the south-west of Cape Town (Figure 2.1b). The average moisture content of the air parcels in

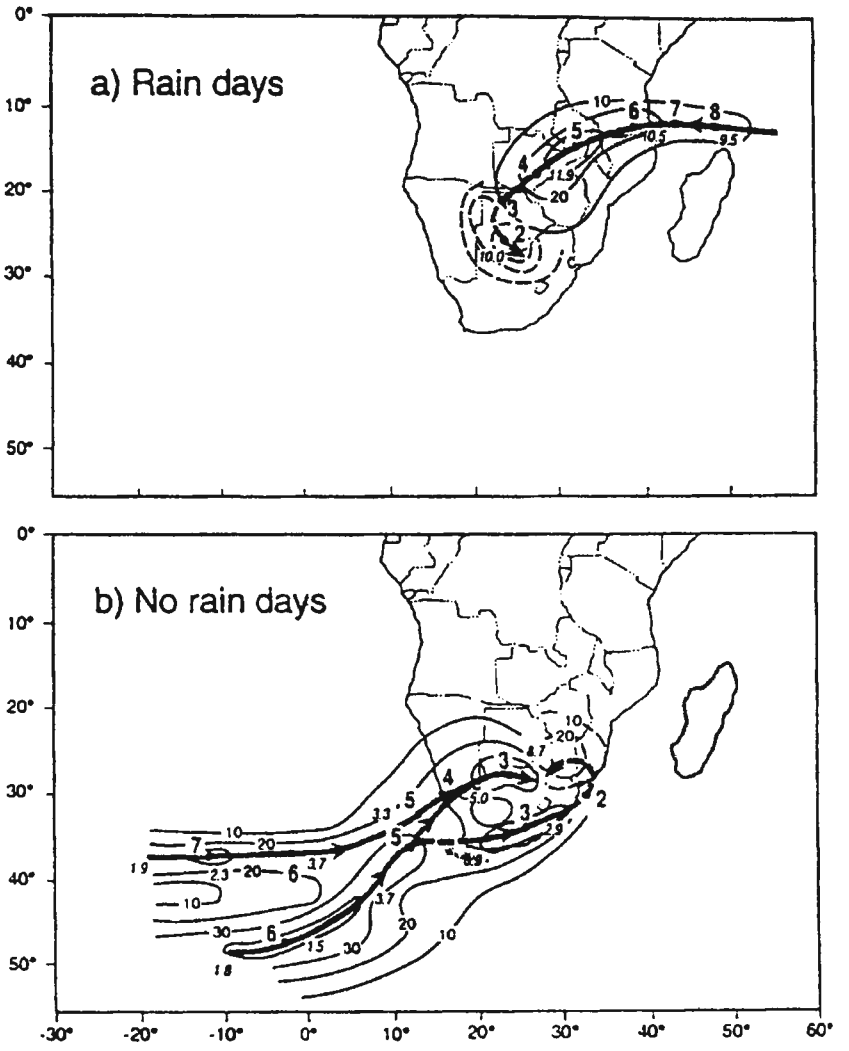


**Figure 2.1.** Mean trajectory fields for (a) rain days and (b) no-rain days in January over the Pretoria-Witwatersrand-Vereeniging (PWV) region. Contours give percentage occurrence of trajectories and heavy lines the maximum frequency pathway of trajectories. Large, bold numbers denote average times of travel (d) from the PWV region. Italicized values give meridionally-averaged specific humidities (g/kg) of mean air parcels at specific longitudes.

Figure 2.1b increases from 3 to 4 g/kg along the south-east coast to more than 8 g/kg at the Witwatersrand. This increase may be explained by the passage of the air over the waters of the Agulhas Current where the latent heat flux has been observed to be five times greater

than over the surrounding waters [Rouault et al. 2000].

It seems that moisture source regions vary depending on the synoptic conditions. D'Abreton and Tyson [1996] have shown that rain days have a significantly different atmospheric circulation than no-rain days. Lindesay and Jury [1991] have shown that an anticyclone over the South-west Indian Ocean and Mozambique Channel is a contributing factor to the synoptic-scale forcing of flood-producing rainfall over central South Africa. However, a definition of the major moisture contributor to an individual heavy rainfall event based on synoptic type has yet to be accomplished.

Moisture derived from high SST waters can be transported and fuel storms far away, as well as affect the atmosphere directly above the anomaly. Tennant [1996] has described the dynamics which underlie the link between the Indian Ocean SSTs and the general circulation over southern Africa. Positive SST anomalies in the Indian Ocean cause a drop in surface pressure and enhanced rainfall in the area of the anomaly. Since the circulation around the anomaly is changed, the convective areas over South Africa will be suppressed. This suppression over South Africa is termed the remote response of positive SST anomalies [Webster 1981]. The added heat flux into the atmosphere above the positive anomaly causes vertical instability in the lower layers, resulting in air parcels rising under buoyancy forces. Moist air would flow in to replace the rising air. The heat is carried upwards in the atmosphere and latent heat is released when the water vapour in the air condenses as the air cools adiabatically.

This research suggests that SST anomalies have a local affect on convection and a remote affect on the atmospheric circulation over South Africa. One may ask whether the positive anomalies in SSTs in the Agulhas Current region also show their greatest affect on

atmospheric circulation in local rainfall patterns. From the literature (e.g. Jury and Courtney [1991], Jury [1993], Jury [1994], Jury and Walker [1988], Reason [1998], Reason and Mulenga [1999], Rouault et al. [2000] and Lee-Thorp et al. [1998a-b]), it seems plausible to postulate that the latent heat released during rainfall in the atmosphere above positive SST anomalies in the Agulhas Current system may act to modify atmospheric systems both locally and remotely in such a way as to increase the quantity of rainfall over land.

Heavy rainfall in the past has resulted in devastating floods in many different regions of southern Africa. The Lainsburg floods were the most severe to date and occurred during the summer month of February 1988. This event resulted in costly destruction and more importantly, many deaths [Triegaardt et al. 1991]. Past research identifies KwaZulu- Natal and the Eastern Cape provinces as regions most susceptible to flooding during the summer months [Van Heerden 1988]. Summer rainfall on the south-east coast of Africa has been shown to be influenced by the temperature of the adjacent Agulhas Current [Jury et al. 1993; Reason 1998; Reason and Mulenga 1999]. However, the degree to which positive SST anomalies within the Agulhas Current system contribute to individual heavy rainfall events in the eastern coastal regions remains unknown.

Thunderstorms are convective cloud configurations, which result in the highest rain rates and thus the greatest probability of flooding. The likeliness of a thunderstorm depends on three factors: moist air near the surface, an unstable moist troposphere and triggering by, for example, surface heating or convergence due to a mountain escarpment. The most severe type of organized circular mesoscale convection is classified as a Mesoscale Convective Complex (MCC) [Linacre and Geerts 1997]. MCCs have been

shown to be favored in south-eastern Africa south of 15° S and east of 25° E with peak activity during summer months [Laing and Fritsch 1993]. That this region encompasses the Agulhas Current suggests that the high SSTs in the Agulhas Current waters may encourage the growth of MCCs by providing moisture at the surface. It is likely that south-eastern Africa being downstream of substantial topography also favors the occurrence of MCCs in this area (Figure 1.6).

Tornadoes are a type of supercell thunderstorm that are known to occur in Africa [Preston-Whyte and Tyson 1988]. The summer of 1998/99 has been identified as an unusually active season for tornado formation over the Eastern Cape [De Coning et al. 2000]. These powerful thunderstorms can spawn from MCCs. The occurrence of tornadoes depends on the development of strong potential and conditional instability. Tornado formation requires at least 2000 J of Convective Available Potential Energy (CAPE) which is possible when the planetary boundary layer (PBL) is sufficiently warm and humid, and the air aloft is sufficiently dry and cool [Linacre and Geerts 1997].

Tornado formation has been shown to occur on the cool side, and in proximity to, baroclinic boundaries [as quoted by Rasmussen et al. 2000]. They have found that storms, which remain on the warm side of the boundary, despite substantial CAPE, will not produce tornadoes. Storms that cross the boundary from warm to cool in general produce significant tornadoes, and evolve very rapidly upon crossing the boundary.

Maddox [1980] has examined four cases in which tornadoes occurred along thermal boundaries that had been produced by earlier thunderstorm activity. Based upon their observations, a physical model (Figure 2.2) was developed to explain the intensification of thunderstorms as they move across and along thermal boundaries. Point

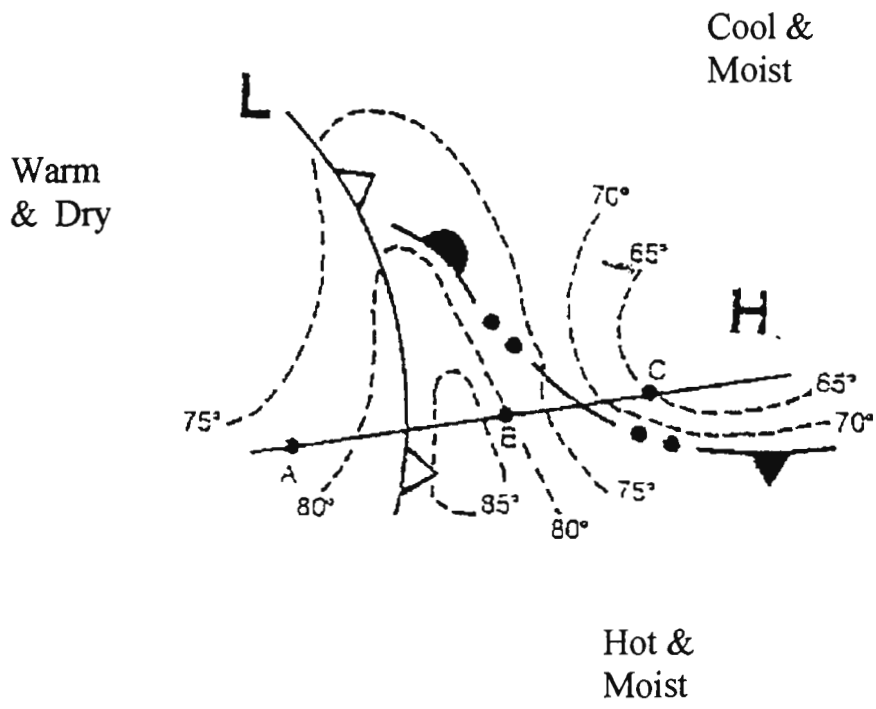


**Figure 2.2.** Conceptual model of flow near a boundary taken from Maddox [1980].

A is within the warm, dry, well-mixed air mass. Point B is a hot, moist and conditionally unstable air mass. Point C is in a region of cool, moist and stable thunderstorm outflow. South Africa's inland plateau region is warm and dry in the summer months due to the sun's heating and the mountain escarpment blocking the influx of moisture from the east. The coastal region is cooler and has a greater moisture content due to the influx of moist air from above the Agulhas Current. This is a common occurrence as the anticyclonic flow in the South-west Indian Ocean is a predominant feature. Whether tornadoes which form in South Africa favor the cool moist side of the baroclinic boundary present between the inland and coastal regions of South Africa has yet to be studied.

# 3. RESEARCH OBJECTIVES

The first chapter of this thesis was written to aid the reader in understanding the general atmospheric and oceanic setting within which South Africa exists. A general overview of the past research regarding the connection between the Agulhas Current sea surface temperatures (SSTs) and rainfall has been given in Chapter 2. To formulate the next logical step towards a more complete picture of the interaction between the warm Agulhas Current and rainfall over the southern African region, a brief reminder of what is known and what is not known follows.

*What is known*:

Certain areas of high SSTs have been identified in the Agulhas Current system as being **key areas** linked to the atmospheric circulation over the subcontinent. Walker and Lindesay [1989] identified the Agulhas Retroflection Region (ARR) as part of this link. Jury et al. [1993] identified a link between the Agulhas Current system and summer rainfall along the south-east coast of the subcontinent. Reason and Mulenga [1999] have shown that eastern South African rainfall is sensitive to SST warming in the South-west Indian Ocean.

During the summer season, floods most commonly occur in KwaZulu-Natal and the Eastern Cape provinces [Van Heerden 1988]. The synoptic situations most often responsible for producing rains in these areas have been extensively studied and classified

by Harrison [1984]. In the KwaZulu-Natal and Eastern Cape provinces, the synoptic systems which are major contributors to rainfall results from tropical or subtropical depressions or frontal disturbances. Cut-off lows are an atmospheric system commonly responsible for flood-producing rains observed over South Africa [Preston-Whyte and Tyson 1988].

The Conditional Instability of the Second Kind (CISK) mechanism explains why the ocean and atmosphere can be treated as a coupled system. The ocean and atmosphere are far more tightly coupled in the tropics than the mid-latitudes because the advection of cold air from the poles is less. Webster [1981] has demonstrated that at high latitudes the climatic response to SSTs was significantly greater in the summer season when cold air advection from the poles had lessened.

Air-sea interaction studies have focused on the Marine Atmospheric Boundary Layer (MABL) and determined flux rates for the key areas in the Agulhas Current system. Walker and Mey [1988] have determined a flux rate of 200/225 $W/m^2$ throughout the year for the ARR. Mey and Walker [1990] have observed an instantaneous flux of 828 $W/m^2$ also in the ARR. During the ACASEX cruise, Rouault et al [2000] observed that the core of the Agulhas Current commonly transferred five times as much water vapour to the atmosphere than the surrounding waters. This high water vapour flux into the atmosphere has been shown to enhance cumulus formations above the Agulhas Current such as cloud bands [Lutjeharms and Rouault 2000; Lee-Thorp et al. 1998b].

Moisture studies have identified two major source regions, which contribute to rainfall over southern Africa. They are the Indian Ocean, encompassing the Agulhas Current system, and the southern extent of the Intertropical Convergence Zone (ITCZ)

[D'Abreton and Tyson 1996]. These trajectories have also shown that the 700 hPa level is a key area for moisture transport from the tropics to southern Africa's inland plateau.

There therefore is little doubt that the Agulhas Current system plays an important role in the climate and weather of southern Africa. Drawing further from the literature [Webster 1981; Van Heerden 1988 and Jury et al. 1993; Reason 1998; Reason and Mulenga 1999], it seems plausible that the strongest signature may be realized during the summer season over KwaZulu-Natal and Eastern Cape provinces.

*What is not known*:

Crimp and Mason [1999] have established that the timing and the contribution of different moisture source regions are important in determining the duration and intensity of events that cause normal rainfall to become heavy rainfall. It remains uncertain whether the tropical moisture input is greater than that from the Agulhas Current during heavy rainfall events. It therefore still has to be determined what the relative contribution of Agulhas Current moisture is to individual heavy rainfall events. In this thesis two heavy rainfall events are identified and the relative contribution of Agulhas Current moisture is determined for each case.

Jury et al. [1993] have suggested that the Agulhas Current may add moisture via the onshore flow of warm marine air, thus providing the necessary moisture for rainfall over the south-east coast of the subcontinent. A strong correlation exists between the adjacent coastal rainfall and SSTs as well as shelf width. These results indicate the influence of the proximity and temperature of the warm Agulhas Current on the local rainfall. Jury et al. [1993] have proposed two potential mechanisms explaining what may

produce the observed alongshore variation in rainfall. These are, the modification of onshore moving air by surface heat fluxes, and the interaction between transient weather systems and the embedded mesoscale circulation over the Agulhas Current.

Research by Tennant [1996] has shown that convection over high SSTs can result in rainfall and subsequent latent heat release that may cause local convection and remote subsidence. This local or remote response to the SSTs in the Agulhas Current system has not been studied for individual case events. This thesis therefore aims to determine whether the Agulhas Current SST enhances or inhibits rainfall in the eastern coastal regions due to the latent heat release in the atmosphere during heavy rainfall events above the current.

Tornado formation has been shown to occur along the cool moist side of a baroclinic boundary [Rasmussen et al. 2000]. A baroclinic boundary exists in South Africa due to the sharp contrast in temperature and humidity between the inland plateau and the eastern coastal regions. The Agulhas Current forms the cool moist side of this boundary by providing the relatively cool moist air along the coast during onshore wind conditions. This thesis addresses whether this baroclinic boundary may enhance the synoptic situation and thus induce tornado formation along the eastern coastal regions of South Africa.

To summarize, this investigation addresses the following three **key questions**:

1. What is the relative contribution of Agulhas Current moisture to individual heavy rainfall events?

2. Does the Agulhas Current enhance or inhibit rainfall in the eastern coastal regions due to the latent heat release in the atmosphere during heavy rainfall events above the current?

3. Does the baroclinic boundary between the Agulhas Current and the inland plateau enhance synoptic events in such a way as to be conducive to tornado formation?

To address these questions properly, the appropriate data and the correct methodology are required.

# 4. DATA AND METHODS

Satellite data, global climate model simulations and observational data provided by the South African Weather Bureau (SAWB) are utilized in this research. The two satellites considered are the Tropical Rainfall Measurement Mission (TRMM) and Meteosat satellites. Global climate model data is taken from the National Center for Environmental Prediction (NCEP) and the European Center for Medium Range Weather Forecasting (ECMWF). The SAWB provided rainguage and radiosonde data over land.

All of the data used in this study were free. These data were either ftp transferred from the Internet, provided by the SAWB or obtained through collaborative efforts in France. Since South Africa is a developing country it was a necessity to exploit the appropriate sources of free data to answer the key questions of this research. The Meteosat satellite is well established as a reliable data source as it has been in use by the scientific community for many years. The TRMM satellite is very new, however it provides the most detailed coverage of rainfall, especially over the ocean. It would be preferable to have a regional model, but in the absence of that, NCEP and ECMWF global model data are a sufficient alternative. All the data were processed using the Matlab software on the Unix Operating System.

*SATELLITE DATA*

The TRMM Mission

The TRMM satellite is a joint US-Japan satellite mission to monitor tropical and

subtropical precipitation and to estimate its associated latent heating. TRMM provides systematic visible, infrared, and microwave measurements of rainfall in the tropics between 35° N and 35° S. TRMM was launched in the year 1997 and will remain in space until at least the year 2000. TRMM provides the first detailed and comprehensive data set on the distribution of rainfall and latent heating over the vast and under-sampled oceanic regions of the world. This new information will help the scientific community to understand better the role latent heat plays in driving the circulation of the global atmosphere and the interaction between the ocean, air and land masses which produce changes in global rainfall and climate.

The satellite orbit

The TRMM orbit is non-sun-synchronous which means that the satellite flies over each position on the Earth's surface at a different local time each day, to allow for the examination of the diurnal cycle of precipitation. The orbit is approximately 350 km

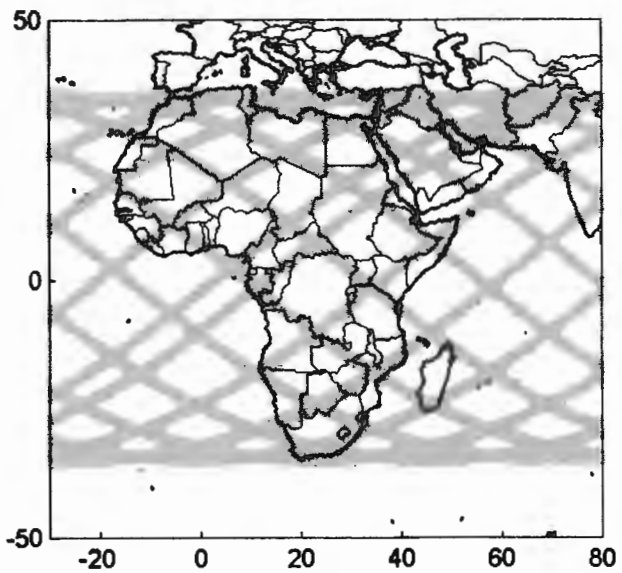


**Figure 4.1.** Characteristic orbits for one 24 h period of the Tropical Rainfall Measurement Mission (TRMM) satellite. The width of the lines indicates the width of the footprint. Note the concentration of lines over northern and southern Africa.

above the earth's surface. To cover the tropical latitudes around the globe, TRMM operates at an inclination of 35 degrees to the equator. TRMM orbits the earth between 15 and 16 times a day. The ground tracks of the orbits over the African continent are shown on Figure 4.1. It is remarkable that the northernmost and southernmost parts of the continent both benefit from a larger number of satellite over-passes than elsewhere. As a consequence, South Africa is in the field of view of the TRMM instruments from three to six times daily, depending on the sensor's swath. It is this advantageous time sampling over South Africa that contributes to the usefulness of this satellite for research in this country.

The TRMM instruments

The satellite carries three rain-measuring instruments. These are the Visible/Infrared Scanner (VIRS), the TRMM Microwave Imager (TMI) and the Precipitation Radar (PR). In addition to these onboard-instruments, there are ground radar systems and rain gauges at various Ground Validation Sites. The ground radar and rain gauge measurements are used to validate the TRMM satellite rain estimation techniques. The two principal rain-measuring instruments are the PR and the TMI and are utilized in this study.

The PR is the first rain radar in space and the most innovative rain-measuring instrument aboard TRMM. The PR is an electronically scanning radar employing active microwave sensors and has a horizontal ground resolution of approximately 4 km and a swath width of 220 km. One of its most important features is its ability to provide vertical profiles of the rain and snow from the surface up to a height of about 20 km. Another

feature is the fine ground resolution, however the 4 km wide footprint of the PR is greater than the scale of some convective rainfall events. This could mean that non-uniform filling of the PR antenna beam might bias the retrieved rain rate profile. Durden et al. [1998] have found that the path-integrated attenuation and the resulting path-averaged rain rate are underestimated. The reflectivity and rain rate near the top of the rainfall column are overestimated. The near surface rain rate is usually underestimated, sometimes severely. In addition, the radar signal of the TRMM satellite is highly attenuated below zero degrees and the precipitation radar is insensitive to reflectivities less than 20 dBz [Steiner and Houze 1998].

Research in recent decades has demonstrated that it is possible to obtain fairly accurate rainfall rates based on the temperature of the microwave spectrum [Bauer and Bennartz 1998]. In general, passive microwave techniques perform exceptionally well for instantaneous applications over the oceans [Bauer et al. 1998]. Thus the TMI aboard TRMM is a passive microwave sensor, which has been developed to provide quantitative rainfall information. The TMI carefully measures the tiny amounts of microwave energy emitted by the Earth and its atmosphere and is able to quantify the water vapor, the cloud water and the rainfall intensity in the atmosphere. It is based on the design of the highly dependable Special Sensor Microwave/Imager (SSM/I), which has been flying continuously on Defense Meteorological Satellites since 1987. TMI provides information over a wide swath width of 760 km and has nine channels, which measure the radiation either vertically or horizontally, polarized at frequencies: 10.7, 19.4, 21.3, 37, 85.5 GHz. These frequencies are similar to those of the SSM/I, except that TMI has the additional 10.7 GHz channel designed to provide a more-linear response for the high rainfall rates

common in tropical rainfall. This frequency is also useful for SST retrievals.

An important feature of microwave retrievals is that SSTs can be measured through clouds, which are nearly transparent at 10.7 GHz. This is a great advantage over the infrared SST observations that require a cloud-free field of view. With TMI, it is now possible to measure the SST over ocean areas with persistent cloud coverage. This advantage is particularly important for measuring surface temperatures of the Agulhas Current as cumulus cloud lines have been shown to commonly occur above this current [Lutjeharms et al. 1986; Lee-Thorp et al. 1998b]. One limitation of this device is that microwave retrievals are sensitive to sea-surface roughness, while the infrared retrievals are not. A primary function of the TRMM SST retrieval algorithm is the removal of surface roughness effects. The algorithm for retrieving SSTs from the microwave radiometer data is described in Wentz [1996].

The TRMM's lower altitude (350 km) compared to the 860 km altitude of the SSM/I results in the TMI having an improved ground resolution, which ranges from 5 km for the 85.5 GHz channels to 45 km for the 10.7 GHz channels. This higher resolution of the TMI over that of the SSM/I, as well as the additional 10.7 GHz frequency, is the reason why the TMI is generally considered to be a better instrument than its predecessors.

Rain products and algorithms

The TRMM Science Data and Information System (TSDIS) perform the real-time processing and post-processing of the TRMM science data [Kummerow et al. 1998]. The products are separated into different levels according to the degree of processing by the TSDIS. Level-1 products are the instrument's data, in full resolution, with radiometric and

geometric calibration. Level-2 data are utilized in this study and are derived geophysical parameters at the same resolution and location as those of the level 1 data, or binned to a regular grid.

The TMI product (2A12) used in this study provides rainfall rates and the vertical structure of rain and latent heat release based upon the nine channels of the TRMM Microwave Imager. This product is also available as a gridded orbital product (G2A12) that gives values at grid points with a resolution of 0.5 × 0.5 degrees corresponding to the orbit swath (760 km). The data are produced by an algorithm that is based on a Bayesian approach requiring the use of a large database of potential rain rate profiles. These profiles are constructed for 14 different layers from the surface to the top of the troposphere using cloud-resolving models such as the Goddard Cumulus Ensemble model.

The brightness temperatures Tb for the nine TMI channels are computed for each rain profile using a radiative transfer model. Each rain profile is then associated with a Tb vector. The whole set of profiles and associated Tb vectors constitutes the database. The rain profile is retrieved by inversion of the Tb measurements using the database. Tb vectors which best fit the TMI-measured Tb vector are obtained by searching the database and allowing for the deduction of the rain profile. A more complete description of this algorithm can be found in Kummerow et al. [1996]. This product also gives the latent heat released in the atmosphere; the algorithm is described by Olson et al. [1999].

The combined TMI/PR product used in this study (2B31) provides the vertical structure of rainfall (rain rates and drop-size-distribution (DSD) parameters) based upon both the data from the microwave imager (TMI) and the radar (PR), within the radar swath of 220 km. This product is also available as a gridded product (G2B31); it has a narrower

swath width, but has a finer resolution of 0.1 × 0.1 degrees. The data are produced by an algorithm also based upon a Bayesian approach that begins by inverting the reflectivity values as measured by radar for every likely value of the DSD parameters [Haddad et al. 1997b]. The resulting rainfall estimates are used to produce the corresponding Tbs, which are then compared to the actual passive, TMI-measured Tb to decide which DSD value was most likely. This DSD is used to calculate the final rain profile. A more complete description of this algorithm can be found in Haddad et al. 1997a.

It is worth noting that discrepancies in rain rate values between the two described products are to be expected because the algorithms are different and have different physics. One is based on microwave emission and scattering of hydrometeors whereas the other combines the microwave measurements with radar reflectivity values obtained from the Precipitation Radar. The spatial resolutions of the products are also different, corresponding to the resolution of TMI and PR respectively. Since the spatial distribution of the rain field is generally highly variable, the two products will not have the same rain rate because their footprints are different. The TRMM science team is currently comparing the different rain products, validating each against ground measurements, quantifying the differences, and trying to improve the rain retrieval algorithms in order to minimize the differences. Therefore, the data are periodically reprocessed and upgraded products are made available to the scientific community. This investigation used Version 5 data, which is the most recent version available from the TSDIS.

Meteosat

The European Space Agency launched the first Meteosat satellite in 1977.

Eumetsat took over formal responsibility for the Meteosat system in January 1987 and by 1991 a new program had been initiated to ensure the continuation of Meteosat operations until the year 2000. The Meteosat Second Generation program will ensure continuity of operations until at least the year 2012.

The Meteosat is a geostationary satellite system, which means it provides a continuous view of the earth disc from a nearly stationary position in space. Geostationary satellites have high spatial and temporal resolutions. Meteosat images of the earth and its atmosphere are provided every half an hour in three spectral channels (Visible, Infrared and Water Vapour). The spatial resolution is 5 km. Only images from the visible part of the spectrum are analyzed in this study.

*MODEL DATA*

NCEP

The NCEP/NCAR Reanalysis Project is a joint project between the National Center for Environmental Prediction (NCEP) and the National Center for Atmospheric Research (NCAR) (Kalnay et al. 1996). This joint effort has produced new atmospheric analyses using historical data from 1948 onwards. This effort involves the recovery of land surface, ship, rawinsonde, aircraft, satellite and other data sources. Quality control and assimilating these data is the responsibility of NCEP/NCAR.

These data are gridded with a resolution of 2.5 X 2.5 degrees. Four different levels of data are available. Level A is strongly influenced by observed data and the most reliable class. The B designation indicates that although there are observational data that directly affect the value of the variable, the model also has a significant influence on the

analysis. Level C is the most unreliable class, as the variables are derived solely from the model fields. Level D represents a field that is obtained from climatological values and does not depend on the model. The NCEP data used in this study are either A or B level parameters. The model outputs forecast values at 0Z, 6Z, 12Z and 18Z, which are used to calculate the daily averages.

BADC

The British Atmospheric Data Centre (BADC) has provided an air parcel trajectory service that derives the air parcel paths from a set of analyzed winds. At present the BADC trajectory model uses European Centre for Medium-Range Weather Centre (ECMWF) 6 hourly pressure level data. This data set is derived from the ECMWF Operational analyses and Re-analyses. The three components of the wind (u, v, and w) are held on a 2.5 x 2.5 latitude-longitude grid. The data used cover the period from January 1979 to present. The pressure levels on which the data are given are not the model levels on which the wind files are produced at the ECMWF. Because of this, the BADC has needed to perform an extra interpolation using software provided by the ECMWF.

The trajectory model is based on a parcel advection code used in the contour dynamics/advection algorithm of Norton [1994] and Waugh and Plumb [1994]. The contour advection technique considers the contours to be made up of a set of particles. These particles are advected around by the winds (which the BADC model uses), and when the particle spacing along the contour becomes too sparse more particles are added. Similarly, when there are too many particles, some are removed.

The particle advection is the solution to the equation:

$$\frac{dr}{dt} = u(r, t) \qquad 1.1$$

where $r$ is the parcel position (latitude, longitude, and height), $u$ is the wind vector at the parcel position $r$ and $t$ is the time. The winds are a function of space and time and are taken from ECMWF analyses. To solve the equations the winds are needed on the particle positions. This is obtained by linear interpolation in both space and time. The time stepping uses a $4^{th}$ Runge Kutta method.

The time-step used in this analysis is 40 minutes. Backward trajectories have been performed from the storm's centers of heavy rainfall as origin to give 3 day backward trajectories for each air parcel analyzed. The output frequency is every 6 hours and has vertical advection included.

*SAWB DATA*

The SAWB has provided this study with daily rainfall data. The daily rainfall data is derived from 100 individual rainguage stations (Figure 4.2). Mean sea level (MSL) synoptic charts provided by the South African Weather Bureau (SAWB) are also used in this study. This data is drawn from both station observations, ship reports, drifting buoys, radiosonde data and satellite imagery. The isobars are drawn at MSL, over the ocean as well as over the continent, in 4 hPa intervals. In some places, where necessary, isobars are drawn in 2 hPa intervals. A key to the chart is shown in Figure 4.3.

In this study, vertical vorticity was calculated to investigate the possible enhancement of tornado formation due to the presence of a baroclinic boundary. This was accomplished using station data across the baroclinic boundary identified in a SAWB MSL synoptic chart (Figure 5.5c ). Vorticity can be expressed as the curl of the

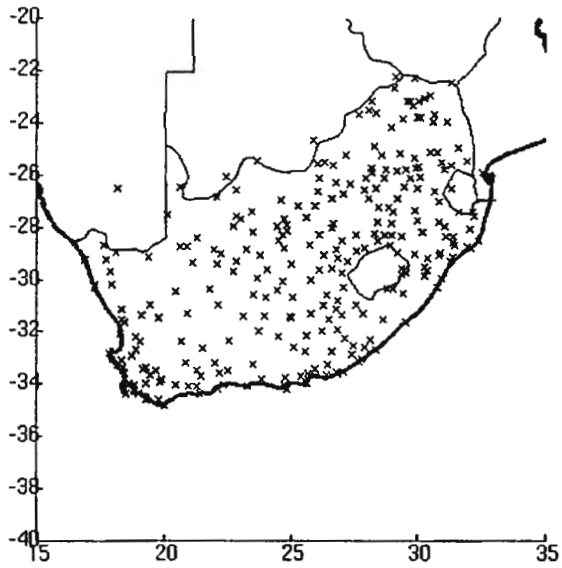


**Figure 4.2.** The 100 daily rainguage stations of the South African Weather Bureau. Each individual station is marked as an X.

velocity $(V_{\phi} \times V_3)$, which is customarily expressed in the Cartesian reference frame with the vertical coordinate $z$ as:

$$curl\ v = i\left(\frac{\partial \omega}{\partial y} - \frac{\partial v}{\partial z}\right) + j\left(\frac{\partial u}{\partial z} - \frac{\partial w}{\partial x}\right) + k\left(\frac{\partial v}{\partial x} - \frac{\partial u}{\partial y}\right) \qquad \textbf{1.2}$$

The vertical component of vorticity is denoted as:

$$\zeta = k \bullet V_z \times V_3 = \left(\frac{\partial v}{\partial x} - \frac{\partial u}{\partial y}\right) \qquad \textbf{1.3}$$

where $x$ is the horizontal distance normal to the baroclinic zone (positive $x$ toward the colder air), and $y$ is the horizontal distance parallel to the baroclinic zone (positive $y$ toward the north). Given the fairly straight geometry of the boundary, the flow can be simplified as two uniform fields, one on either side of the boundary, with a narrow transition zone

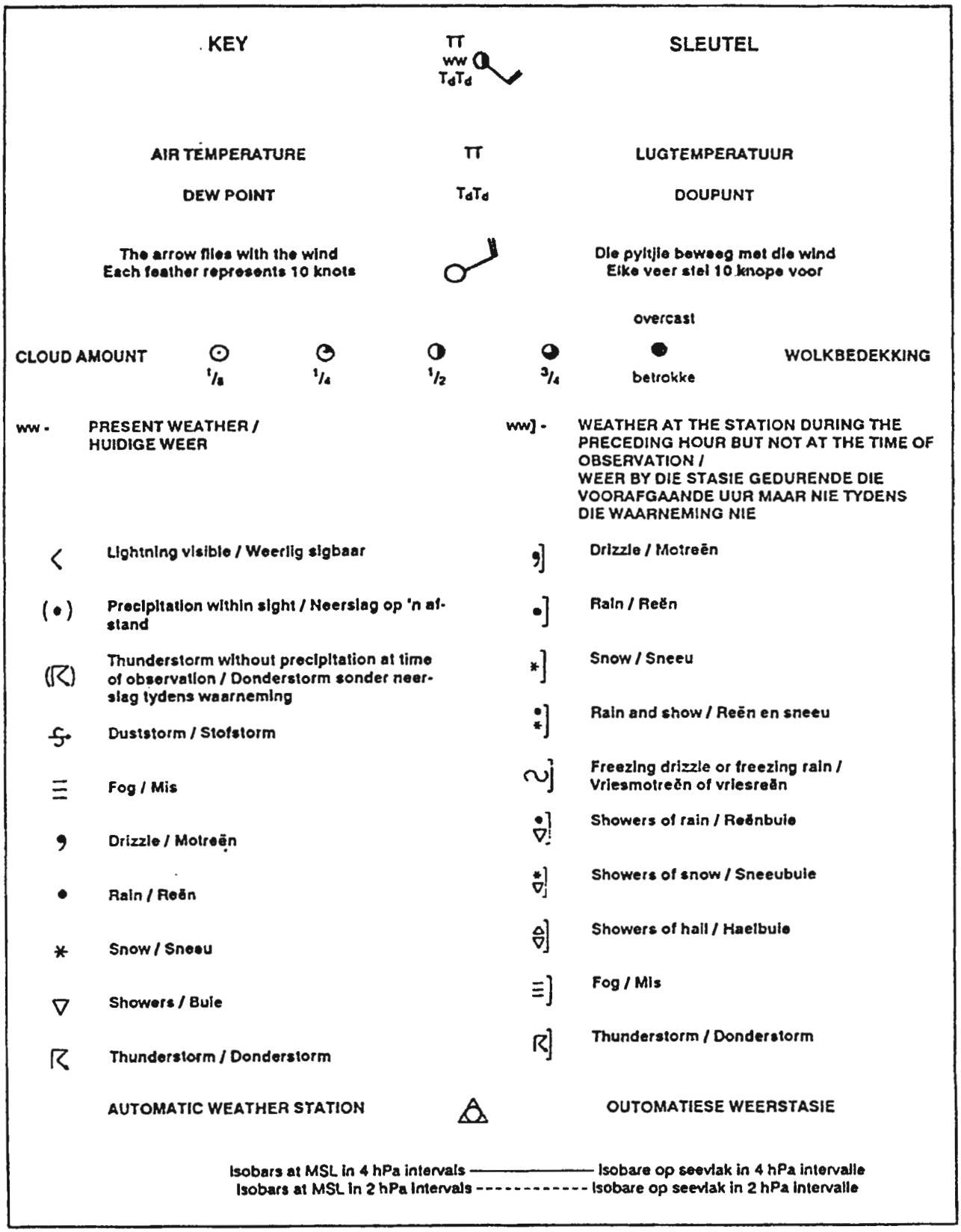


**Figure 4.3.** A key to the Mean Sea Level synoptic charts provided by the South African Weather Bureau.

between. Therefore, to estimate the vertical vorticity, the simplification used by Rasmussen et al. [2000] will be introduced that the along-boundary variations in the wind are much smaller than the cross-boundary variations. With the coordinate system [as in Eq. (**1.3**)] so that $x$ is normal and points toward cooler air, the equation for vertical vorticity using the foregoing assumption becomes:

$$\zeta = \frac{\partial v}{\partial x} \qquad \textbf{1.4}$$

The SAWB has also provided radiosonde data for this study. Radiosonde stations from De Aar, Bethelehem, Bloemfontein and Irene (near Pretoria) were selected from the available inland stations. On the coast, all radiosonde stations available were used in this study. These were stations located in the coastal cities of Cape Town, Port Elizabeth and Durban (Figure 1.1). The radiosonde ascents at all stations occurred twice daily, once in the early morning and again in the afternoon. Temperature and dewpoint temperature values as well as wind values were used, however for some stations wind values were missing. The radiosonde station in Port Elizabeth had only one ascent per day due to financial problems at the SAWB.

From the radiosonde stations the convective available potential energy (CAPE) was calculated using a package supplied by Bob Hart [http://www.ems.psu.edu/wx/grads/plotskew.gs]. The CAPE is useful to establish the susceptibility of a given temperature and moisture profile to the occurrence of deep convection [Holton 1992]. The CAPE provides a measure of the maximum possible kinetic energy that a statically unstable parcel can acquire (neglecting effects of water

vapour and condensed water on the buoyancy), assuming that the parcel ascends without mixing with the environment and instantaneously adjusts to the local environmental pressure.

The momentum equation for such a parcel can be rewritten following the vertical motion of the parcel:

$$\frac{D\omega}{Dt} = \frac{Dz}{Dt}\left(\frac{D\omega}{Dz}\right) = \omega\left(\frac{D\omega}{Dz}\right) = b' \qquad \textbf{1.5}$$

Where $b'(z)$ = buoyancy, given by:

$$b' = g\left(\frac{\rho_{env} - \rho_{parcel}}{\rho_{parcel}}\right) = g\left(\frac{T_{parcel} - T_{env}}{T_{env}}\right) \qquad \textbf{1.6}$$

$T_{env}$ designates the temperature of the environment. If the last term in Eq. **1.6** is integrated vertically from the level of free convection, *LFC*, to the level of neutral buoyancy, *LNB* (or limit of convection), following the motion of a parcel the result is:

$$\frac{(w_{CAPE})^2}{2} = \int_{LFC}^{LNB} g\left(\frac{T_{parcel} - T_{env}}{T_{env}}\right)dz = b \qquad \textbf{1.7}$$

where $w_{CAPE}$ is the maximum kinetic energy per unit mass that a buoyant parcel should obtain by ascending from a state of rest at the *LFC* to the *LNB* near the tropopause [Holton 1992 and Stull 1988]. Pressure coordinates and virtual temperature were used instead of temperature to account for the change in buoyancy resulting from a moist or dry environment [Doswell and Rasmussen 1994].

$$w_{CAPE} = \int_{LF}^{LN} R * \frac{(T_{parce} - T_{env})dp}{p} \qquad \textbf{1.8}$$

The trapezoid method for integrating vertically was then used to solve for $w_{CAPE}$. In equation 1.8, R is the gas constant for air and p is the pressure. It is important to note that CAPE calculations are greatly influenced by the humidity of the air parcel at its initial level since this affects the value of the *LFC* and the resultant air parcel trajectory.

# 5. RESULTS and DISCUSSION

During the 1998/99-summer season, South Africa's Eastern Cape experienced an unusual number of storms, floods and tornadoes [De Coning et al. 2000]. A survey of TRMM (Tropical Rainfall Measurement Mission) satellite surface rainrate data for this entire season was analyzed to discover the events with the most extreme TRMM rain rates which occurred over the Greater Agulhas Current system. There may have been more extreme rainfall events that took place over this region during the summer season, which were not observed by TRMM. TRMM orbits South Africa between 3 to 6 times a day resulting in an orbit path that may or may not capture images of the surrounding ocean areas.

The TRMM satellite, during the summer season 1998/99, observed intense rainfall over the Agulhas Current system, which corresponded to two significant storm events over land. As the sea surface temperatures (SSTs) in the Agulhas Current system and rainfall over the subcontinent have been linked in past research, these case studies were selected with the following key questions, identified in the previous chapter, in mind: was Agulhas Current moisture the dominant moisture source to these storms? Did the latent heat release during local rainfall above the current enhance these storms?

*CASE DECEMBER*

The most extreme of the two cases chosen occurred on 14 and 15 December 1998. Flood producing rainfall occurred over the Western Cape on 14 December. On 15 December heavy rain fell over the Eastern Cape as well as tornadoes in the cities of Umtata and Hogsback. Positively anomalous SSTs occurred over the Greater Agulhas Current system during the week surrounding this event (Figure 5.1). A TRMM SST composite from the week surrounding this event shows the Agulhas Current temperature ranged from 21° to 27° C (Figure 5.2).

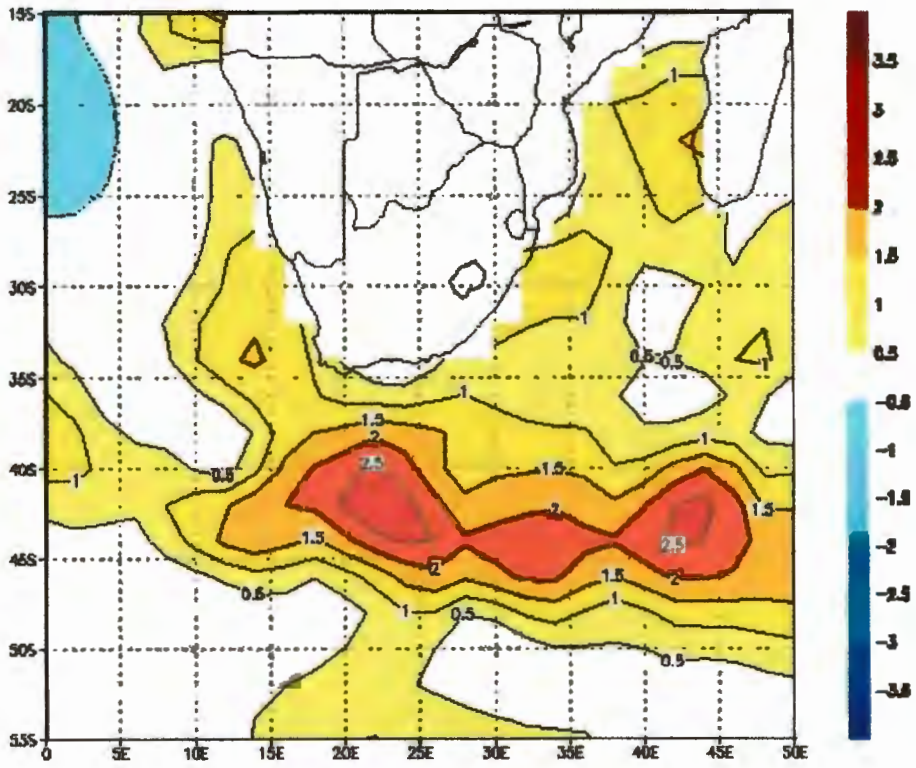


**Figure 5.1.** Optimal interpolation of sea surface temperature anomalies for the South-west Indian Ocean and the South-east Atlantic Ocean for the period 13 - 20 December 1998 (Reynolds and Smith 1994). Red is positive; blue negative.

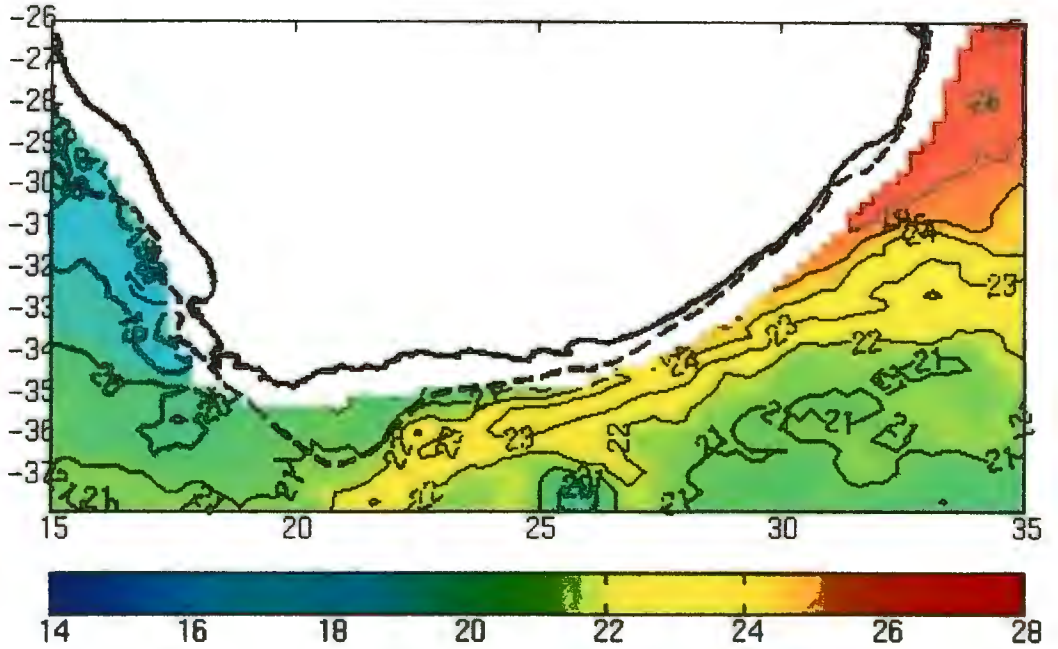


**Figure 5.2.** Weekly composite of SSTs in °C from 10 to 16 December 1998. These values were derived from TRMM Microwave Imager (TMI) on board the TRMM satellite.

Flood-producing rainfall occurred over the Western Cape at Tygerhoek (34° 9' S, 19° 5' E) on 14 December (93 mm) and similarly heavy rainfall (98 mm) the next day at East London (33° S, 27° 5' E) over the Eastern Cape (Figure 5.3). Tygerhoek is a predominantly winter rainfall area and heavy summer rains are rare. Thus, the flood-producing rainfall of 93 mm on 14 December accounted for 90 percent of Tygerhoek's rainfall for that month. The heavy rainfall (98 mm) on 15 December at East London represents 58 percent of the month's total. Unlike Tygerhoek, East London receives more rain in summer than in winter on average.

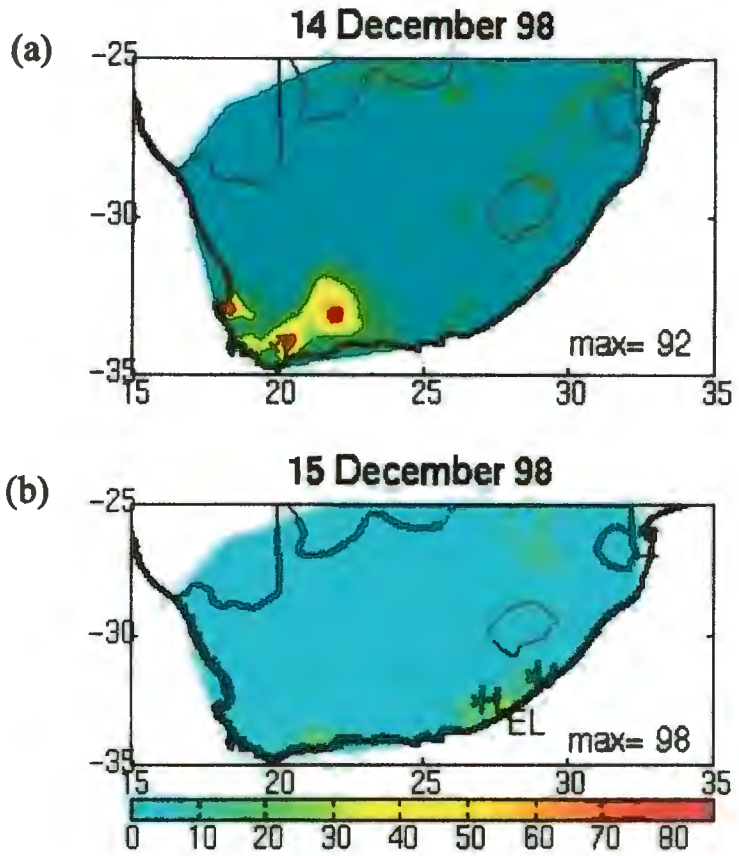


**Figure 5.3.** (a). SAWB rainfall for 14 December from 100 stations. Heavy rainfall occurred over Tygerhoek (T). (b). SAWB rainfall for 15 December. Tornado locations are shown as H for Hogsback and U for Umtata. Heavy rainfall occurred over East London (EL). The color bar is the daily total in mm/day and the maximum rainfall (max) which fell in the heavy rainfall locations appears in the bottom right-hand corner of each panel.

In addition to this heavy rainfall and local flooding, tornadoes were reported at Hogsback (32° 35' S, 26° 56' E) and in the city of Umtata (31° 32' S, 28° 40' E) (Figure 5.3b). The tornado event in Umtata received extensive media coverage because it threatened the life of South Africa's president at the time, Nelson Mandela. Eleven people were killed and buildings were destroyed in a 70 km radius. A picture of the tornado

damage in Umtata shows the vulnerable nature of these areas to unforeseen extreme events that go unforecasted (Figure 5.4). Van Niekerk and Sampson (1999) have classified the tornado as F2 on the Fujita scale.

**Figure 5.4.** Evidence of the tornado damage in the city of Umtata located in Figure 5.3(b) as U.

Synoptic Setting

Mean Sea Level (MSL) synoptic charts (Figure 5.5) and Meteosat visible imagery (Figure 5.6) show the general development and dissipation of the storm system. On 13 December a weak cold front was present south of the continent with a heat low over the interior (Figure 5.6a). A well-developed anticyclone was present in the South-west Indian Ocean with associated easterly advection of moist air above the Agulhas Current along the south-east coast (Figure 5.5a). Cloud lines over the Agulhas Current (Figure 5.6a) on 14 December provide further evidence of the low level moisture available along the south-east coast of South Africa. On 14 December, the inland heat low deepened from 1010 hPa to 1008 hPa as it shifted eastward (Figure 5.5b). Figure 5.6b-d shows the eastward moving system of organized convective thunderstorm cells at this time. The weak cold front that

was situated south of the country on 14 passed the subcontinent on 15 (Figure 5.5c). The continental heat low moved further eastward on 15 and deepened to 1006 hPa as it extended further north. This corresponds with the most intense convective thunderstorm cloud imagery (Figure 5.6d-g).

(a)

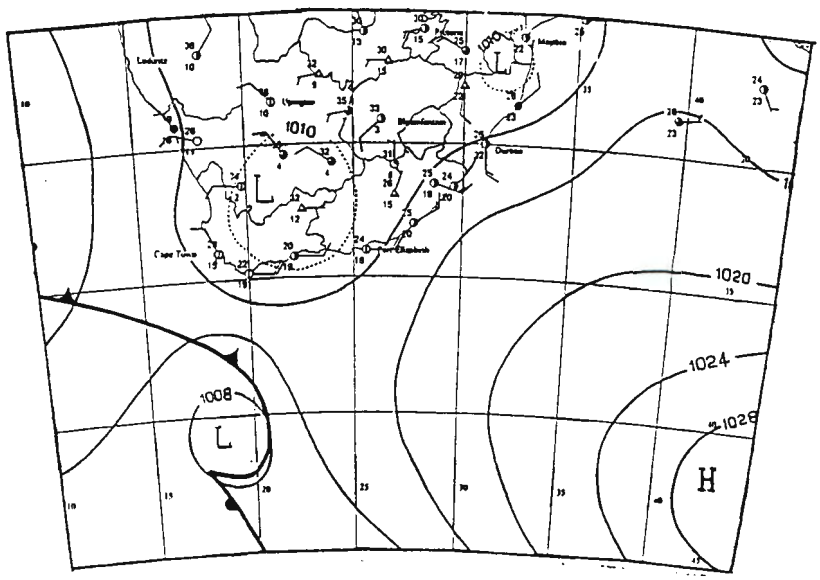


(b)

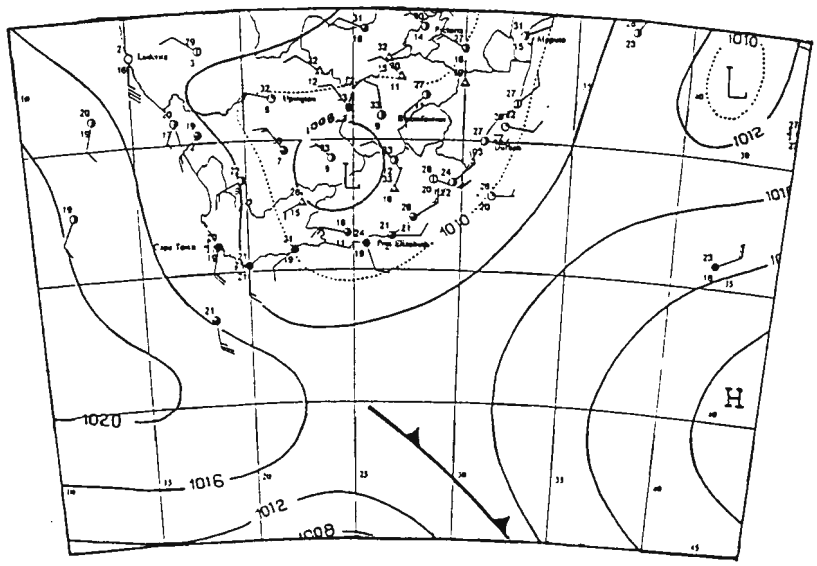


**Figure 5.5.** Synoptic chart of atmospheric pressure at mean sea level (a) for 13 December 1998, (b): for 14 December 1998, (c): for 15 December 1998, (d): for 16 December 1998 at 1400 SAST.

(c)

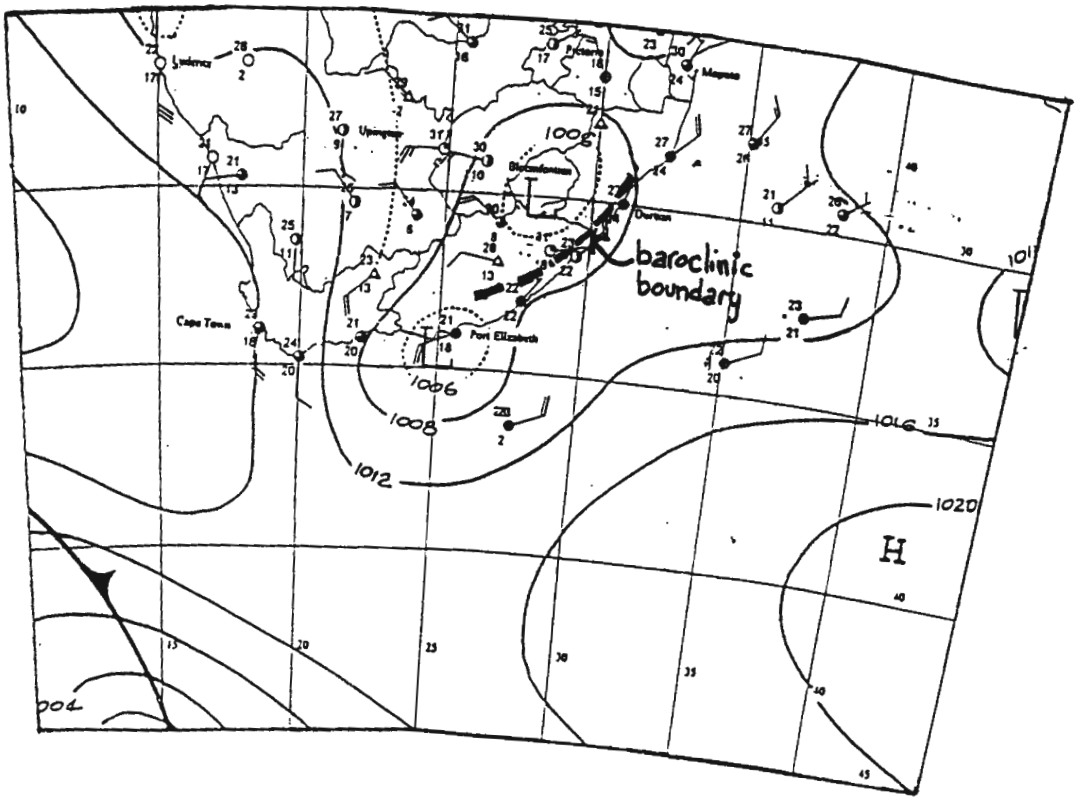
baroclinic boundary
1004
1006
1008
1012
1016
1020
H

(d)

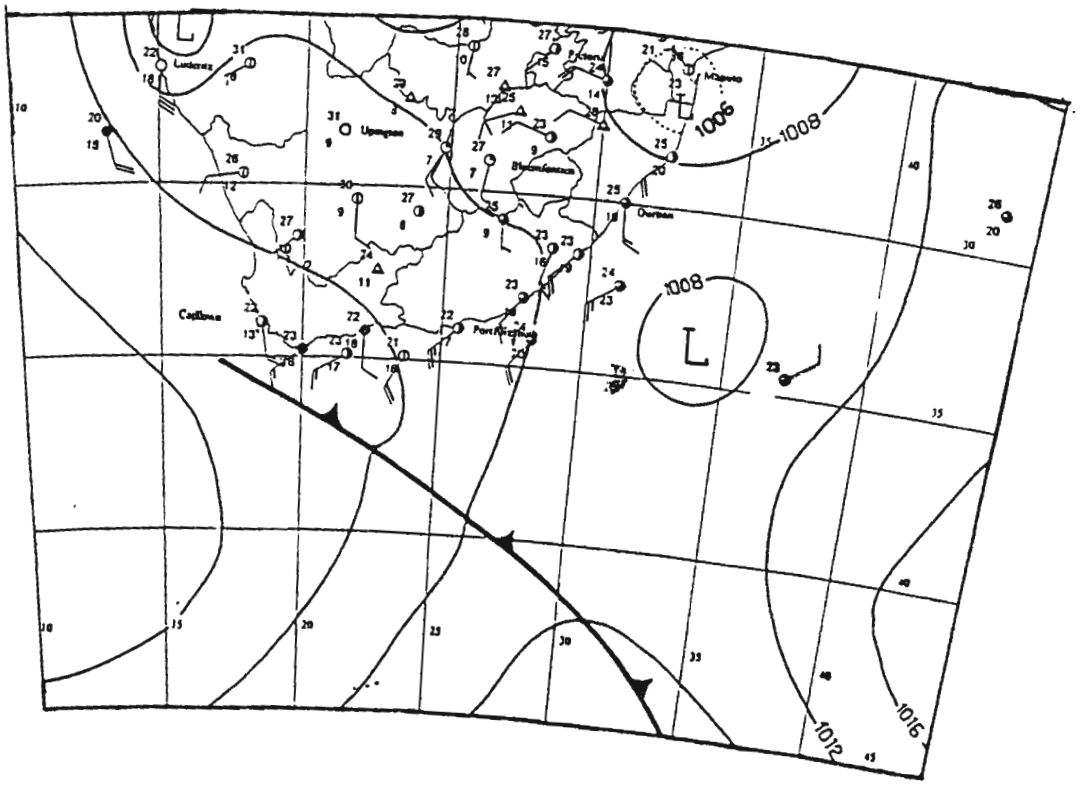
1006
1008
1008
L
1012
1016

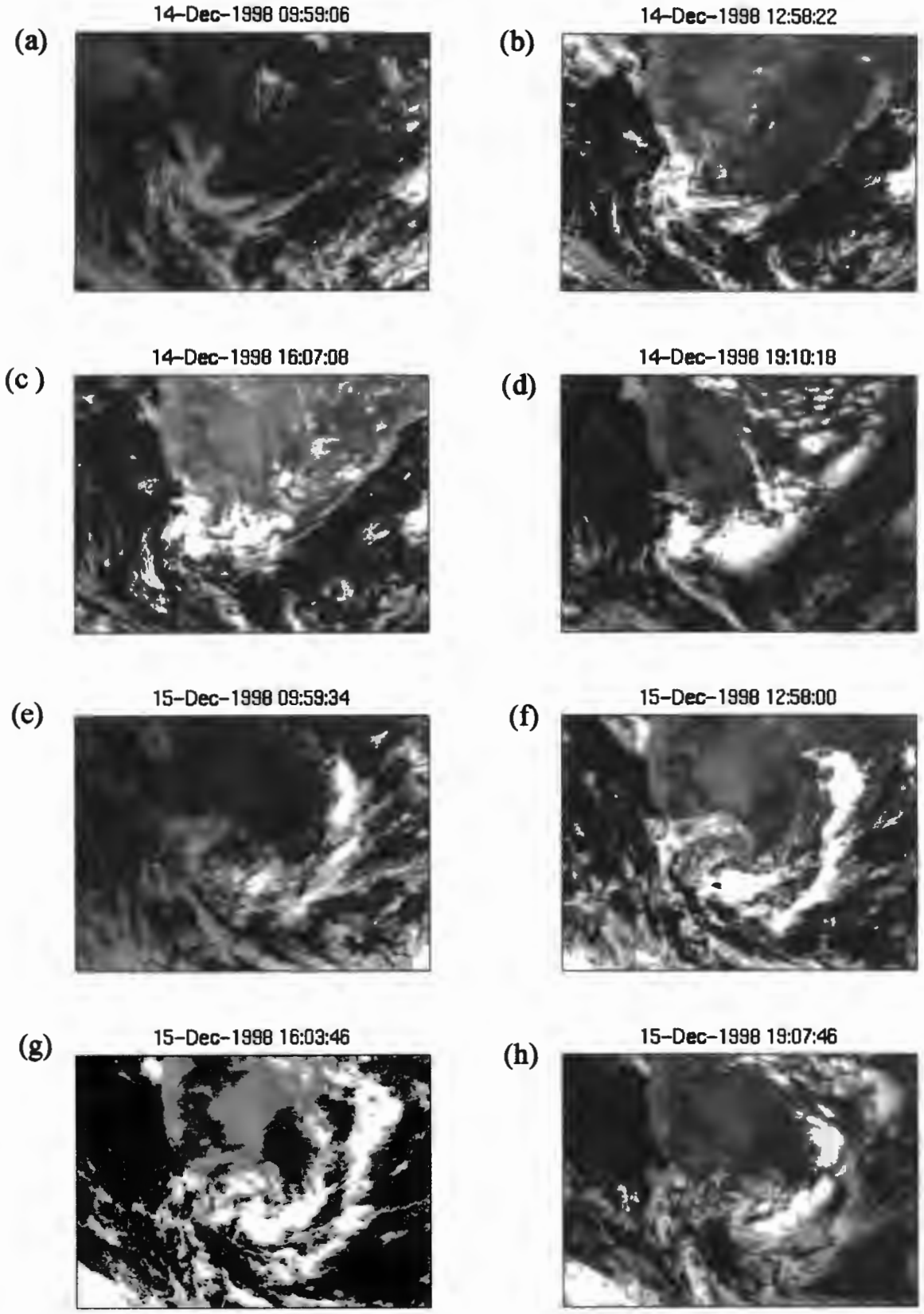


**Figure 5.6.** Satellite images in the visible frequency band for southern Africa and adjoining ocean regions for 14 and 15 December 1998 from METEOSAT. Clouds are in white.

Late on 14 and early 15, the organized convection became more linear in form and lasted long enough and was sufficiently extensive to be classified as a squall line (at least 6 h and 650 km long) (Figure 5.6e-g). The Atlantic anticyclone approached from the west on 16 (Figure 5.5d), with associated advection of cooler, drier air into the region. As a result, the surface low over the Eastern Cape was displaced well out into the South-west Indian Ocean and rainfall over land ceased.

NCEP Analysis

The National Center for Environmental Prediction (NCEP) daily averages of atmospheric parameters were analyzed to better understand the progression of the storm on a daily basis. Temperature data at the surface (Figure 5.7a) confirm the presence of the intense near-surface thermal low over the interior previously seen in the MSL charts (Figure 5.5). This thermal low can be identified because of the closed isobar pattern. On 13-14 December the temperatures at 1000 hPa reached a maximum of 34° C with a strong thermal gradient of approximately 16° C existing between 30° S and 35° S that enhanced the baroclinicity of the approaching trough. This strong gradient weakened by 5 degrees on 15 and 16 December. At the 850 hPa level the heat low is still evident. It shows a similar pattern of dissipation on 15 and 16 December at 1000 hPa as at 850 hPa. There is no evidence of the heat low at the 500 hPa level (Figure 5.7b) consistent with the fact that thermal lows have small vertical extension and usually remain below the 700 hPa level. It is interesting to note at the 200 hPa level the existence of a warm core (32.5° S, 24° E) in conjunction with the passage of the trough mentioned in the MSL charts (Figure 5.5). That the vertical extent of this trough reaches such a high atmospheric level indicates the great

magnitude of convective energy present in this storm.

(a)

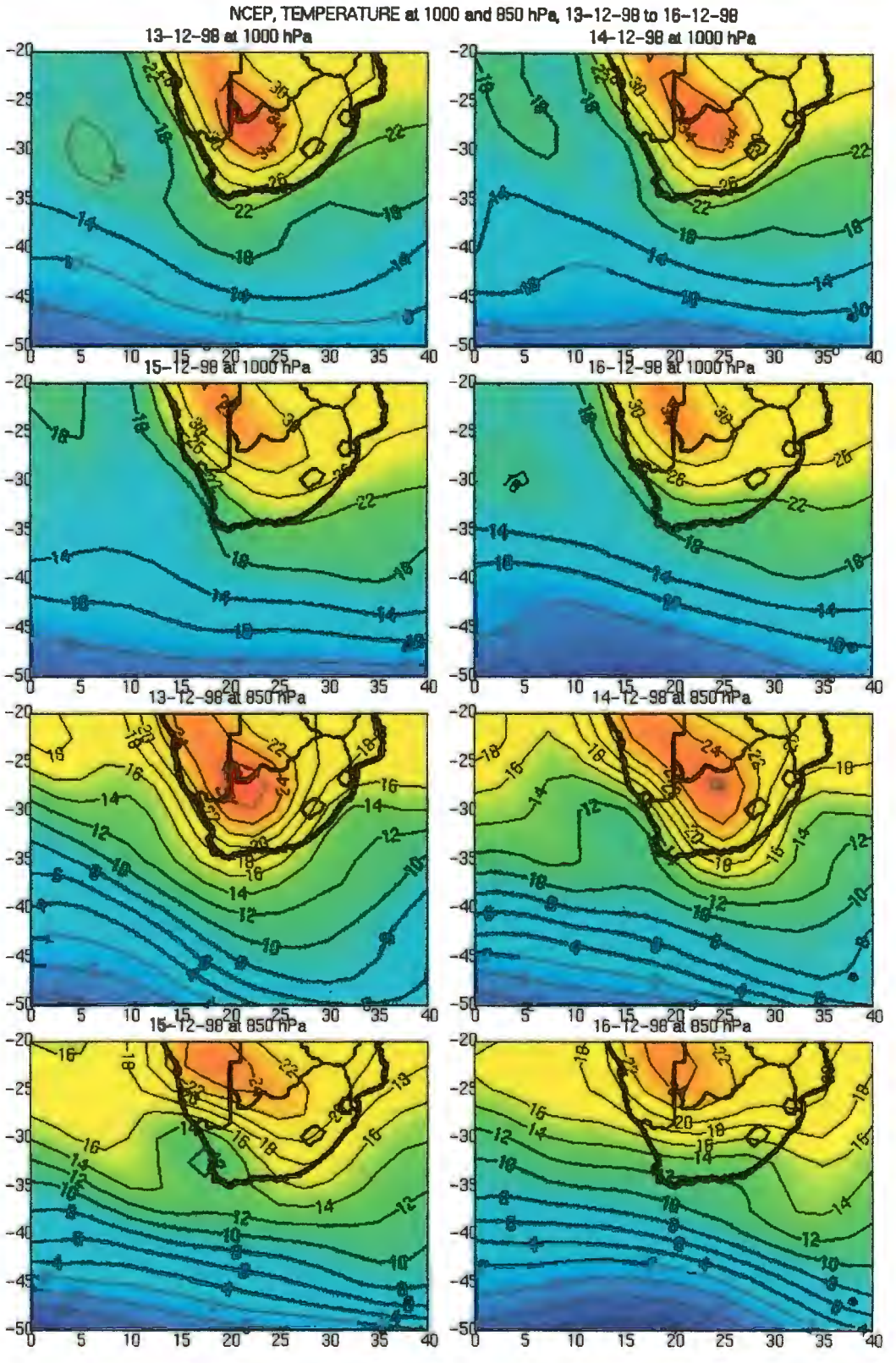


**Figure 5.7.** NCEP daily temperature values in °C for (a) 1000- 850 h-Pa and (b) 500-200 h-Pa levels from 13 until 16 December 1998.

(b)

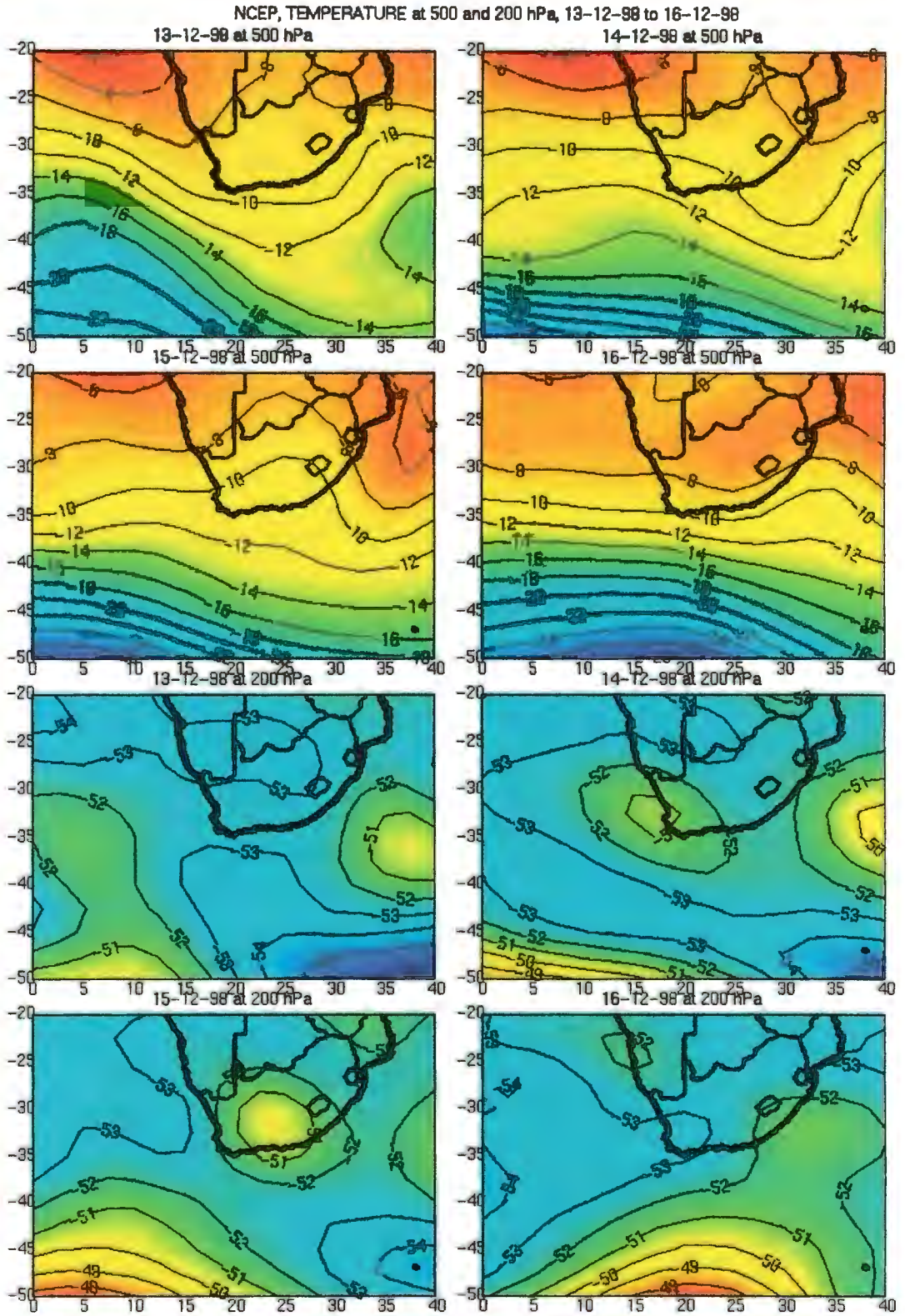
NCEP, TEMPERATURE at 500 and 200 hPa, 13-12-98 to 16-12-98
13-12-98 at 500 hPa
14-12-98 at 500 hPa
15-12-98 at 500 hPa
16-12-98 at 500 hPa
13-12-98 at 200 hPa
14-12-98 at 200 hPa
15-12-98 at 200 hPa
16-12-98 at 200 hPa

NCEP geopotential height data at the 1000, 850, 500 and 200 hPa level shows a weak westerly trough tracking above the surface heat low (Figure 5.8a-b). The heat low moved approximately 5 degrees east between 13 and 14 December with the westerly trough axis (at 500 hPa) displaced west of the heat low during the 14 and 15 December. Divergence occurs along the descending branch of a trough line owing to changes in radius

(a)

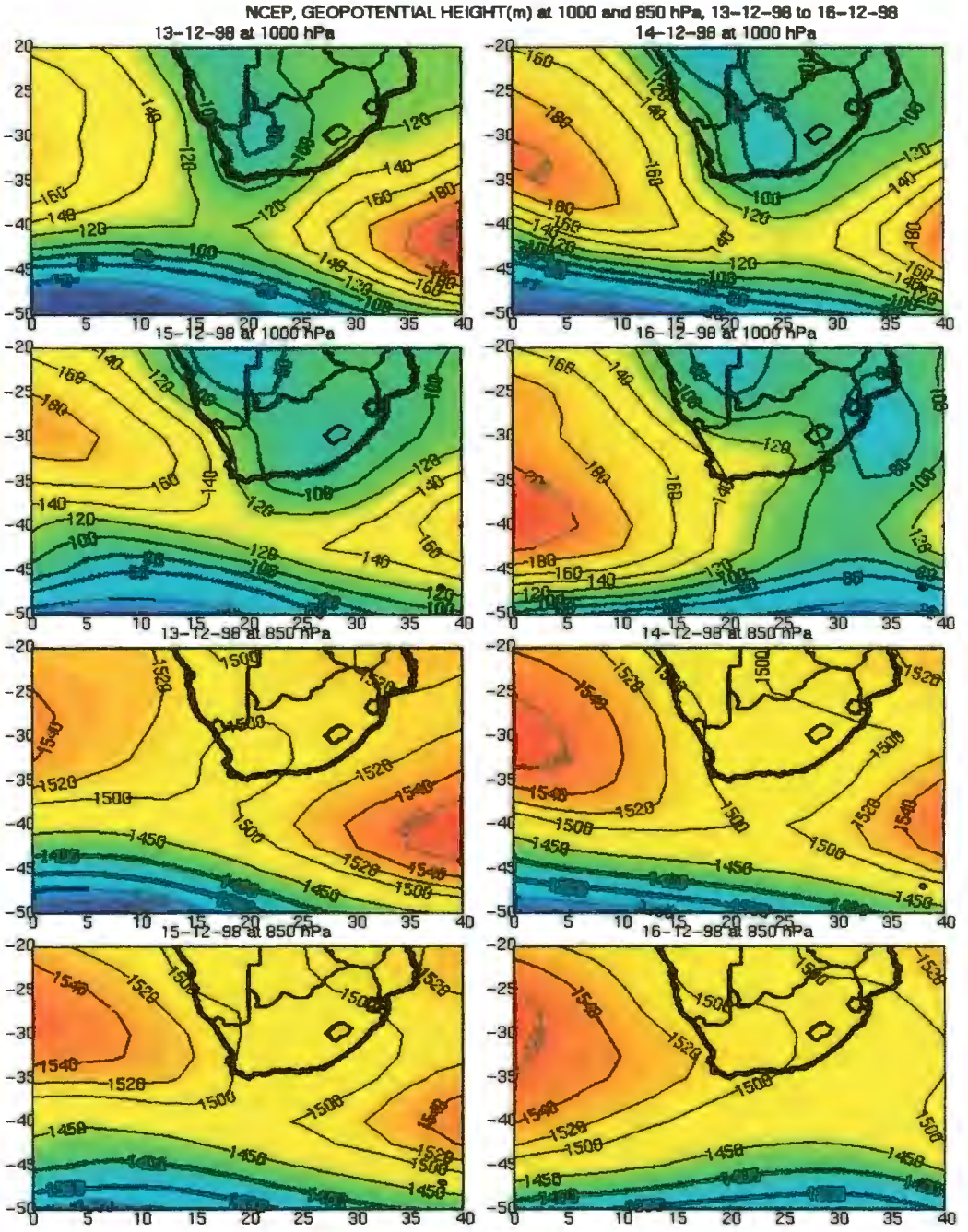


**Figure 5.8.** NCEP daily geopotential height (m) values for (a) 1000-850 hPa and (b) 500-200 hPa levels from 13 until 16 December 1998.

(b)

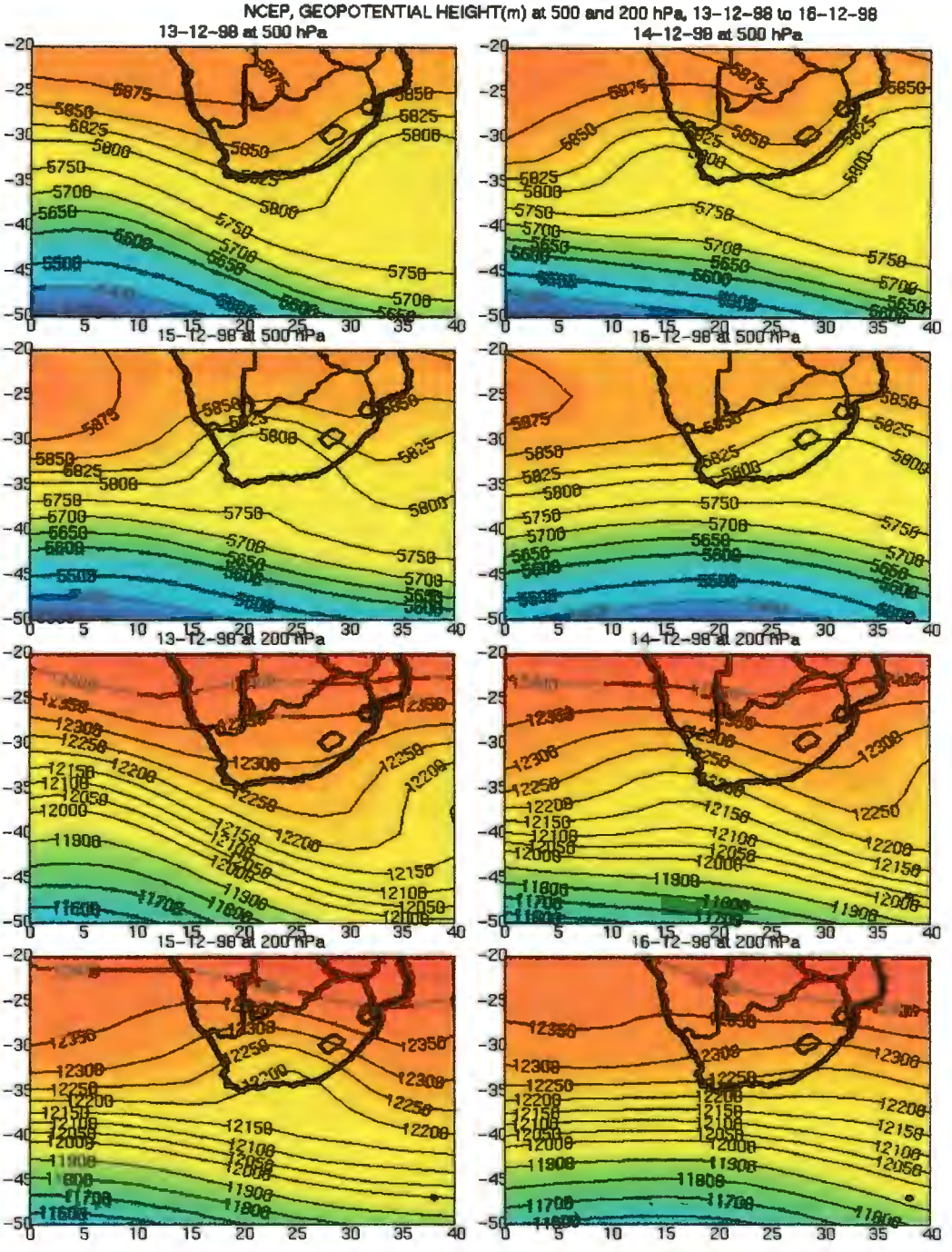


of curvature in Rossby waves. This divergence along the descending branch at 500 hPa corresponds to the low geopotential height values at 1000 hPa, which are indicative of surface convergence.

(a)

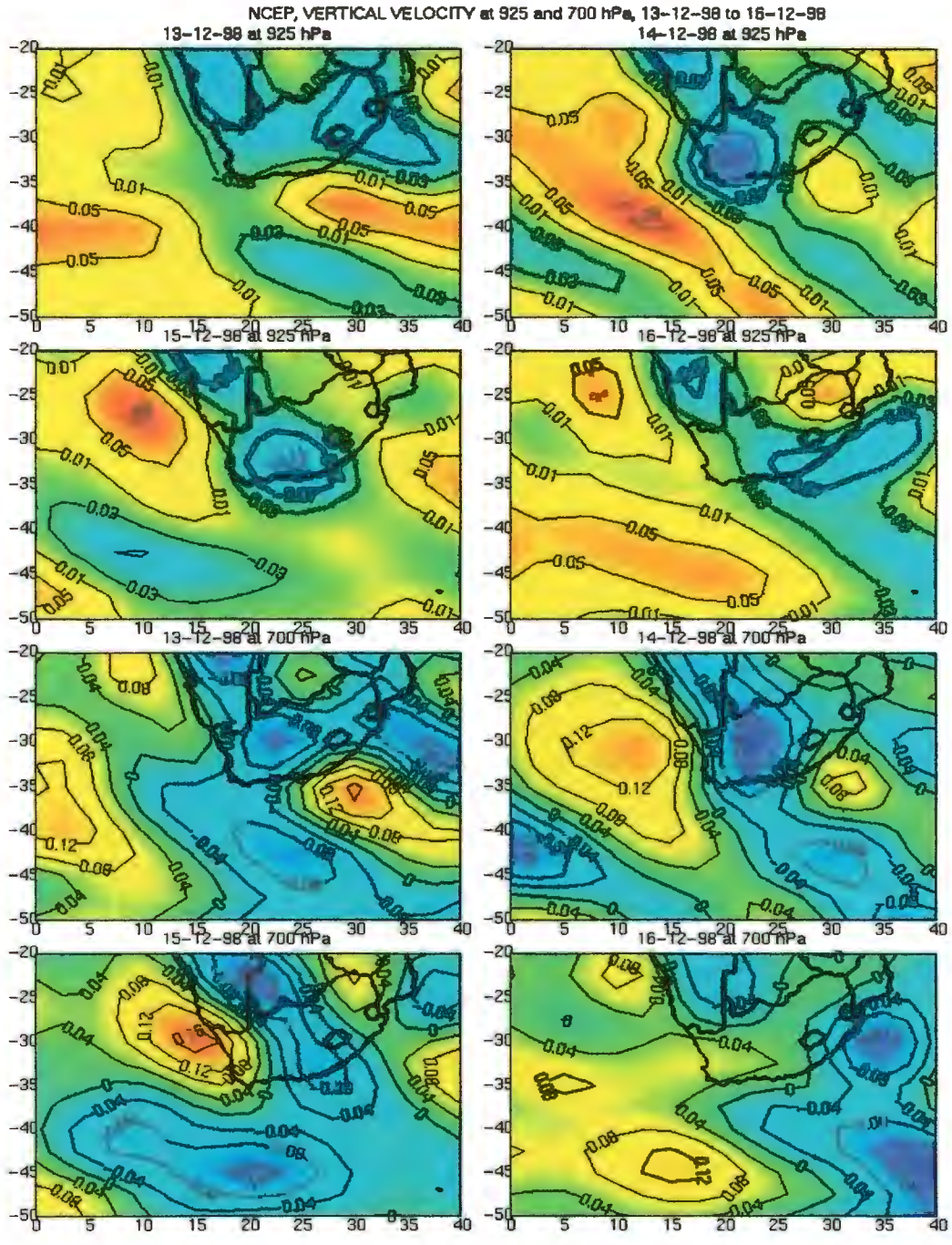


**Figure 5.9.** NCEP daily vertical velocity values (hPa/s) for (a) 925-700 hPa and (b) 500-200 hPa levels from 13 until 16 December 1998.

(b)

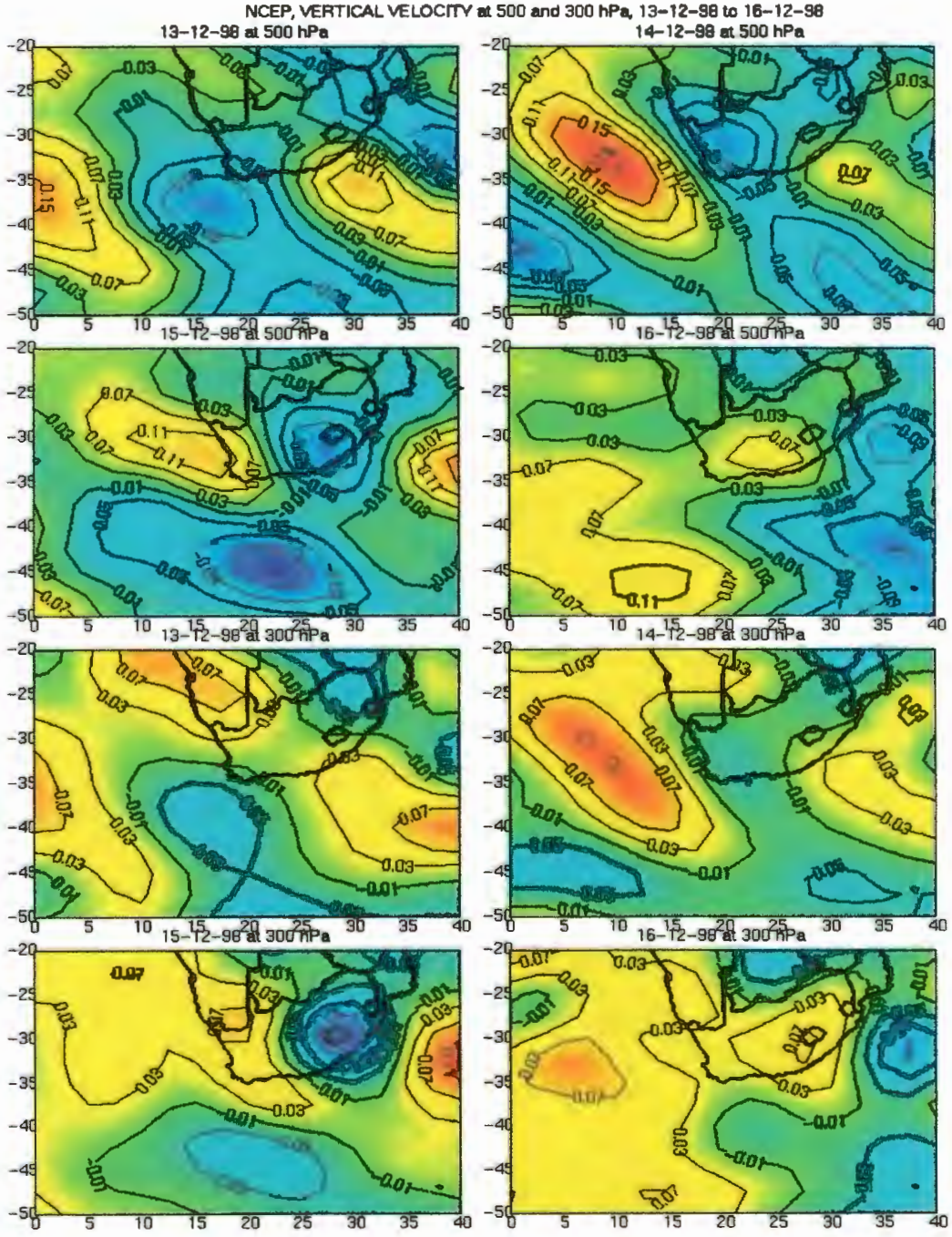


Vertical velocity (NCEP) values at 925 hPa show a closed pattern of strong ascent developed over western South Africa on 14 December which then tracked east on 15 December as the storm evolved (Figure 5.9a). A maximum vertical velocity of 0.11 Pa/s was reached on both days in the same region as the geopotential height trough axis (Figure 5.8b). Distinct ascending and descending limbs are present at all levels, reflecting

the subsidence in the South Indian Ocean and South Atlantic anticyclones and the uplift in between them which is associated with the trough. It is interesting to note that the greatest vertical velocity (0.13 Pa/s) was reached at great vertical extent (the 300 hPa level) on 15 December, which is consistent with deep convection and the satellite image from that day (Figure 5.9b and Figure 5.6). An important feature can be seen on 15 December

(a)

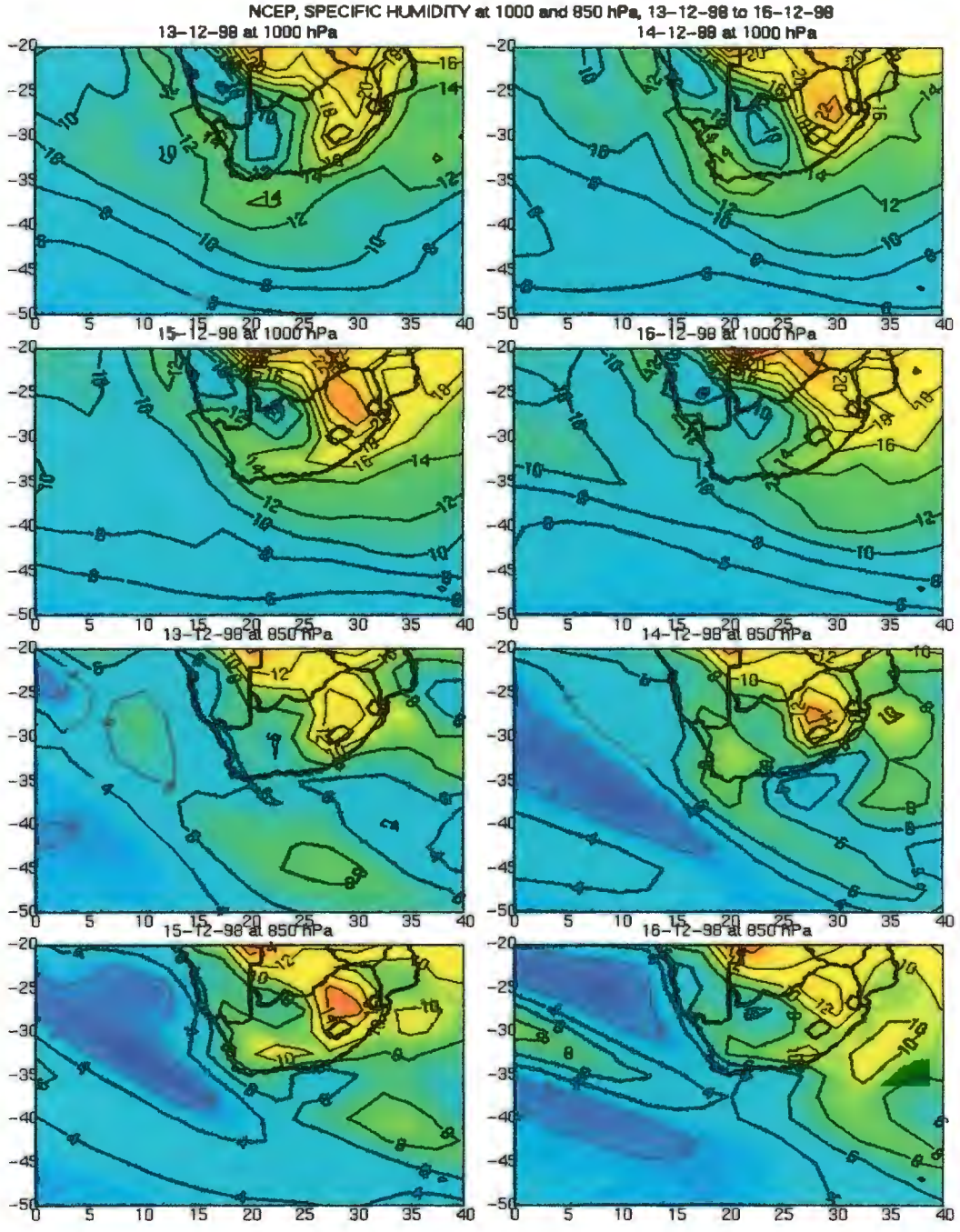


**Figure 5.10.** NCEP daily specific humidity (g/kg) values for (a) 1000-850 hPa and (b) 700-500 hPa levels

(b)

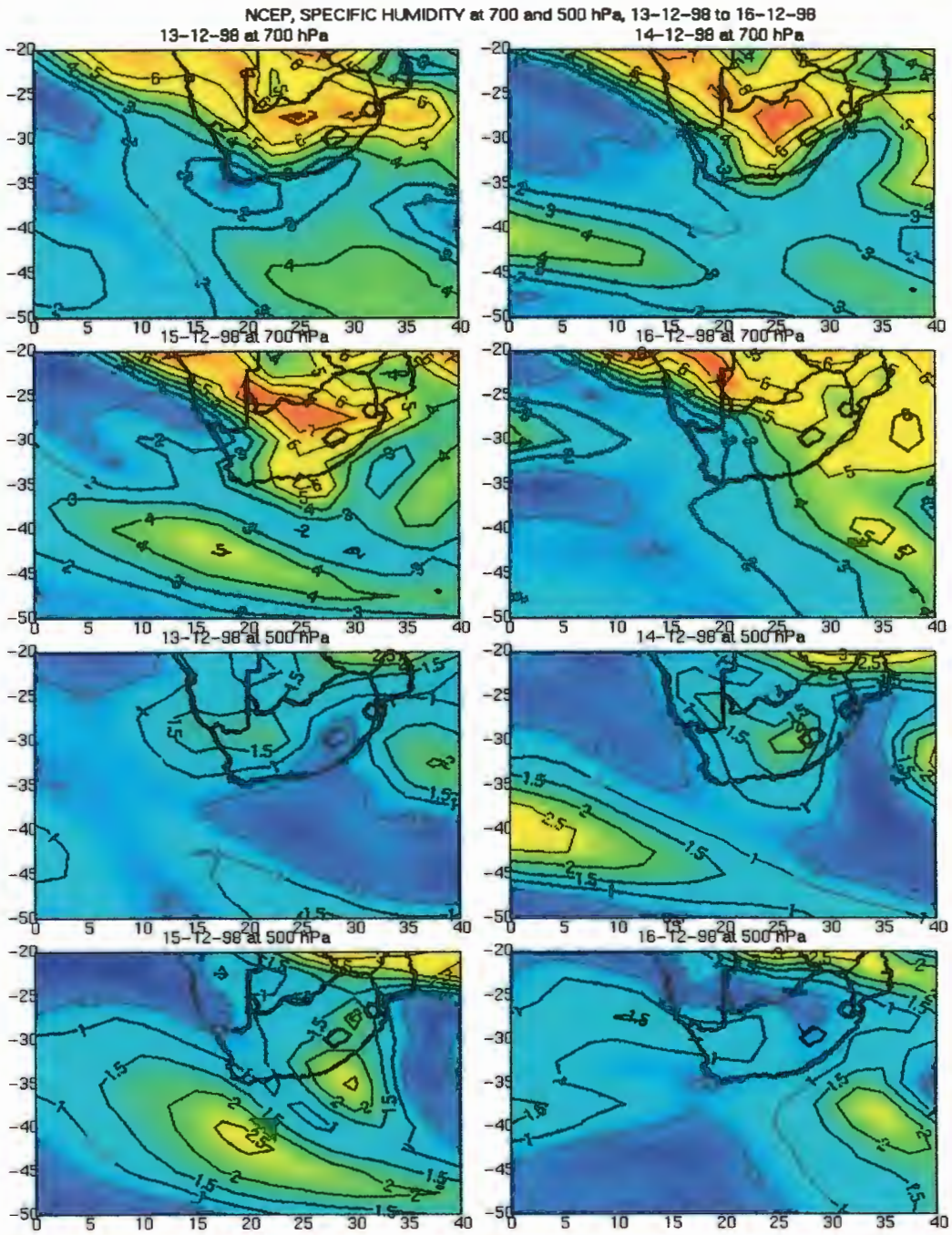


from 13 until 16 December 1998. at the 300 hPa level as an area of intense vertical motion over the Eastern Cape province and KwaZulu-Natal province (Figure 5.9b). The upward motion aloft may be attributed to the deepening of the storm on 15 (Figure 5.6e-g). This deepening may have resulted in a significant latent heat release due to rainfall in the

atmosphere and corresponds well with the warm core observed at 200 hPa in the temperature diagram of Figure 5.7b.

The specific humidity at 1000 hPa (Figure 5.10a) shows more moisture available in the Northern Province region associated with the southern extent of the Intertropical Convergence Zone (ITCZ) than above the Agulhas Current. Values from 12 to 14 g/kg occurred above the Agulhas Current while in the Northern Province they ranged from 14 to 22 g/kg. At 850 hPa moisture was slightly less but was still dominated by the same regions. On 15 December at 700 hPa the tropical moisture was clearly the most significant source in the atmosphere (Figure 5.10b). At 500 hPa the only significant moisture in the atmosphere seems to be linked to the position of the trough indicating that rainfall may have occurred at this level related to the storm. There was significant moisture to the south of the country which was most likely related to the weak cold front undercutting warm air as it approached the subcontinent on 13 and passed to the south on 14 December (Figure 5.5a-d).

Only considering the specific humidity diagrams, it appears that tropical moisture was the major contributor to this storm. However, the moisture flux diagram Figure 5.11a at the 1000 hPa level shows 140 g·m/kg·s of moisture advected into the storm region on 13 and 14 December (the moisture flux calculation neglects the effects of density changes with moisture since the specific humidity rather than the relative humidity has been used to calculate the flux). This moisture was most likely advected from above the Agulhas Current by the easterly to northerly winds, which compose the trailing edge of the anticyclone located in the South-west Indian Ocean (Figure 5.5a-b). It appears in Figure 5.11a that little tropical moisture was advected towards the storm region. The winds in the

tropical regions of greatest specific humidity were weak and not consistently in the same direction over a large fetch area as those in the South-west Indian Ocean. At 850 hPa, there was still anticyclonic motion over the South-west Indian Ocean but the moisture at that level was less than at the surface so it does not appear to be contributing as much

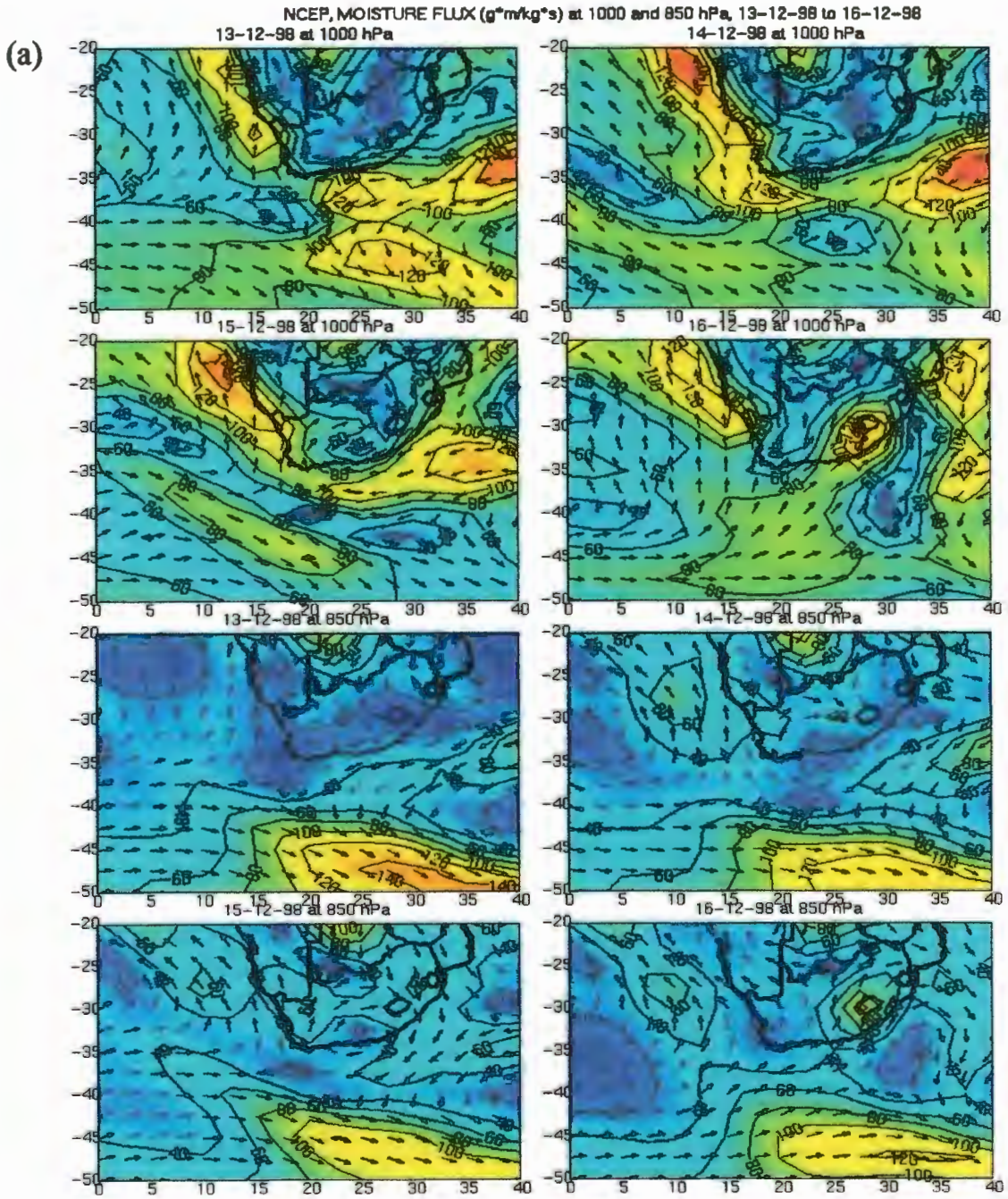


**Figure 5.11.** NCEP daily moisture flux (g·m/kg·s) values for (a) 1000-850 hPa and (b) 700-500 hPa levels from 13 until 16 December 1998.

(b)

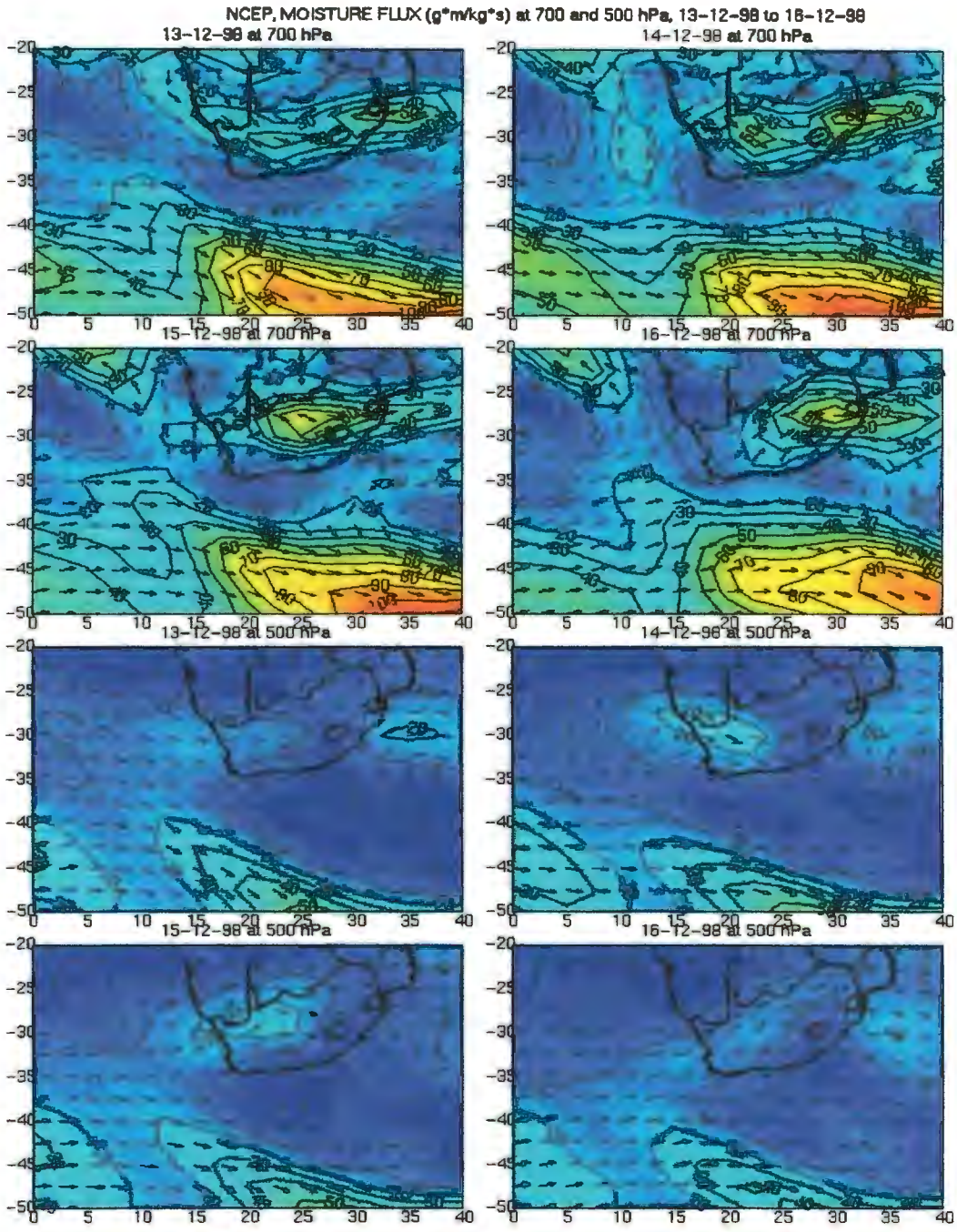


moisture to the storm. The tropics contributed little moisture at 850 hPa as well, most likely because of the light and variable wind at this level. Looking at the 700 hPa level (Figure 5.11b) it appears that moisture was advected from the tropics into the storm region but its magnitude (50 g·m/kg·s) was less than that originating at the surface from the Agulhas Current region (140 g·m/kg·s). At 500 hPa, there was negligible moisture available and the winds reflect a westerly wave motion associated with the passage of the midlevel trough mentioned in Figure 5.8b.

Vertical cross sections of the moisture flux across longitude 25° E on 13 December (Figure 5.12a) show 80 g·m/kg·s of moisture above the Agulhas Current advecting into the storm region from the east to west up to approximately 875 hPa. There was a significant eastward flux at 700 hPa from 30° S up to 25° S, which corresponds to Figure 5.11b and is most likely of tropical origin. North of 25° S, the moisture was

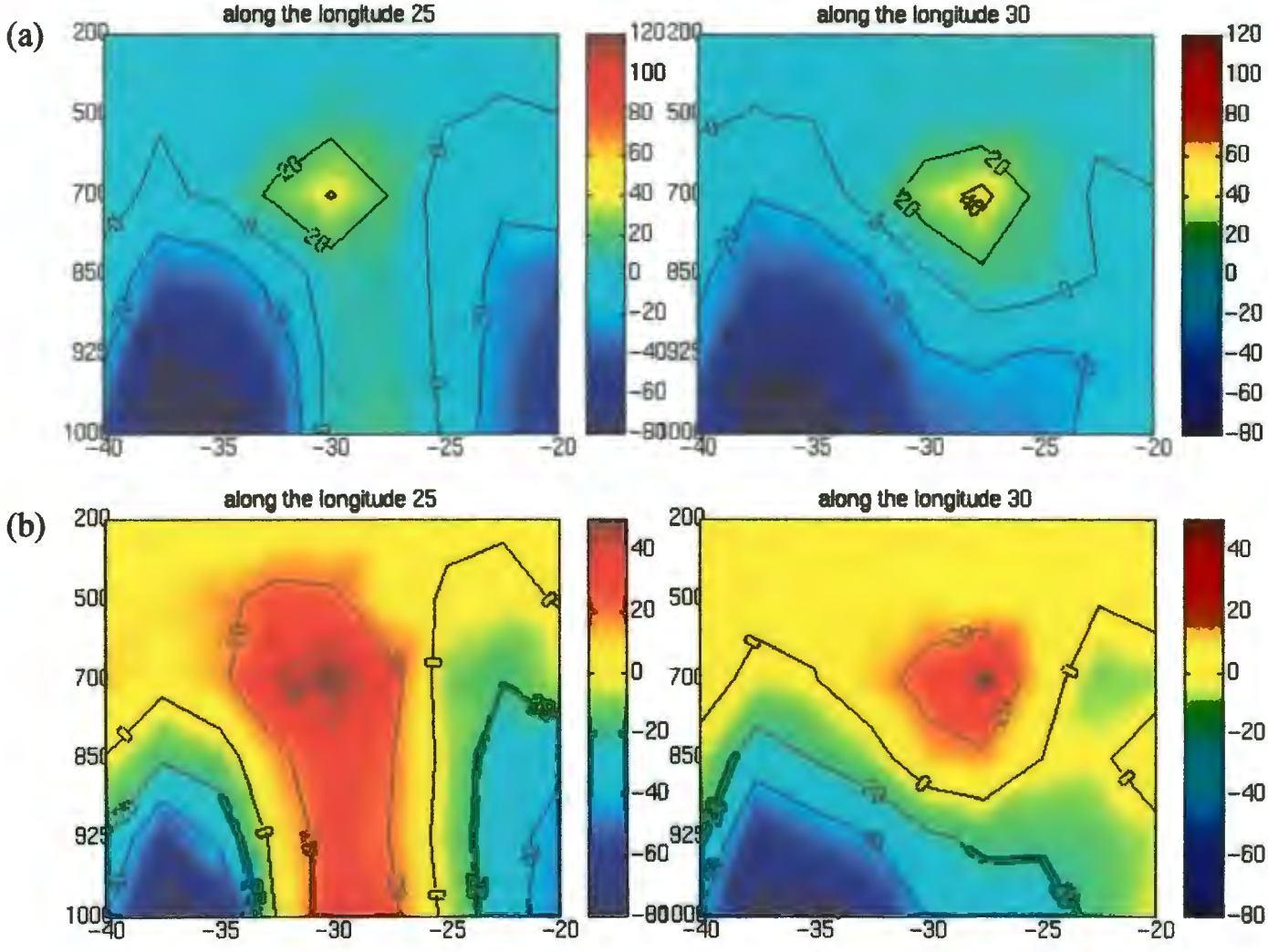


**Figure 5.12.** NCEP daily moisture flux (g·m/kg·s) values for longitudinal profiles (a) on 13 December, (b) on 14 December, (c) on 15 December and (d) on 16 December 1998 (eastward fluxes are positive values; westward fluxes are negative values).

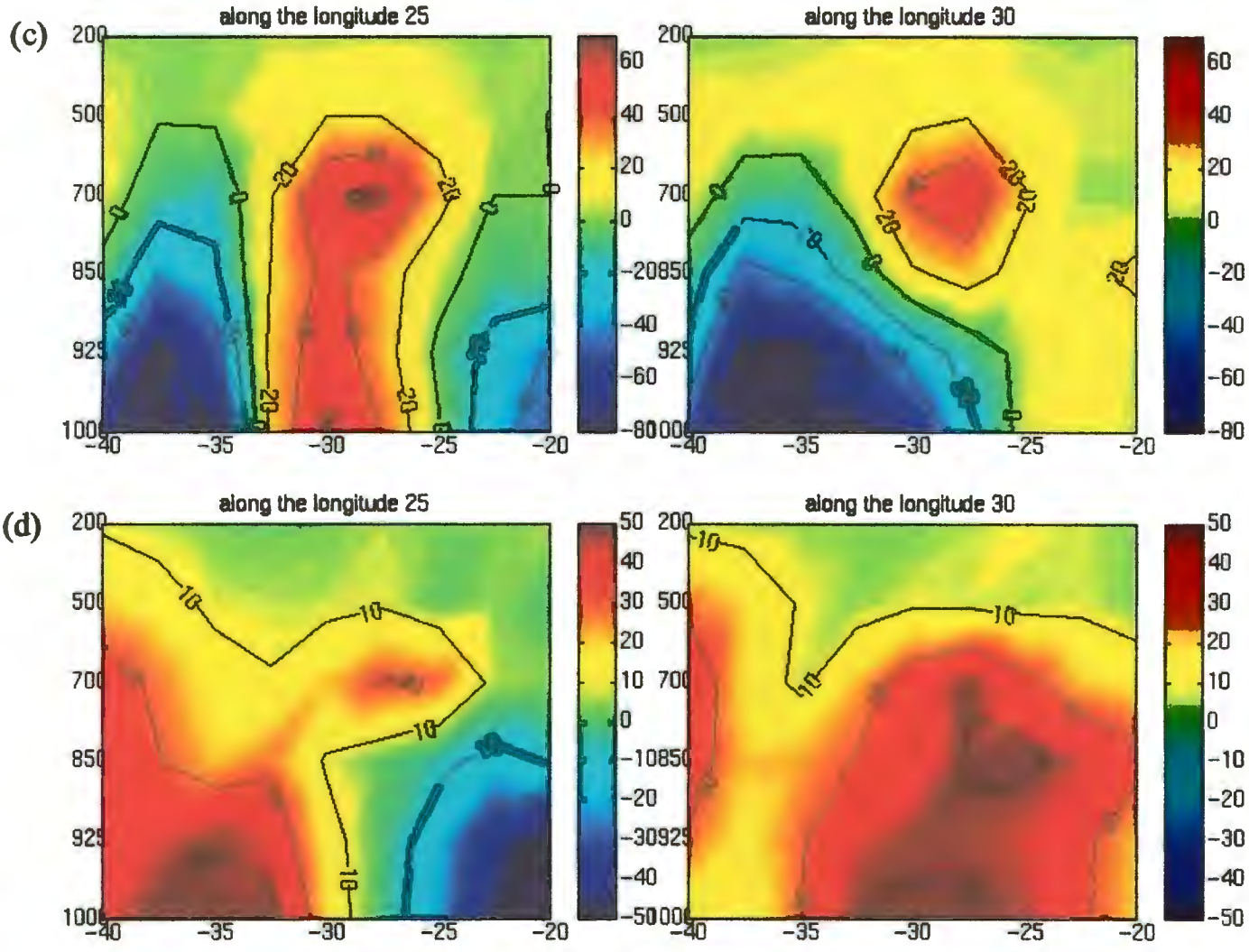


advected by the prevailing low latitude easterlies. It is interesting to compare the cross section at 25° E with that at 30° E. At 30° E the fetch above Agulhas Current water below the subcontinent is greater than at 25° E. Along the 30° E cross section, Agulhas Current water and Agulhas Return Current water can extend from 31° S to 40° S (Figure 1.1 and Figure 5.12a). It is along this section that there was significant westward moisture originating from the greater Agulhas Current system.

On December 14 (Figure 5.12b), the Agulhas Current region's input was twice that which came in at lower latitudes. From the cross section at 30° E, low level moisture appears to underlie moisture aloft that was advected in the opposite direction. The 850 to

700 hPa level seems to be dominated by eastward propagating moisture over the northern reaches of South Africa. However, the region of greatest moisture flux (80 g·m/kg·s) was westward into the storm center at the surface level, directly above Agulhas Current water.

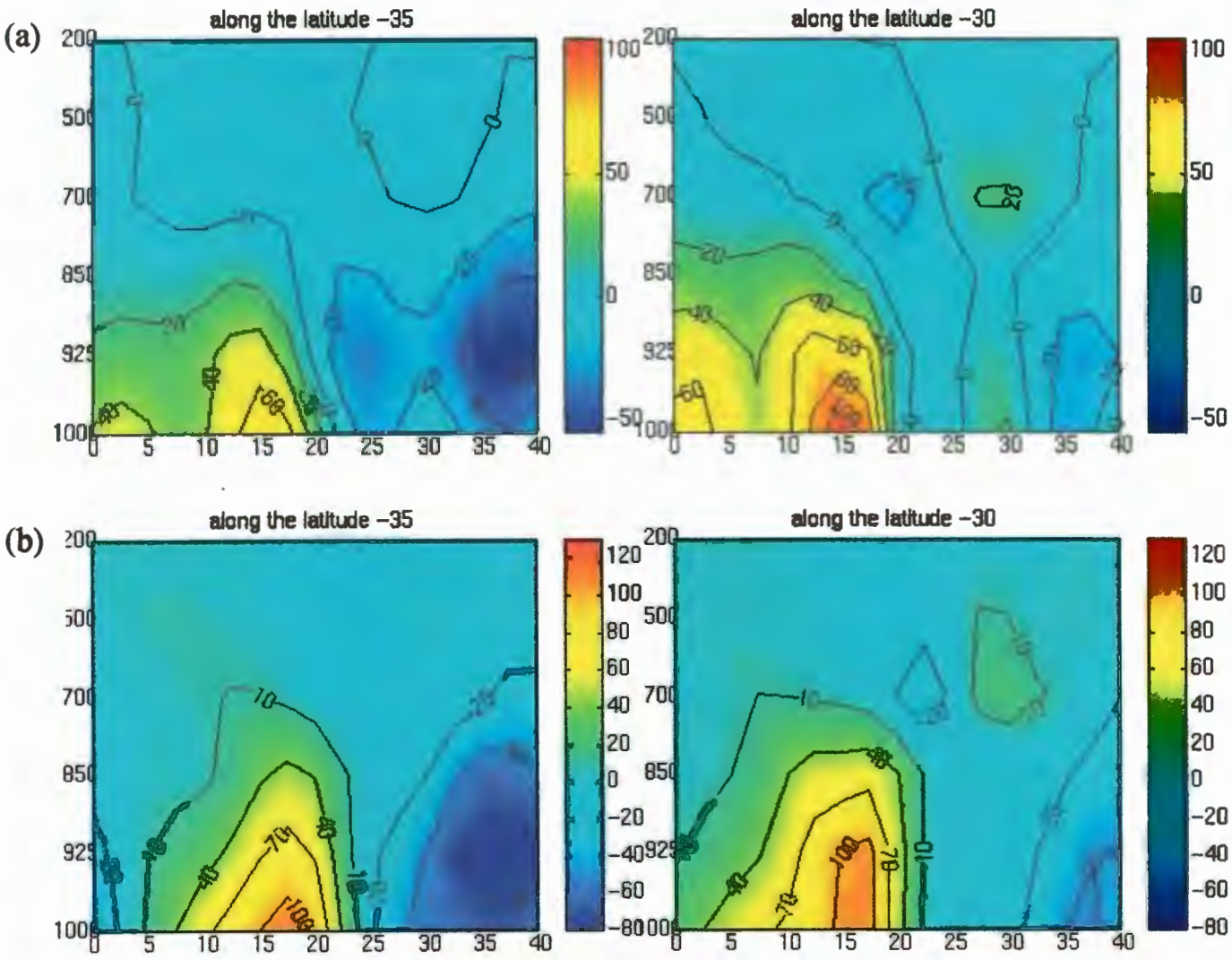


**Figure 5.13.** NCEP daily moisture flux (g·m/kg·s) values for latitudinal profiles (a) on 13 December, (b) on 14 December, (c) on 15 December and (d) on 16 December 1998 (northward fluxes are positive values; southward fluxes are negative values).

c)

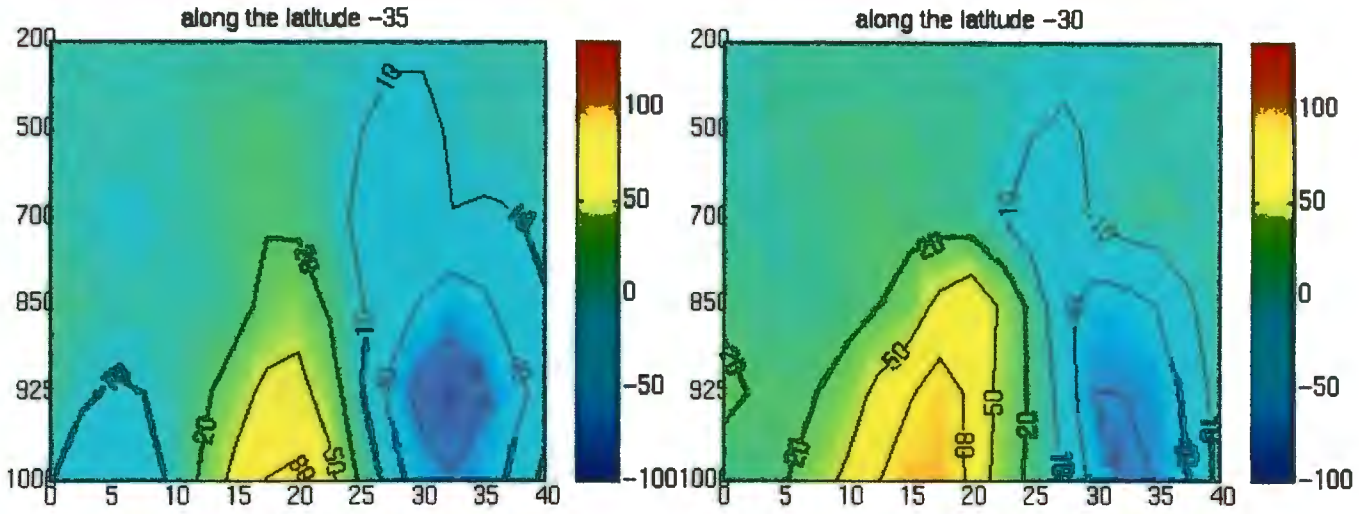


d)

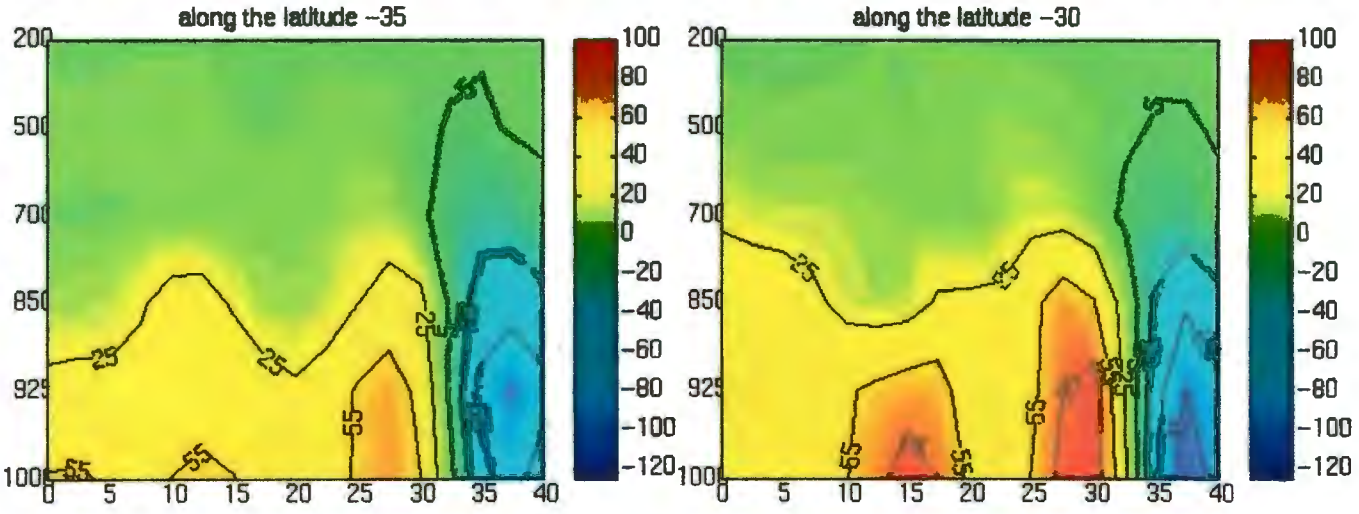


On 15 December (Figure 5.12c), there was again a westward flux of moisture from the Agulhas Current region toward the subcontinent. By contrast, the moisture flux over the Agulhas Current was eastward on 16 December (Figure 5.12d). The synoptic charts (Figure 5.5a-d) show that the winds veered from the east to the south-west on this day. This corresponds well with the NCEP geopotential height at 1000 hPa (Figure 5.8a), which shows that on 16 December the storm dissipated over land and moved offshore over the Indian Ocean.

Latitudinal cross sections on 13 December at 35° S and 30° S show that centered at 15° E a moisture flux from 60 to 100 g·m/kg·s moved north and was mostly confined to

the surface layers (Figure 5.13a). East of 20° E, the pattern reverses and the moisture moved south from both the northern extent of Agulhas Current water and the north-east eastern coastal regions of South Africa and Mozambique. It is difficult to distinguish whether this southward moving moisture came more from the tropics or from above Agulhas Current water. From this data it is impossible to distinguish the relative input of each individual source. The pattern remains the same on 14 December (Figure 5.13b) and 15 December (Figure 5.13c), however the boundary between the northward and southward moisture flux shifted from 20° E on 13 to 25° E on 15 December. Since this boundary shift represents a substantial increase of about 500 km in the fetch of the winds above the Agulhas Current, it suggests that on 15 December the Agulhas Current moisture that was advected from the south played a larger role than on the previous days (Figure 5.13c). On 16 December the wind shifted from east to south-west (Figure 5.11a) at the surface and the low pressure cell over land moved eastward over the ocean (Figure 8a), which can be seen in the latitudinal profile as a eastward shift to 30° E in northward moving moisture (Figure 5.13d).

The latitudinal and longitudinal cross sections discussed above, show horizontal shear present in the north-south and east-west directions. Horizontal shear in the atmosphere increases the vertical vorticity of the system and thus enhances upward motion. These cross sections also show the presence of vertical shear. This change in direction of the moisture flux with height in the atmosphere increases the horizontal vorticity which is also favorable for atmospheric instability. As a result, it is not just the flux of moisture from the Agulhas Current and tropical sources that contributes to the storm development but also the horizontal and vertical shear in these fluxes that is significant.

So far only the synoptic scale features have been discussed. Remembering the key questions, it is clear that further data are required to answer them. NCEP specific humidity data (Figure 5.10a-b) show that more moisture was available to this storm from the tropical regions than from above the Agulhas Current. Moisture flux diagrams (Figure 5.11a-b) show that the most significant moisture advected into the storm region was at the surface from above Agulhas Current. At the 700 hPa level less significant amounts of moisture was advected towards the storm from the north. There were large amounts of tropical moisture available at 700 hPa (Figure 5.10b), however the relatively weak winds were unable to advect much of it into the storm region. To examine the tropical and Agulhas Current moisture sources in greater detail, backward air parcel trajectories are considered.

Trajectory Analysis

At the 900 hPa level, a 3 day backward air parcel trajectory ending at Tygerhoek(34° 9' S, 19° 5' E) on 14 December, shows a pathway of air over the Agulhas Current prior to the flooding there (Figure 5.14a). This trajectory through moist air at 900 hPa (or within the marine boundary layer) further suggests that the major moisture source at the surface was the Agulhas Current system. At the 700 hPa level, the air parcels do not come from the north as expected by looking at Figure 5.11b. This suggests that the moisture available from the north at this level never reached the storm. At the 500 hPa level, the trajectory shows that air was derived from the north-west of the country, suggesting that it may be part of the descending branch of the westerly trough seen in Figure 5.8b. The air at 200 hPa is also part of the westerly wave which is evidence of the

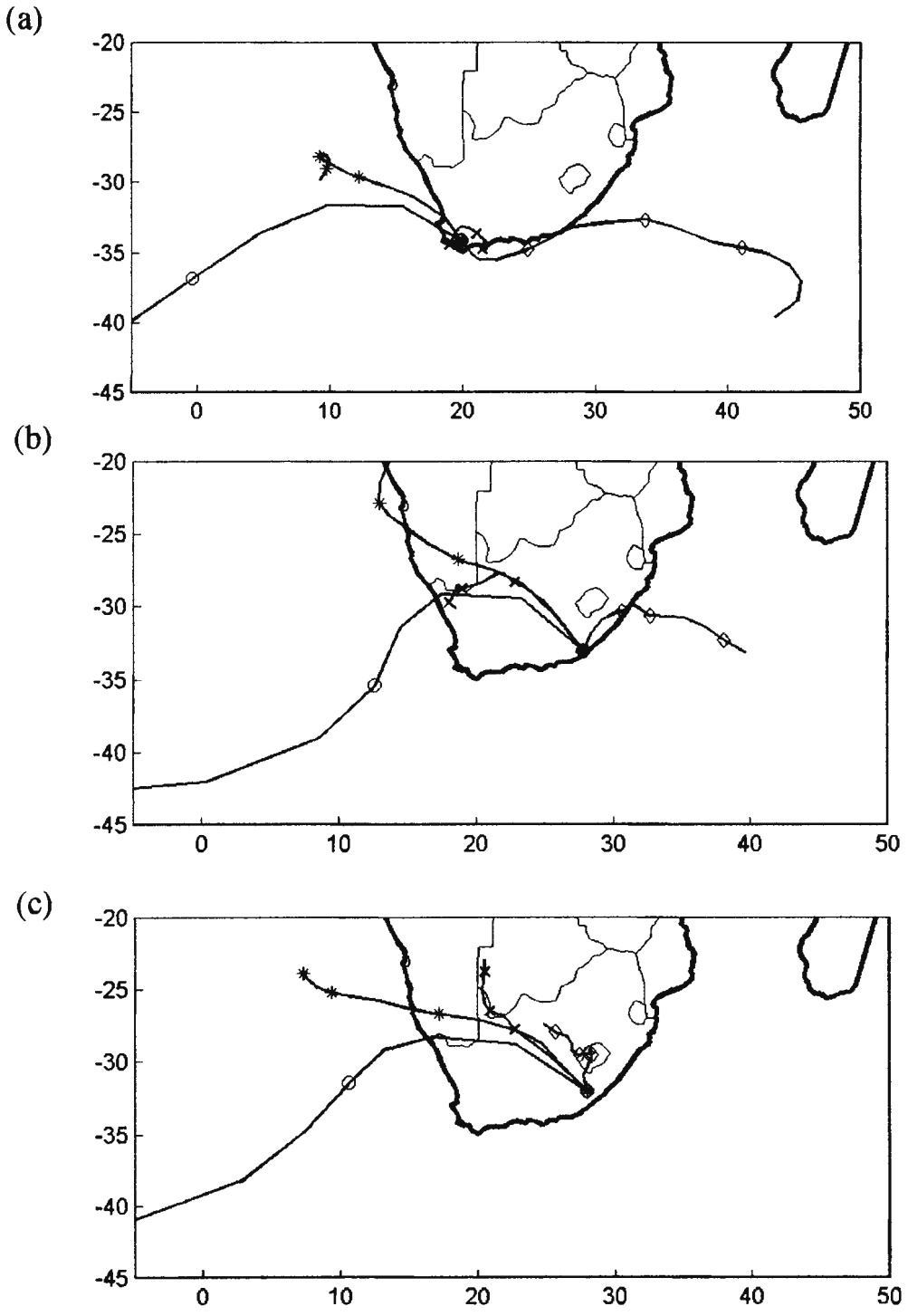


**Figure 5.14.** BADC backward trajectories for air parcels at the (a) 900 hPa (◊), 700 hPa (+), 500 hPa (*) and 200 hPa (o) 3 days prior to 14 December at 12:00 UTC and originating from the Tygerhoek flood location, (b) 900 hPa (◊), 700 hPa (+), 500 hPa (*)and 200 hPa (o) 3 days prior to 15 December at 12 UTC originating from the East London heavy rainfall location, and (c) 850 hPa (◊), 700 hPa (+), 500 hPa (*) and 200 hPa (o) 3 days prior to 15 December at 12:00 UTC originating midpoint between the tornado locations.

cold dry air advection aloft. These trajectories therefore suggest that air parcels over the storm region traveled through a warm, moist surface layer at 900 hPa with an influx of cold dry air between the 500 and 200 hPa level. Figure 5.14b shows backward air parcel trajectories for 15 December for the heavy rainfall location of East London (33° S, 27° 5' E). At the 850 hPa level, the air parcel pathway passes above the northern branch of Agulhas Current. Trajectories at the 500 hPa and 200 hPa levels show a similar pattern to Figure 5.14a for Tygerhoek and reflect the westerly trough motion.

Backward air parcel trajectories at 850 and 700 hPa for a location centered midway between the two tornadoes (32° S, 28° E) on 15 December, shows the air to be originating from the north (Figure 5.14c). Note that the terrain at this location lies just below the 850 hPa level. Figure 5.14c suggests that the air arriving at the storm was coming from the north to north-west at midlevels, consistent with Figure 5.14b. The trajectories at 500 and 200 hPa show a similar pattern to that in Figure 5.14a, again reflecting the approaching westerly trough. Similar to the trajectories for the other locations and consistent with the moisture flux diagrams (Figure 5.11, 5.12 and 5.13), the basic situation is one favorable to instability and convection, namely, warm moist air near the surface with cold dry air aloft.

Regional Features

*a. Radiosonde*

Radiosonde stations are geographically sparse in South Africa and none exist close to the tornado locations at Hogsback or Umtata. The most relevant station for the

current purpose is the coastal station of Durban which lies about 250 km north-east of Umtata. The Convective Available Potential Energy (CAPE) values at this station were assessed to give further insight into the relative susceptibility of the atmosphere to deep convection. The maximum CAPE of 2800 J occurred on 15 December at Durban as revealed by the 12:00 UTC sounding (Figure 5.15). For this time, the satellite imagery (Figure 5.6f) shows a squall line passing through the Durban region. This CAPE value of 2841 J was due to the relatively humid air in the 1000-900 hPa interval and the subsequent drop in the environmental temperature from 800 hPa and above. The temperature remained high up to 700 hPa and dropped rapidly above this level. The presence of a low level warm, moist layer overlain by a cold, dry layer of air is a profile highly conducive to instability and is consistent with the air parcel trajectory for East London (Figure 5.14b).

Since radiosonde data in South Africa is sparse, only a rough picture of the evolving atmospheric conditions can be derived. Tornadoes require at least 2000 J of CAPE. Thus, the CAPE at Durban (2841 J) was sufficient for tornado formation. Rasmussen et al. [2000] have shown that at baroclinic boundaries, the occurrence of significant tornado formation (e.g. F2 or stronger on the Fujita Scale) almost always occurs on the cool moist side (Figure 2.2) of a boundary. This research has furthermore shown that storms that remained on the warm side of the boundary, despite substantial CAPE, did not produce tornadoes. It is evident from the SAWB MSL charts that a baroclinic boundary existed between the coastal and inland stations (Figure 5.5c) close to the tornado event. The inland stations were warm and dry at the surface whereas the coastal stations were relatively cool and moist.

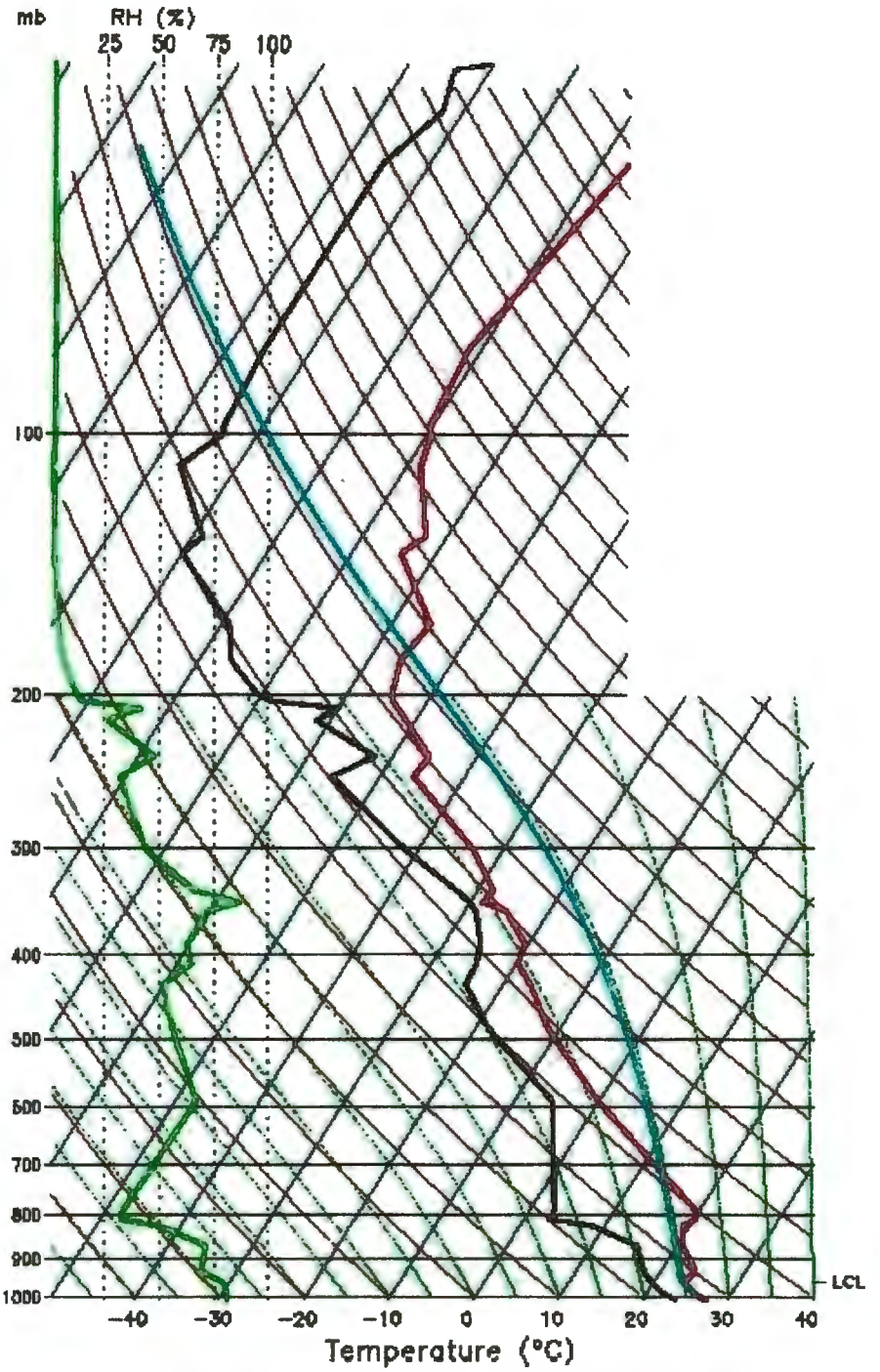


**Figure 5.15.** Stability profiles constructed from radiosonde data provided by the South African Weather Bureau. Temperature lines are blue, dry adiabat lines are red, moist adiabat lines are green, the parcel trace is cyan, the temperature sounding line is magenta, the dewpoint sounding is black and the relative humidity sounding is the thicker green line. The lifting condensation level is indicated as LCL in the bottom right hand corner.

It has been shown using radiosonde data that sufficient CAPE was available near the tornado event (Figure 5.15). The SAWB has classified the tornado event as F2 [Van Niekerk and Sampson 1999] on the Fujita Scale [Fujita 1973]. A baroclinic boundary existed on 15 December and can be seen in Figure 5.5c. The weather station data from the MSL charts shows a difference in temperature of up to 7° C across the boundary. The moisture difference across the boundary was significant, ranging from dewpoint temperature 22° C on the coast (cool moist region) to 18° C across the boundary on the hot moist side and then dropping to 8° C in the country's interior (warm dry region).

For conditions like those shown in Figure 5.5c, the wind profiles at the surface were modified by the presence of the boundary so as to maximize the cyclonic vertical vorticity within a narrow zone between the hot moist region and the cool moist region. Using the equation 1.4:

$$\zeta = \frac{\partial v}{\partial x}$$

The vertical vorticity was calculated using SAWB wind data as $7.0 \times 10^{-5}$ $s^{-1}$. This value would be of the same order of magnitude as for a tornado event studied by Rasmussen et al. [2000] ($9.5 \times 10^{-4}$ $s^{-1}$) had the data points in this study (100 km) been the same as Rasumussen's (10 km). This back of the envelope calculation demonstrates that baroclinic boundaries can enhance the vertical vorticity and suggests that the tornado event in this study may have been enhanced by such a boundary.

*b. TRMM analysis*

TRMM rain rate and latent heat data from above the Agulhas Current may yield more insight into the role the regional environment above the Agulhas Current played in the synoptic event CASE DECEMBER. The most intense surface rainfall events available

from TRMM's passes over the Agulhas Current during CASE DECEMBER were selected, and the atmospheric profiles of rain rate and latent heat release above these events were analyzed. Three TRMM passes above the Agulhas Current on 15 December provide useful data for this study (Figure 5.16). The combined PR and TMI product consistently estimated a surface rain rate greater than the TMI derived surface rain rate. These discrepancies are expected and commented on in Chapter 4.

TRMM derived SSTs give the weekly mean of SSTs surrounding the days of CASE DECEMBER (Figure 5.2). The maximum surface rain rates occurred in all four orbit passes between 25° - 26° E and 34° - 36° S. This corresponds geographically to SSTs ranging from 22° - 23° C. It is important to note that the maximum rain rates at the surface occurred in line with the tongue of warm Agulhas Current water. Comparing surface rain rate plots and Figure 5.2 shows that the events do not extend into the cooler water south of the tongue which suggests that these intense regional rain events may be directly related to the high SSTs of the Agulhas Current. At 08:49 until 08:53 UTC, TRMM passed above the Agulhas Current and provided the only imagery of heavy rainfall available from both the PR and TMI swaths for CASE DECEMBER. This event was approximately 45,000 $km^2$ with a maximum surface rain rate of 28 mm/h according to TMI and 94 mm/h according to combined TMI/PR (Figure 5.16). At 50 km increments across the heavy rainfall event, longitudinal cross sections (as in Figure 5.17) of the vertical rain rate were analyzed. Rainfall was found at a maximum vertical height of 9000 m (Figure 5.18). The bulk of precipitation in the atmosphere ranged from 1000 to 4000 m. Most of the rain in the atmosphere occurred between 34.6° and 35° S which corresponds well with the high SST region in Figure 5.2.

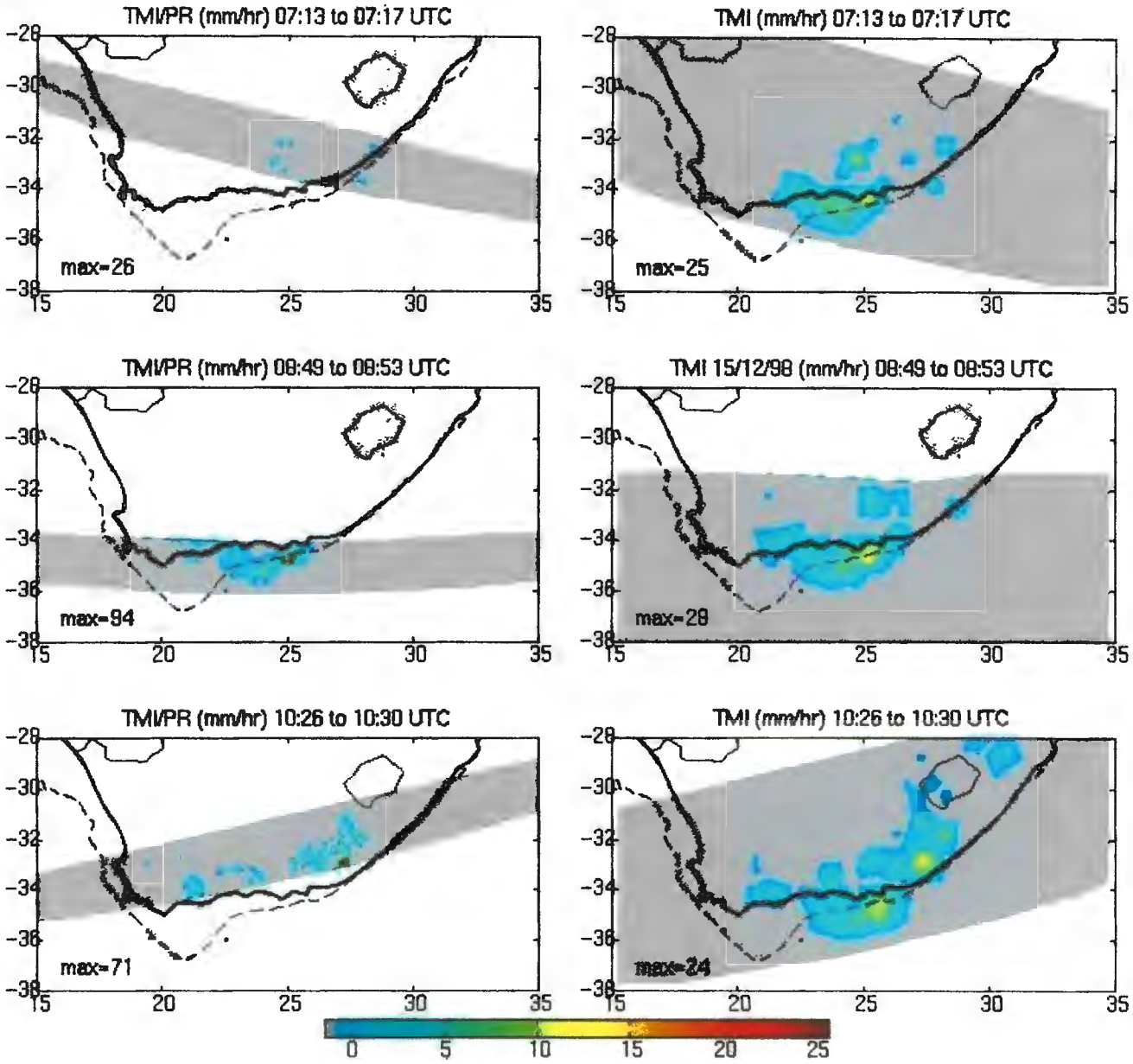


**FIG. 5.16.** TRMM-derived surface rain rates on 15 December 1998 for three consecutive orbit passes from TMI on the right side and from TMI/PR on the left side (mm/h).

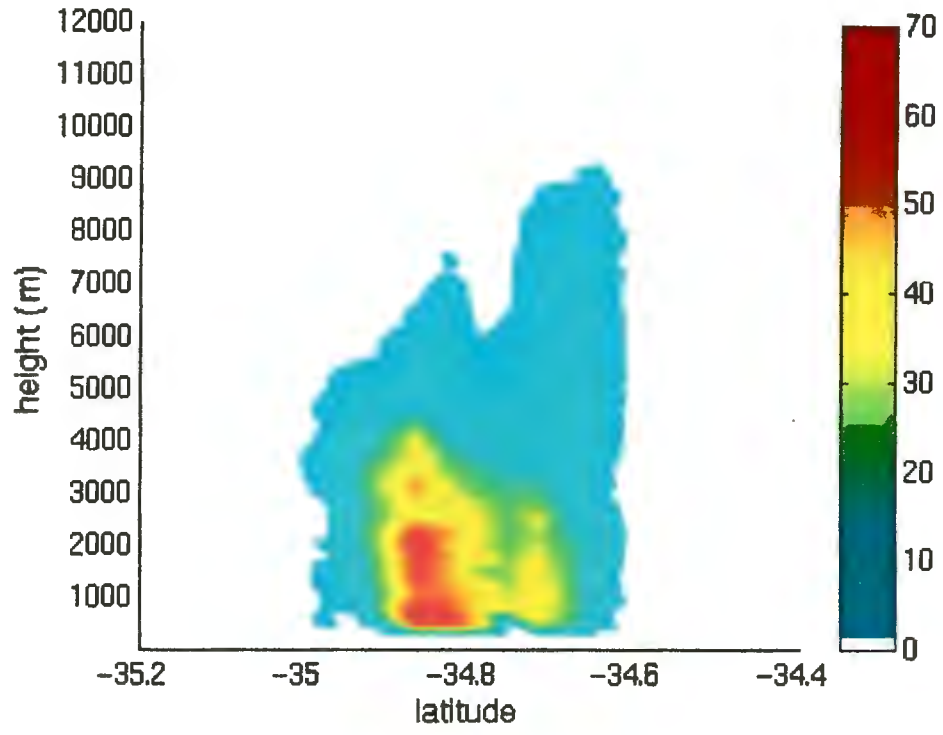


**Figure 5.18.** A vertical profile of the rain rate in the atmosphere derived from PR measurements in mm/h corresponding to the cross section B—A given in Figure 5.17 from left to right respectively.

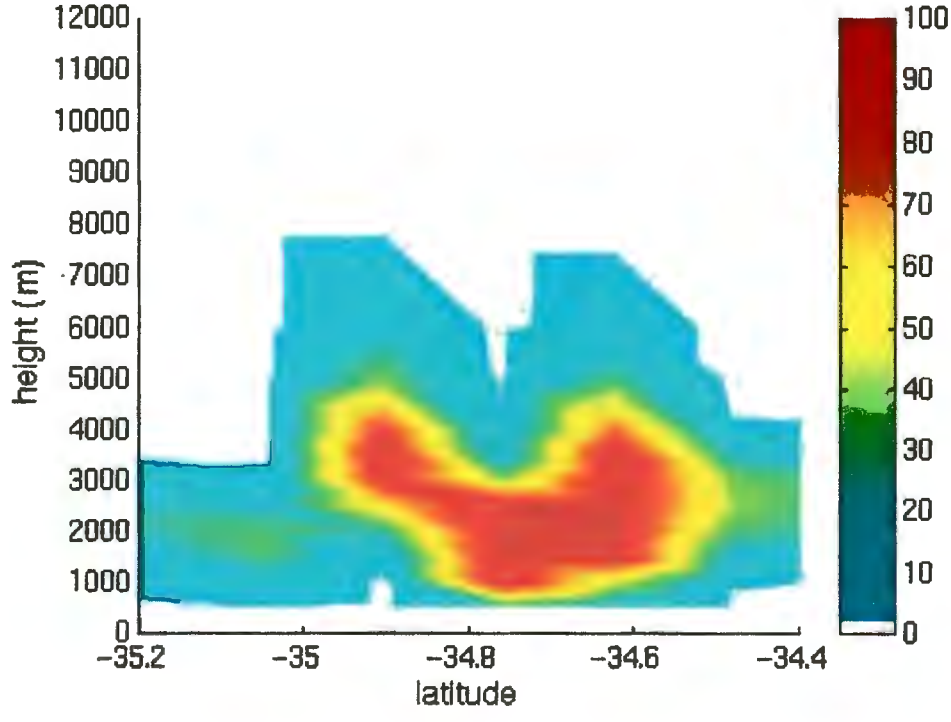


**Figure 5.19.** A vertical profile of the latent heat in the atmosphere derived from TMI measurements in °C/day corresponding to the cross section B—A given in Figure 5.17 from left to right respectively.

an area which corresponds to the same area in which rain was falling in the atmosphere according to TMI data (Figure 5.17). This supports the concept that the latent heat was released during the condensation process and existed at high levels in the atmosphere.

Vertical profiles at longitudinal increments of 50 km were analyzed for all the TRMM passes in Figure 5.16. Convective rainfall remained centered between 1000 and 4000 m in the atmosphere. A corresponding latent heat release ranging from 50° to 150° C/day also remained centered at this height. Latent heat released directly above the Agulhas Current seems to correspond well with convective rain rates at the surface and in the atmosphere. The surface air parcel trajectory (Figures 5.14a), shows the pathway of air over the Agulhas Current through the location where the heavy rainfall events (Figure 5.16) occurred. The surface air parcel trajectory in Figure 5.14a did not pass through the specific rainfall events shown in Figure 5.16 because these events happened on 15 December. However it seems possible that air parcels entrained in the South-west Indian Ocean anticyclone may advect latent heat in the atmosphere above the Agulhas Current over land. Since the current is close to shore and has been shown to influence the weather over the eastern coastal regions in the past [Jury et al. 1993], it seems reasonable to suggest that the latent heat released in the atmosphere above the current may enhance the synoptic situation over the eastern coastal regions.

*CASE NOVEMBER*

During November 1998, a heavy rainfall event occurred over the Western and Eastern Cape on 19 November followed by heavy rains above the KwaZulu-Natal Province on 20 November. The storm over land was accompanied by heavy rainfall over

the Agulhas Current. From a survey of TRMM rainfall images during the 1998/99 summer season, this event was identified as an intense heavy rainfall event over both the coastal regions and the Agulhas Current, second only to CASE DECEMBER. By conducting a compare-contrast exercise between the two events, more insight into the different moisture sources for the two events as well as the interaction between the environment above the Agulhas Current and the synoptic event is sought.

CASE NOVEMBER seemed to be less severe than CASE DECEMBER as the heavy rainfall did not result in flooding and there were no recorded tornado occurrences. A maximum daily rainfall of 59 mm on 19 November was recorded in Swellendam (34° 2' S, 20° 27' E) (Figure 5.20a). Swellendam is most commonly a winter rainfall region. Thus, CASE NOVEMBER resulted in 43 percent of the month's total rainfall. On 20

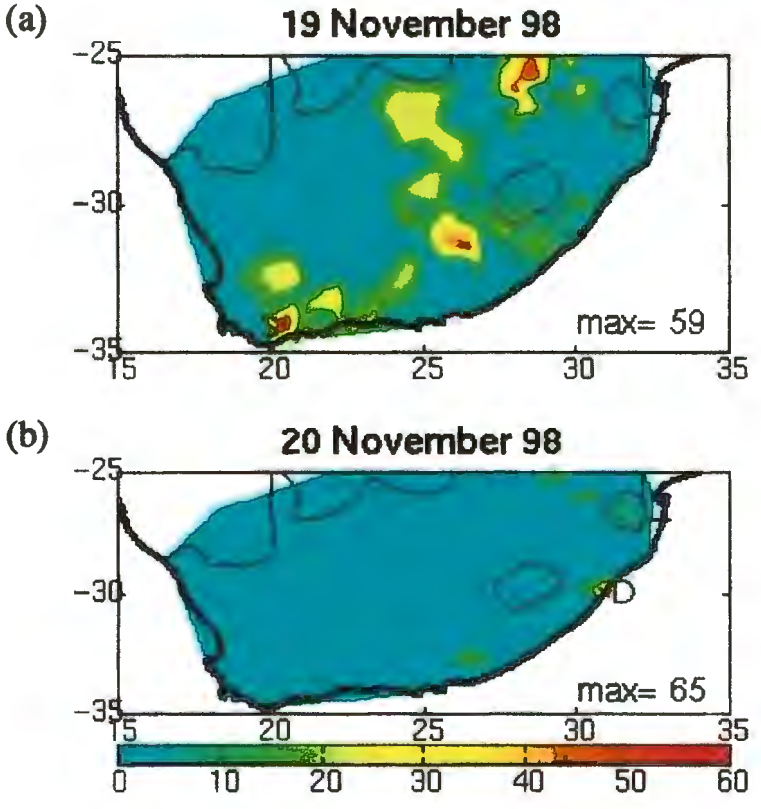


**Figure 5.20.** (a). SAWB rainfall for 19 November from 100 stations. Heavy rainfall occurred over Swellendam (S). (b). SAWB rainfall for 20 November. Heavy rainfall occurred over Durban (D). The color bar is the daily total in mm/day and the maximum daily rainfall (max) at the heavy rainfall locations

is given in the bottom right hand corner.

November, Durban (29° 58' S, 30° 57' E) received 62 percent of the month's total rainfall (Figure 5.20b). November marks the beginning of South Africa's summer rainfall season of which Durban is a part. Since Durban received over half of the months total rainfall on this day means this storm contributed a large part to an already rainy month.

It is interesting to note that the composite of SST anomalies for the week surrounding this event (Figure 5.21) shows warming to the south-west of the continent while in the Greater Agulhas Current system there is no anomaly. Comparing Figure 5.22 to Figure 5.2, a slightly broader tongue of 23° C water than in December can be seen. A

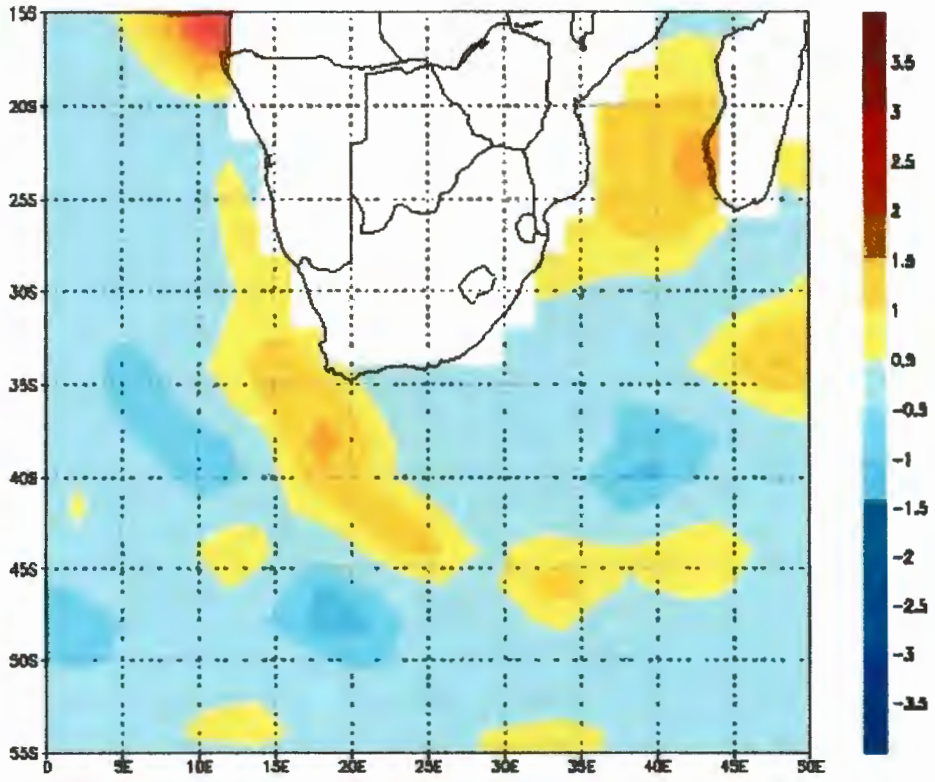


**Figure 5.21**. Optimal interpolation of sea surface temperature anomalies from for the South-west Indian Ocean and the South-east Atlantic Ocean for the period 15- 21 November 1998 (Reynolds and Smith 1994).

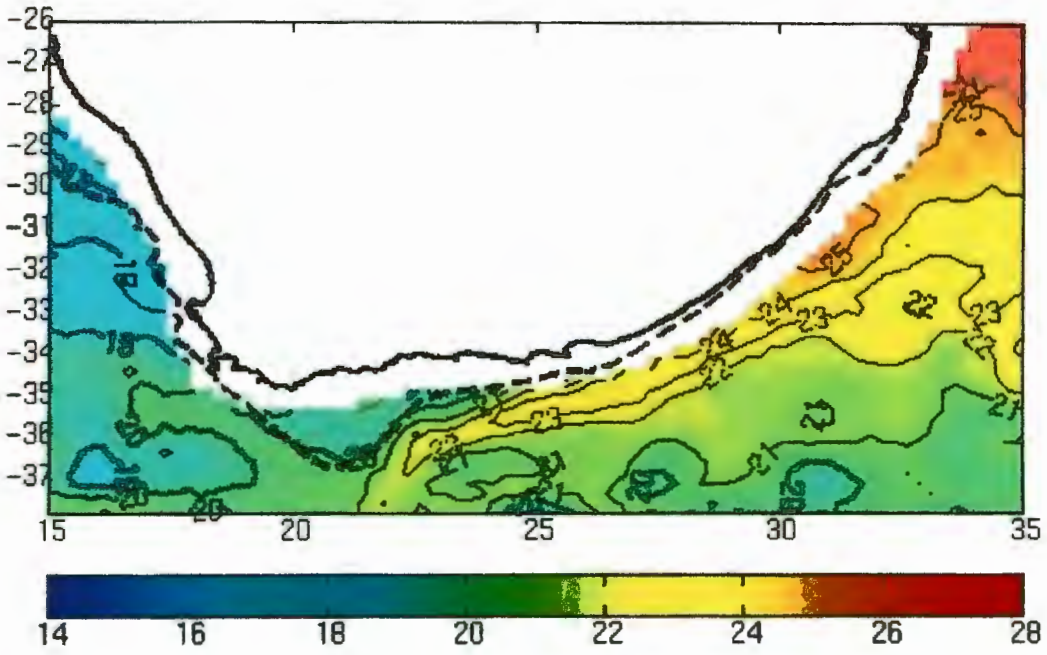


**Figure 5.22.** Weekly composite of SSTs in °C from 19 to 25 November 1998. These values were derived from TRMM Microwave Imager (TMI) on board the TRMM satellite.

similar temperature range between 21-26° C exists in Figure 5.22 but the southward extent of warm water is diminished. Even though the temperature anomalies are greater in Figure 5.1 (CASE DECEMBER) than in Figure 5.21 for CASE NOVEMBER, the actual Agulhas Current SST distribution looks very similar.

Synoptic Setting

The Mean Sea Level (MSL) synoptic chart on 17 November (Figure 5.23a) of November shows the presence of a cold front moving east over the country. This is also observable in the Meteosat imagery (Figure 5.24b-c) as a linear band of convective clouds associated with the frontal boundary extending in a north-south direction. High temperatures recorded at inland stations are indicative of a heat low (1008 hPa) centered over the western interior. Significant amounts of rainfall were recorded on 17 and 18 and were mostly centered over the interior regions. By 19 the front had passed and an

(a)

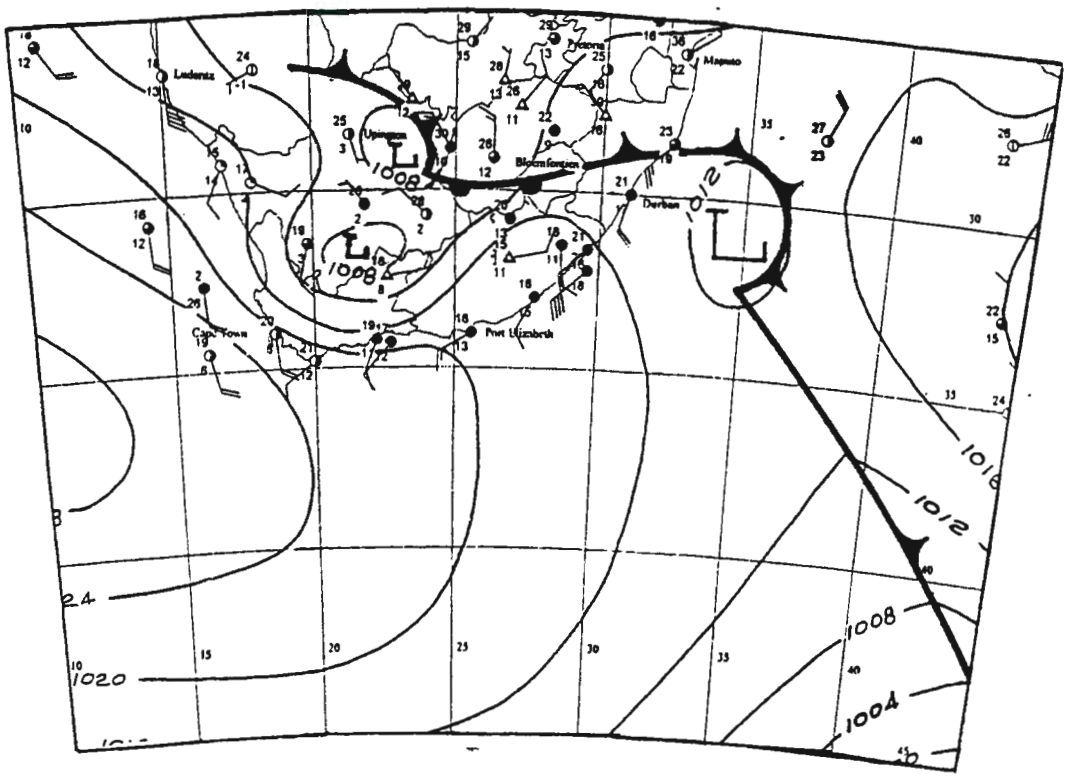


(b)

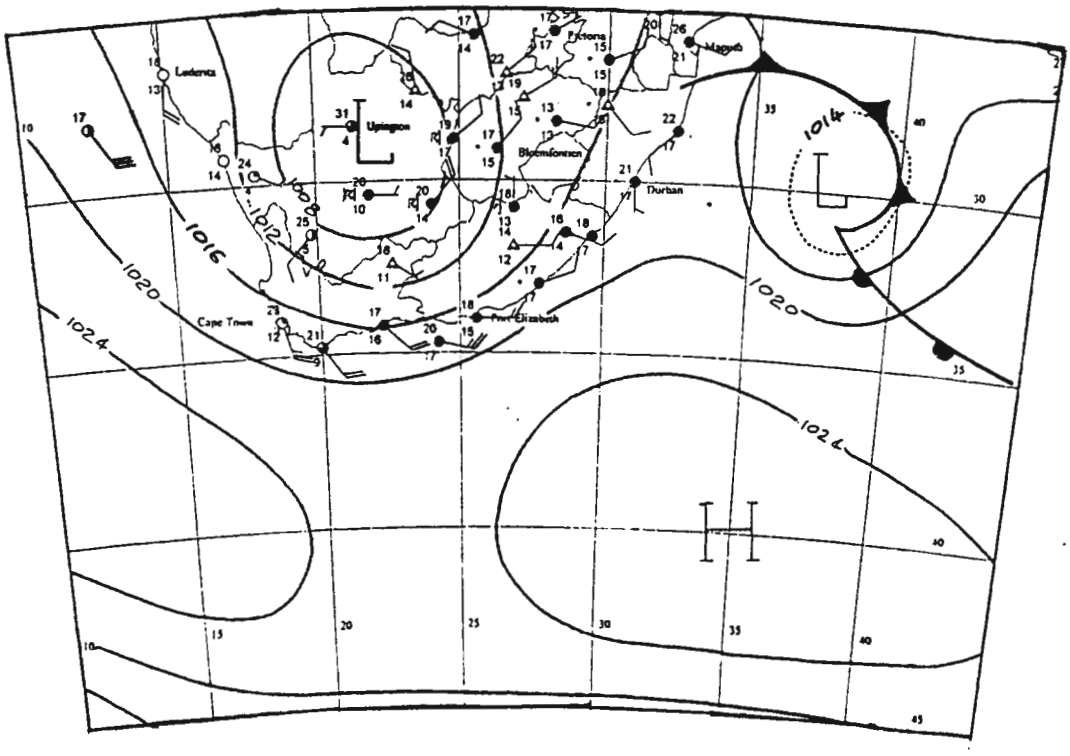


**Figure 5.23.** Synoptic chart of atmospheric pressure at mean sea level (a) for 17 November 1998, (b): for 18 November 1998, (c): for 19 November 1998, (d): for 20 November 1998, (e): for 21 November 1998 at 1400 SAST.

(c)

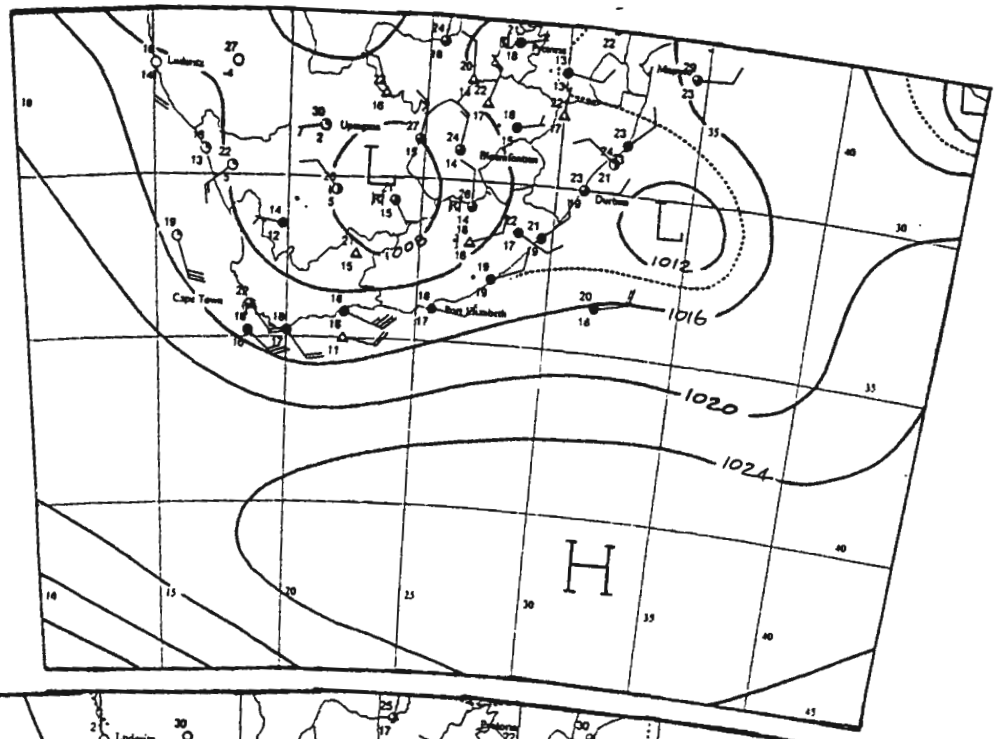
Upington
Durban
Cape Town
1012
1016
1020
1024
H

(d)

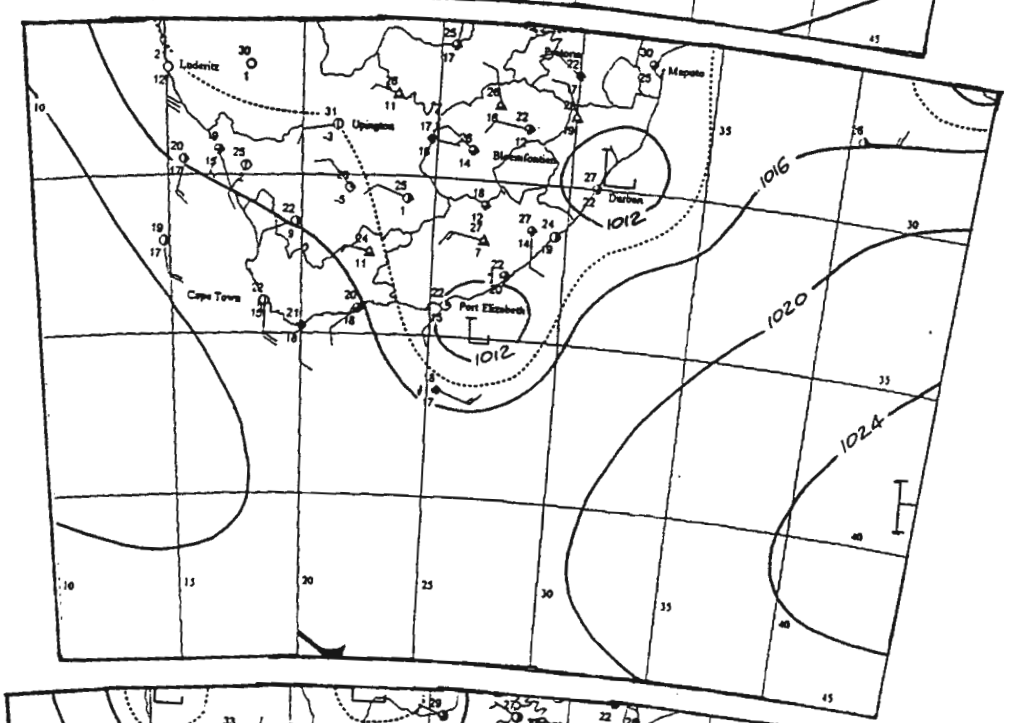
Upington
Durban
Cape Town
Port Elizabeth
1012
1016
1020
1024

(e)

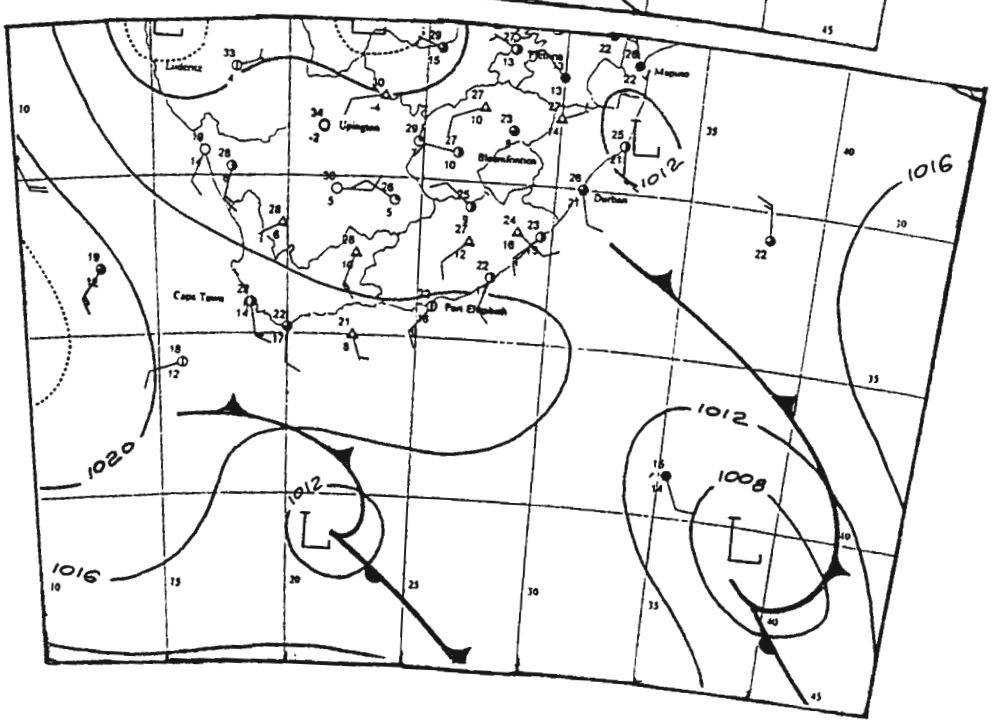
Upington
Durban
Cape Town
Port Elizabeth
1012
1016
1020
1008

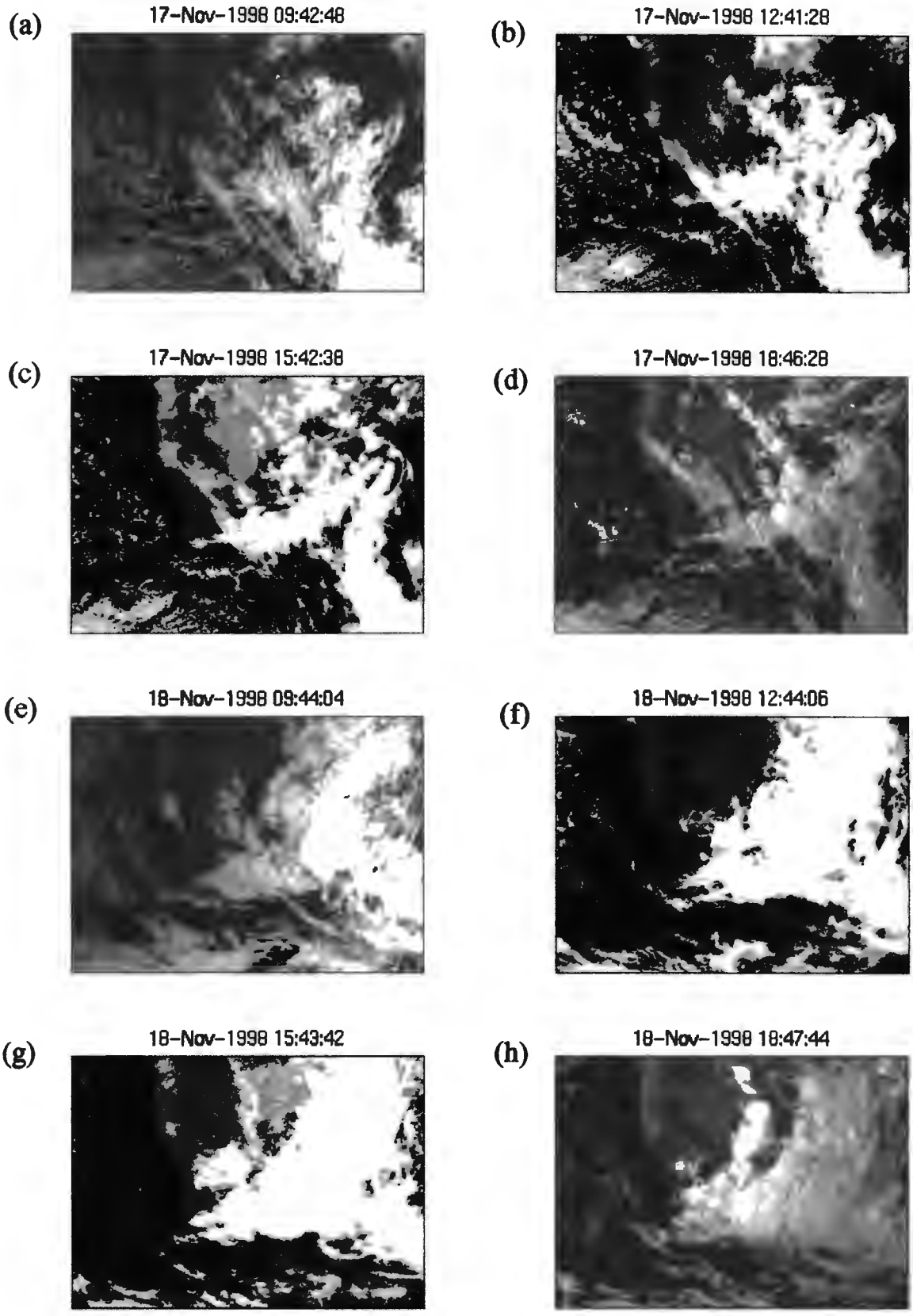


**Figure 5.24** Satellite images in the visible frequency band for southern Africa and adjoining ocean regions from 17- 18 (a-h) until 19-20 (I-p) November 1998 from METEOSAT. Clouds are in white.

(i)

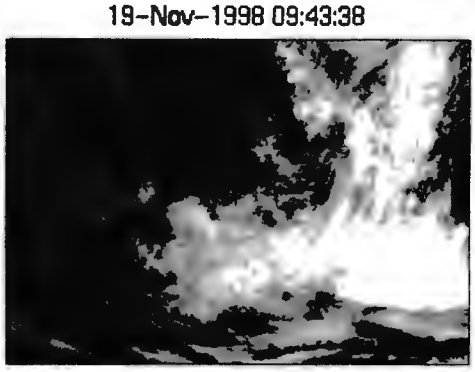


(j)

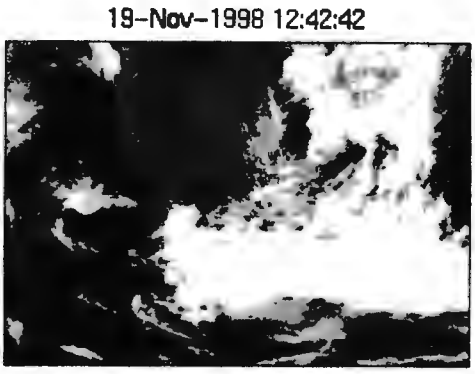


(k)

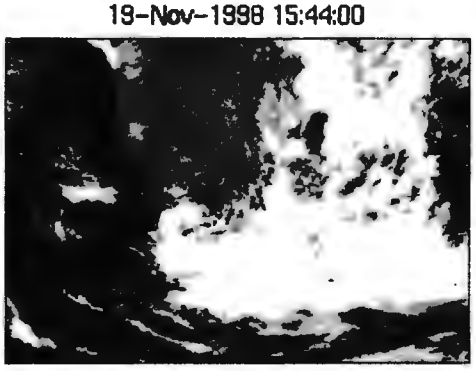


(l)


(m)

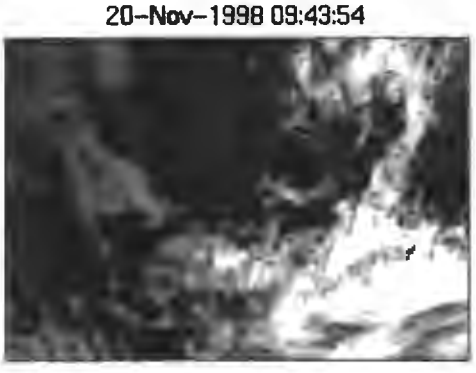


(n)

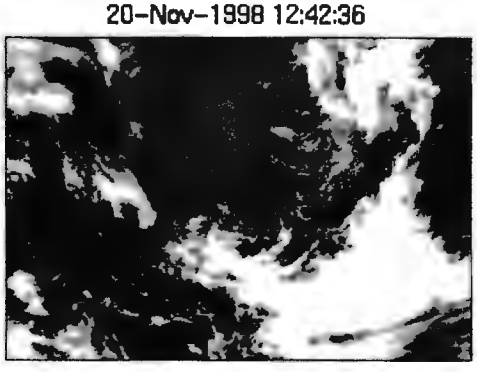


(o)

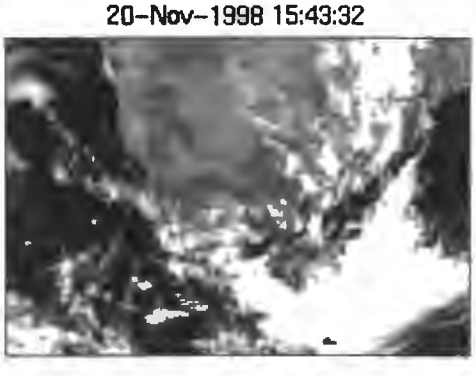


(p)

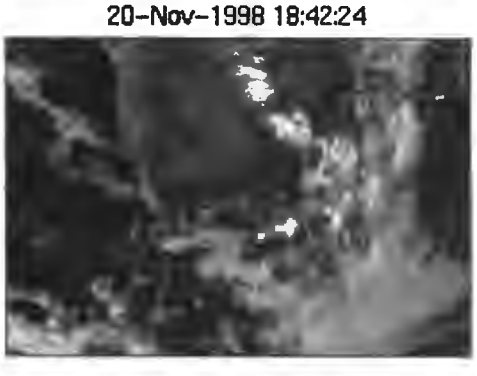


extensive surface trough was present over the eastern half of the subcontinent (Figure 5.23c). Meteosat imagery on 19 shows that the linear shape of the frontal boundary had

changed into a more cyclonic pattern associated with a deep low pressure (Figure 5.24j-k). This large mass of convective clouds remained centered along the edge of the subcontinent which suggests that the system was blocked from the interior due to the mountain escarpment. Heavy rainfall associated with this cloud cover occurred (Figure 5.24i-l) over the Eastern and Western Cape on this date (Figure 5.20a). The surface trough on 20 resulted in heavy rainfall mainly over the KwaZulu-Natal province (Figure 5.23d and Figure 5.20b). Meteosat imagery shows that by midday on 20 November, the cloud cover had significantly decreased over land and the low pressure system moved over the Agulhas Current (Figure 5.24m-p). By 21 November, heavy rainfall had ceased over most of the country (Figure 5.23e).

NCEP Analysis

The National Center for Environmental Prediction (NCEP) temperature data (Figure 5.25a) at the surface gives evidence of the heat low over the interior identified in Figure 5.23. This thermal low is situated farther north than in CASE DECEMBER (Figure 5.7a) and is less developed as it does not have a closed isobar pattern. On 18, 19 and 20 November, the temperatures at 1000 hPa reached 34° C centered to the north over the bordering country of Botswana. A temperature gradient of approximately 8° C existed between 30° S and 45° S on 18 and 19 and weakened to 6° C on 20 November. This is much weaker than the 16° C gradient calculated for CASE DECEMBER which suggests the baroclinicity in this synoptic situation was less. The heat low is still present at 850 hPa and the gradient has steepened as cold air has extended farther north. The 500 hPa level depicts the westerly wave motion as a midlevel cold core trough traveling from west to

east over the Western and Eastern Cape (Figure 5.25b). At 200 hPa the warm core similar to that found in CASE DECEMBER (Figure 5.7b) moved over the eastern Cape on 19 and 20 November. This warm core feature may be the result of latent heat released during

(a)

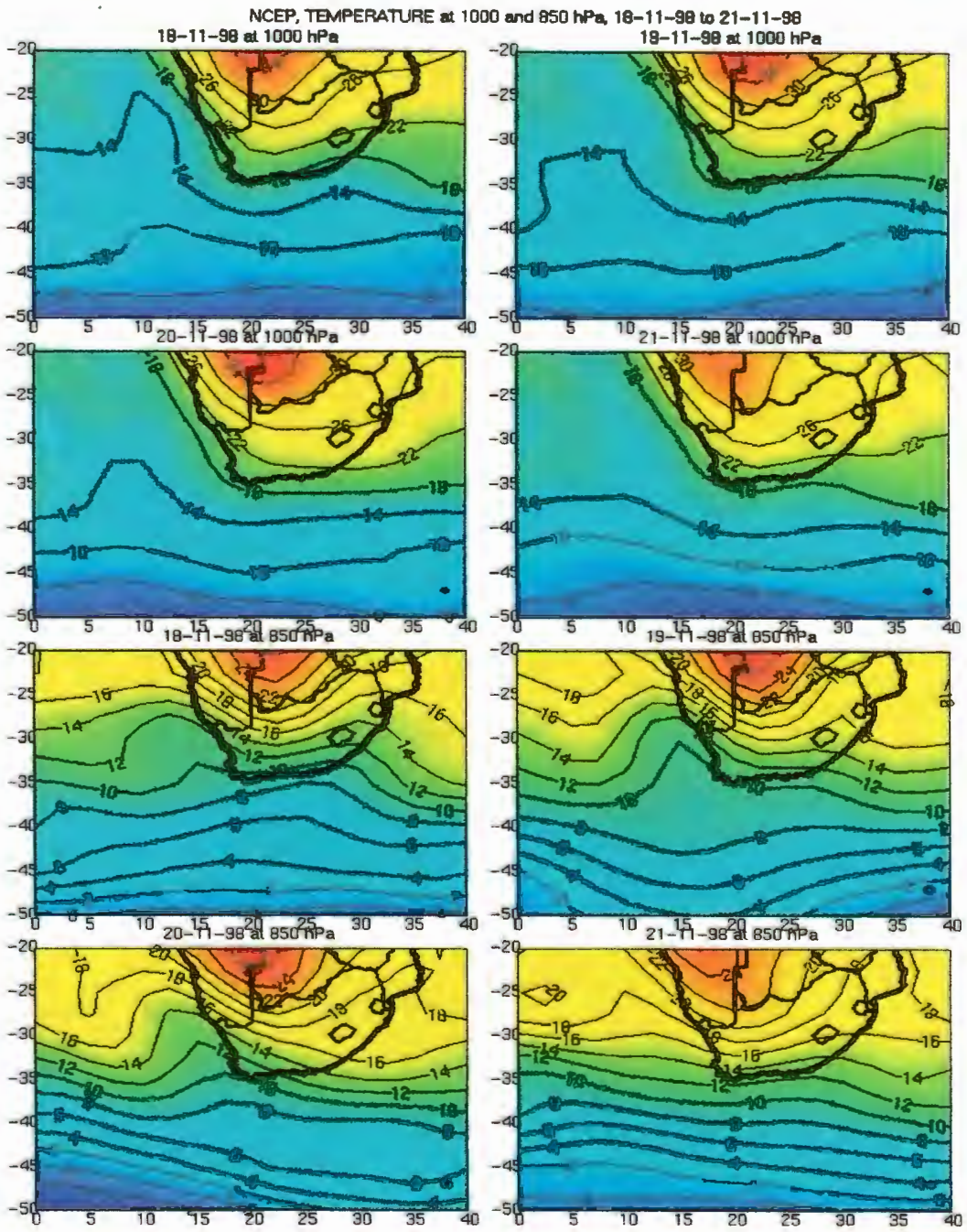


**Figure 5.25.** NCEP daily temperature values in °C for (a) 1000- 850 h-Pa and (b) 500-200 h-Pa levels from 18 until 21 November 1998.

(b)

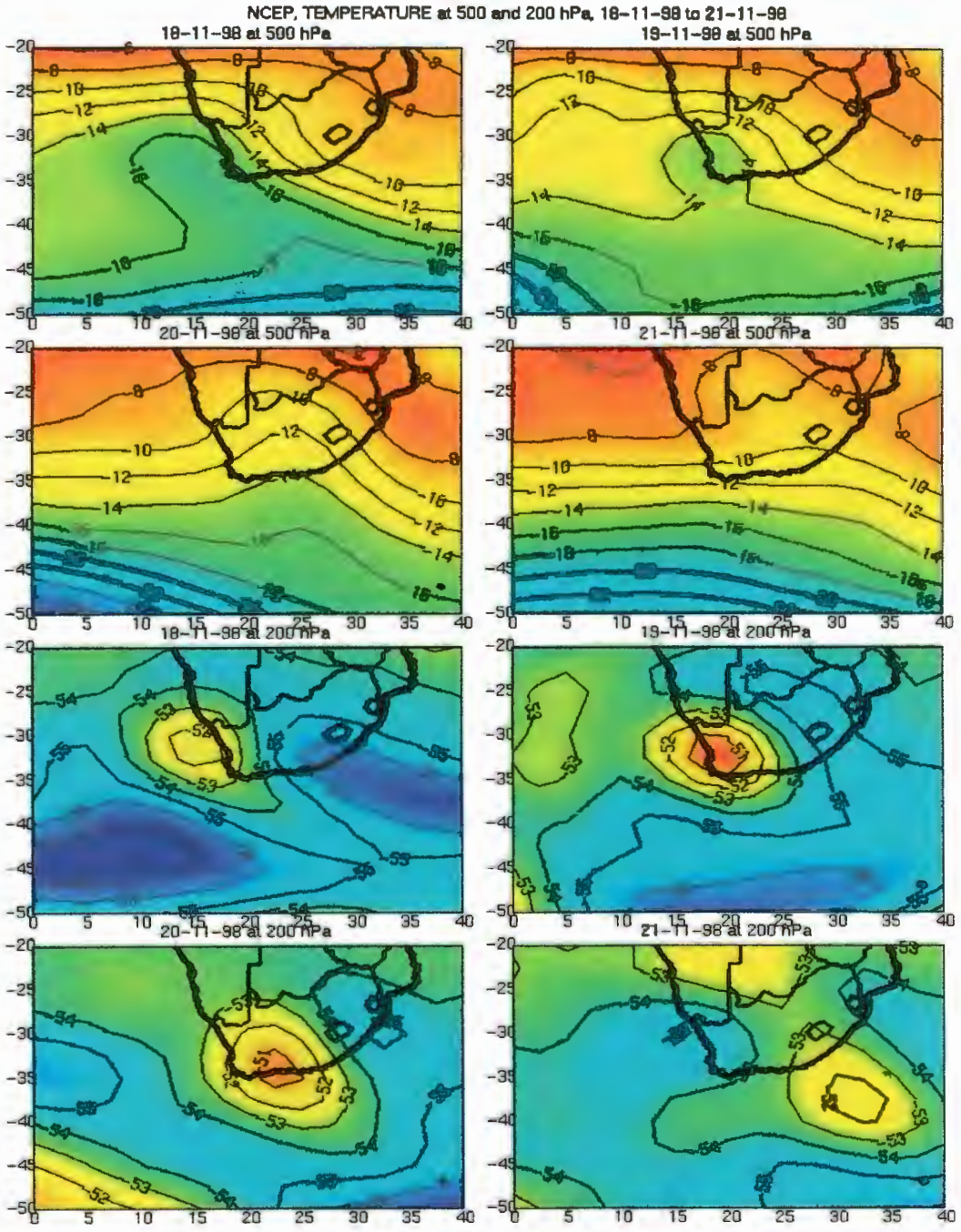


convective rainfall associated with this trough.

Geopotential Height values (NCEP) at 1000, 850, 500 and 200 hPa show a midlevel westerly wave trough tracking above the surface heat low (Figure 5.26a-b). This is similar synoptic situation to that found in CASE DECEMBER (Figure 5.8a-b). The presence of the cold front, which passed over the country on 17, is not visible

on 18 November in Figure 5.26a. The surface heat low is clearly situated farther north than in CASE DECEMBER and thus is not as strong over the southern parts of the subcontinent. This is in agreement with the temperature distribution shown in Figure 5.25a. The midlevel westerly trough however is stronger than that in CASE DECEMBER as it forms a cut-off low on 19 November (Figure 5.26b). This is observable as an isobar

(a)

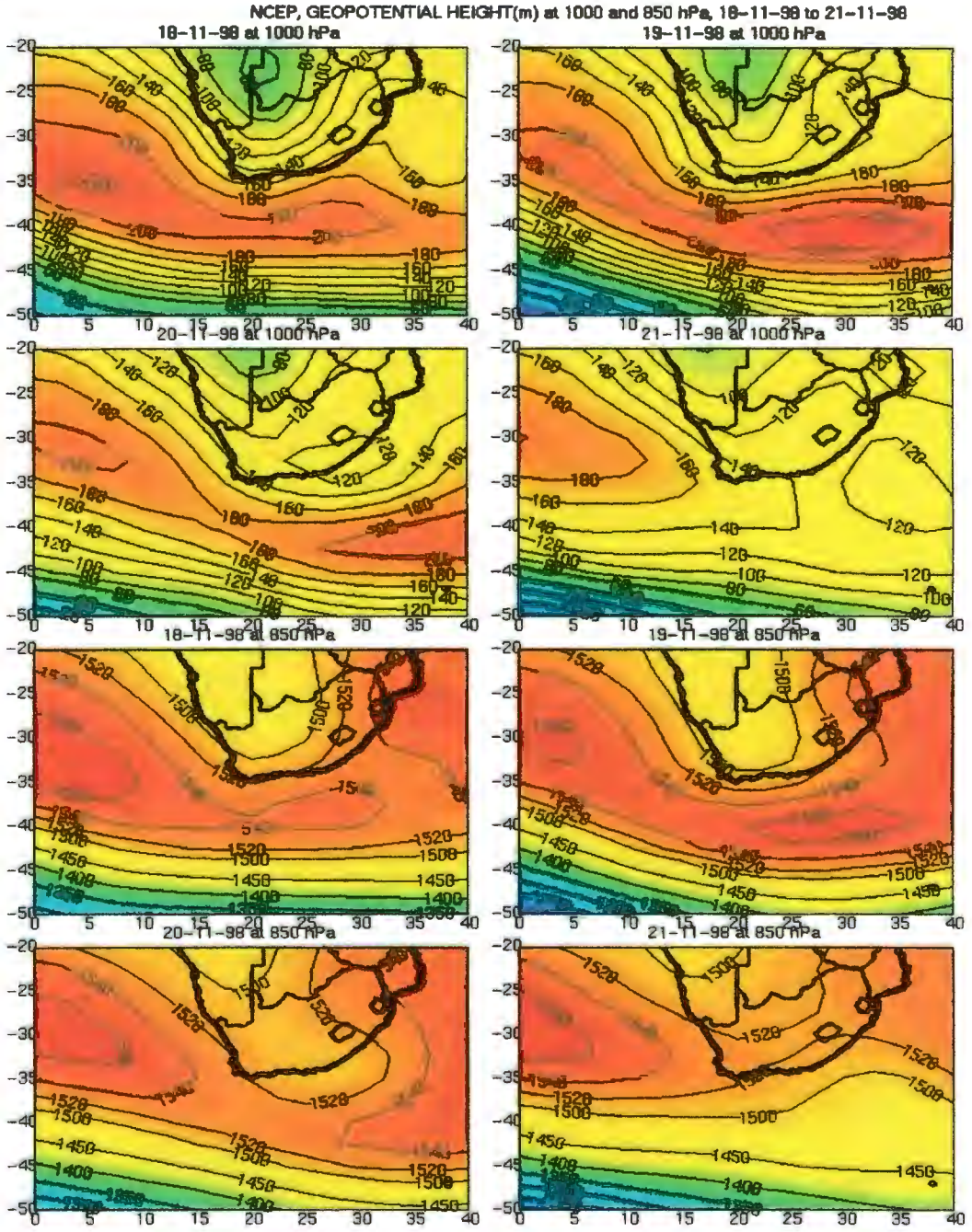


**Figure 5.26.** NCEP daily geopotential height values (m) for (a) 1000- 850 h-Pa and (b) 500-200 h-Pa levels from 18 until 21 November 1998.

(b)

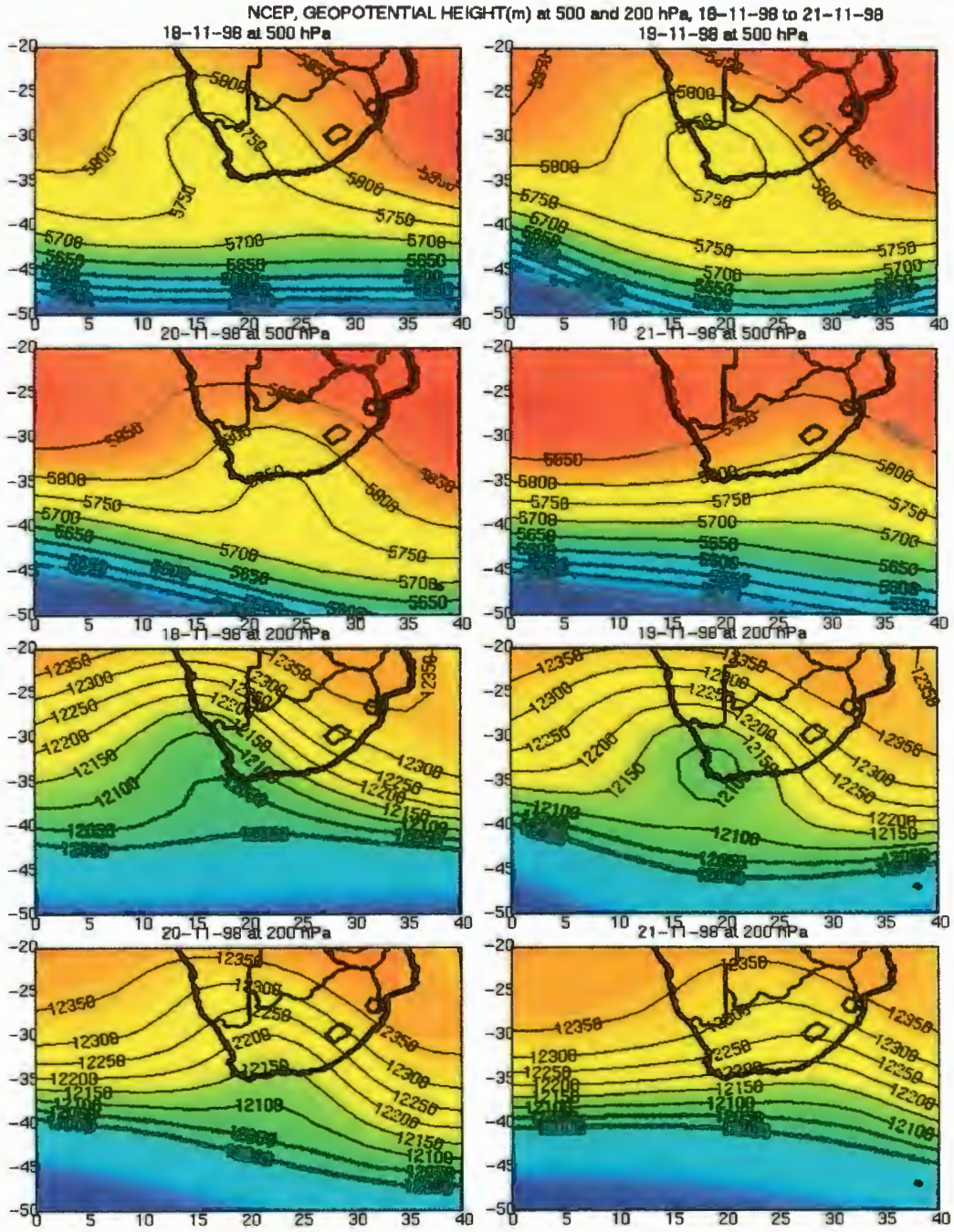


pattern which has closed off at the 500 hPa and 200 hPa level. The descending branch of the westerly wave at 200 hPa is in alignment with the area of heaviest rainfall on 19 and 20 November. This suggests divergence aloft and consequently, convergence at the surface, due to the changes in radius of curvature of westerly waves.

Vertical velocity (NCEP) values at 925, 700, 500 and 300 hPa (Figure 5.27a-b) look significantly different to the vertical velocity Figure 5.9a-b of CASE DECEMBER.

Intense vertical motion (up to 0.39 Pa/s at 500 hPa) was reached at all levels on 18 November, and is most likely associated with passage of cold front over the east coast on that day. At 700 hPa, the ascending limb of the trough and descending limbs of Atlantic and Indian Ocean anticyclones west and south of the continent respectively, are obvious

(a)

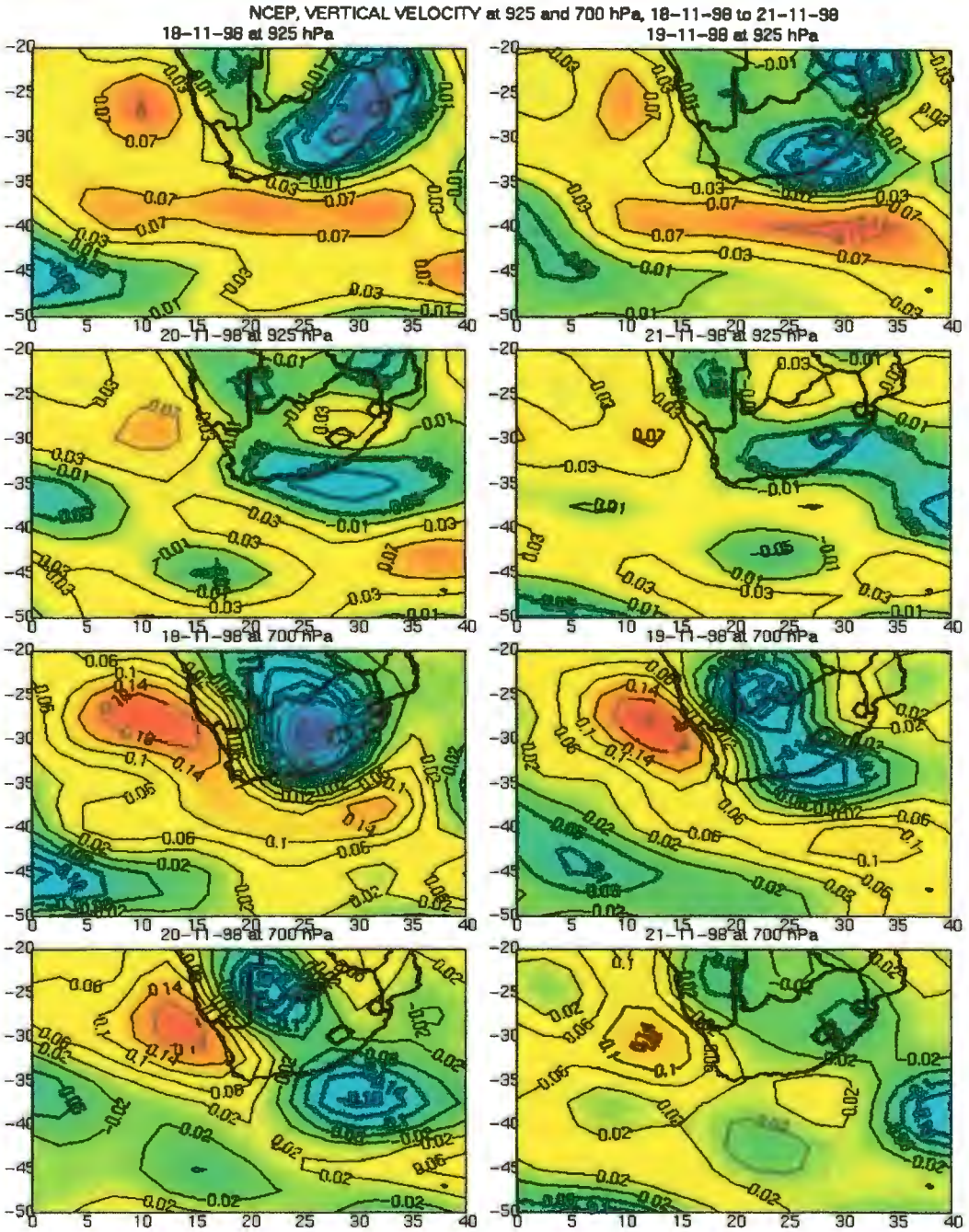


**Figure 5.27.** NCEP daily vertical velocity values (Pa/s) for (a) 925- 700 h-Pa and (b) 500-200 h-Pa levels from 18 until 21 November 1998.

(b)

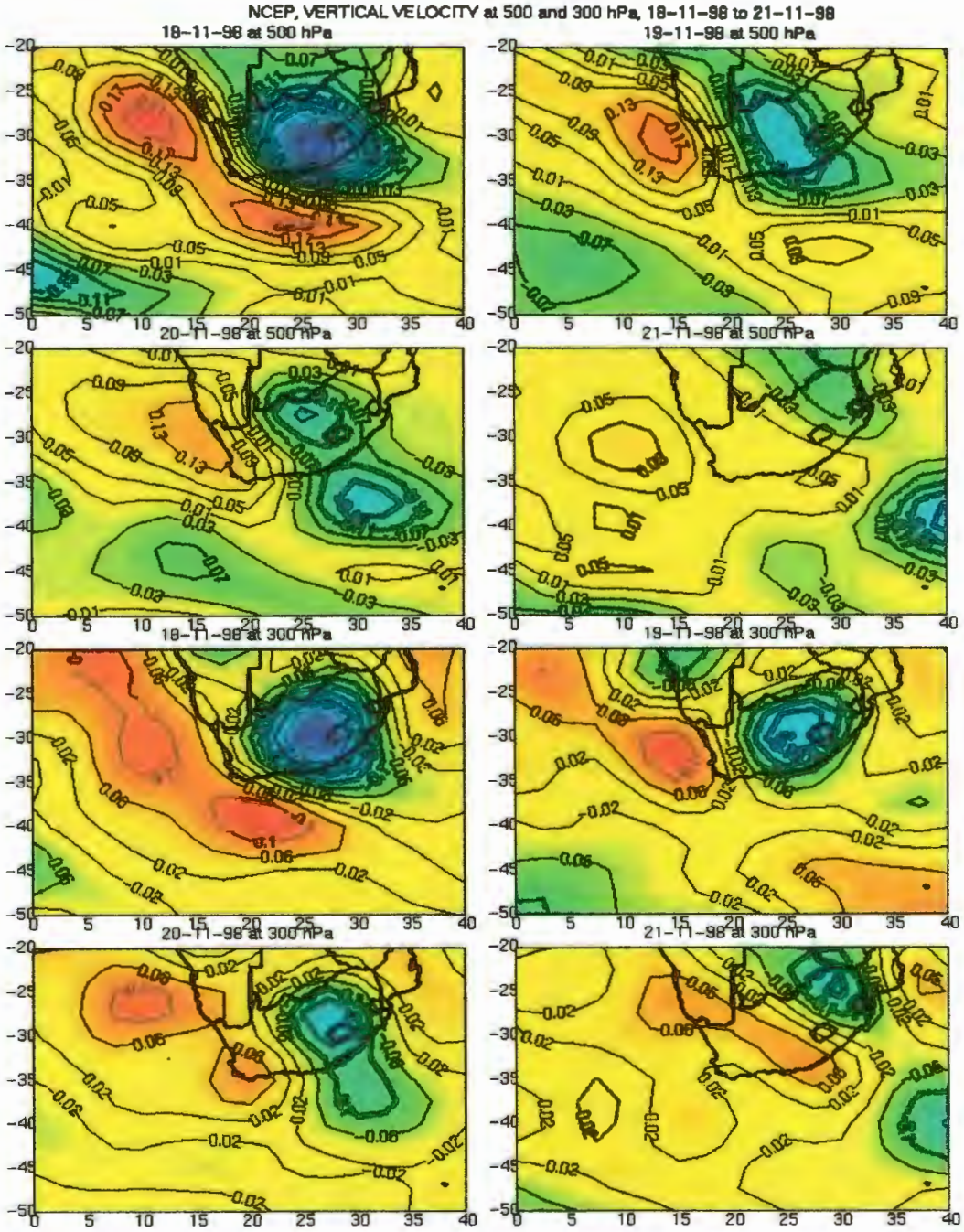


throughout the period. The area of vertical velocity over the Agulhas Current broadened on 19 and 20 November. The Meteosat imagery (Figure 5.24j-k) captures this as a broad east to west sheet of clouds. Also, two distinct areas of vertical motion are obvious at all levels on 19 and 20 November. One region is centered farther north and inland while the other is centered above eastern coastal regions and the Agulhas Current. This bipolar

vertical velocity structure suggests that the heat low and midlevel cut-off low maintained there own continuity. The heat low was centered farther north and the cut-off low remaining above the eastern coastal regions and the Agulhas Current. In contrast, CASE DECEMBER had one clearly defined cell of upward motion which maintained its continuity throughout the period and at all levels (Figure 5.9a-b).

(a)

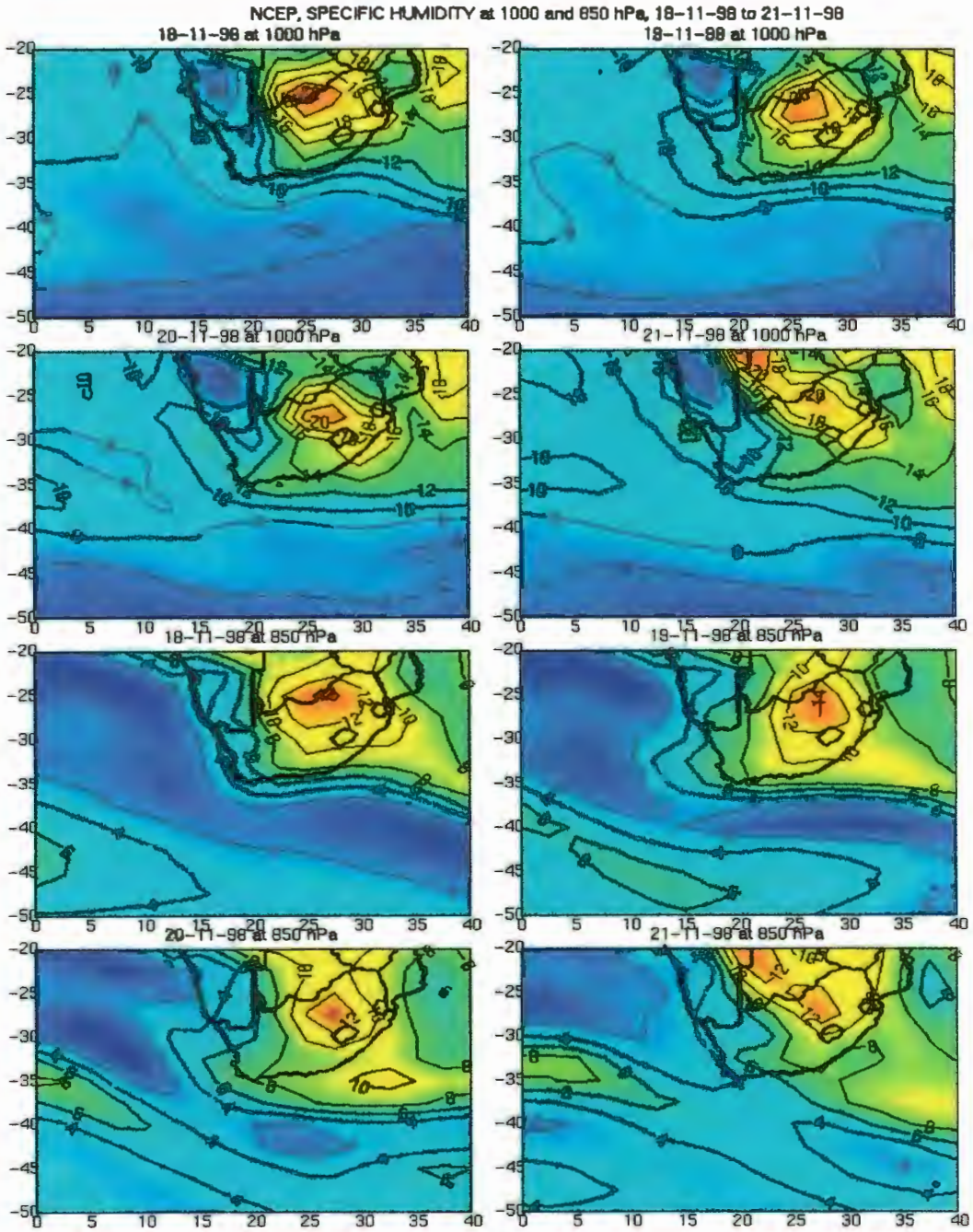


**Figure 5.28.** NCEP daily specific humidity values (g/kg) for (a) 1000- 850 h-Pa and (b) 700-500 h-Pa levels from 18 until 21 November 1998.

(b)

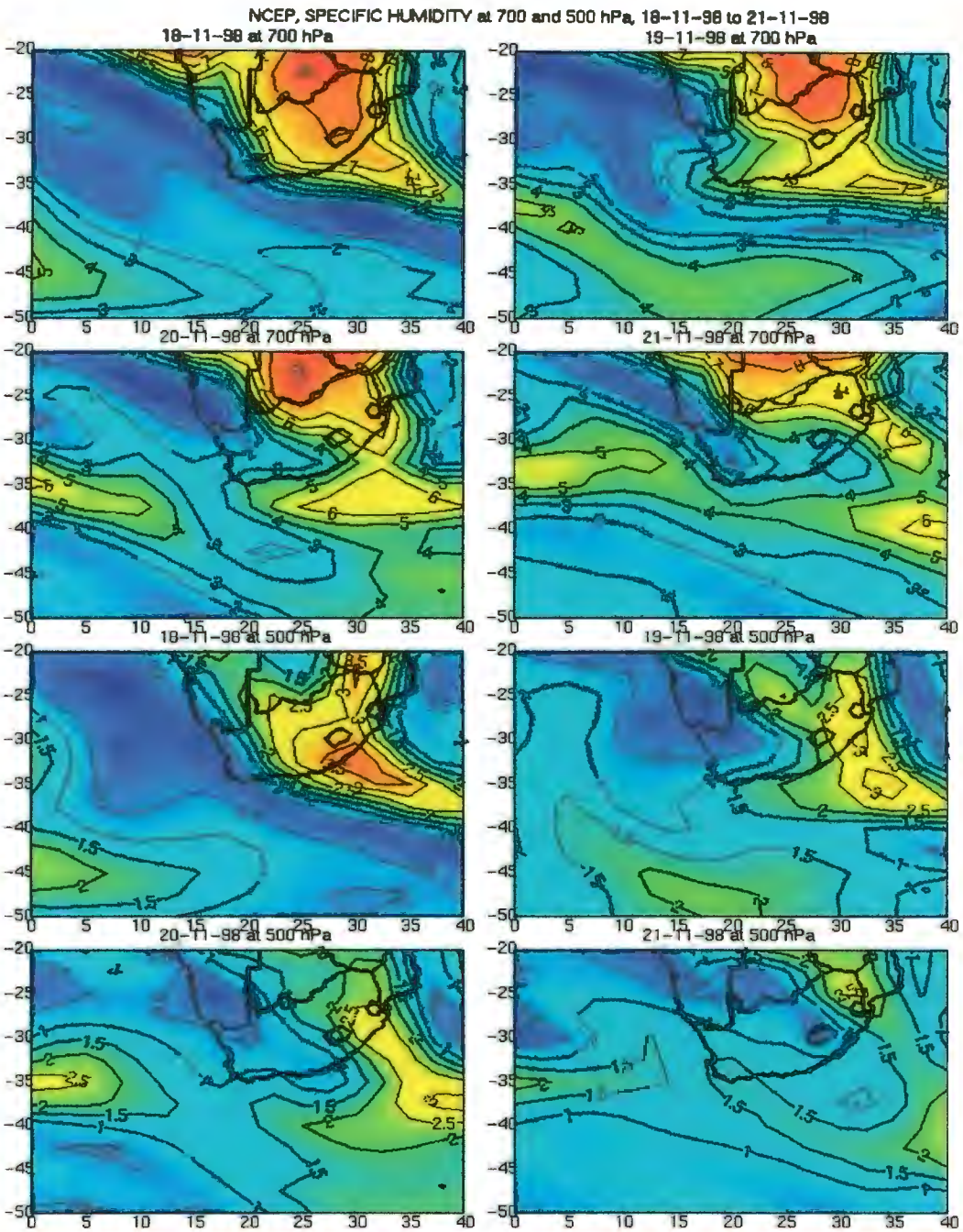


As in CASE DECEMBER (Figure 10a-b), more moisture existed in the Northern Province region than above the Agulhas Current at the 1000 hPa level for CASE NOVEMBER (Figure 5.28a). Higher values reached farther south in CASE NOVEMBER reaching 20 g/kg in the Northern Province regions. Similar values to CASE DECEMBER occurred above the Agulhas Current region ranging between 12 to 14 g/kg. CASE

NOVEMBER specific humidity diagram Figure 5.28a shows moisture in a similar position at 1000 hPa to 850 hPa as CASE DECEMBER, however there was less total moisture available. At 700 hPa a clearly bipolar distribution (as in Figure 5.27b) can again be seen in CASE NOVEMBER on 19 and 20 (Figure 5.28b). Similar values exist in the tropics (8 g/kg) and above the Agulhas Current (6 g/kg) and appear as separate entities. At 500 hPa

(a)

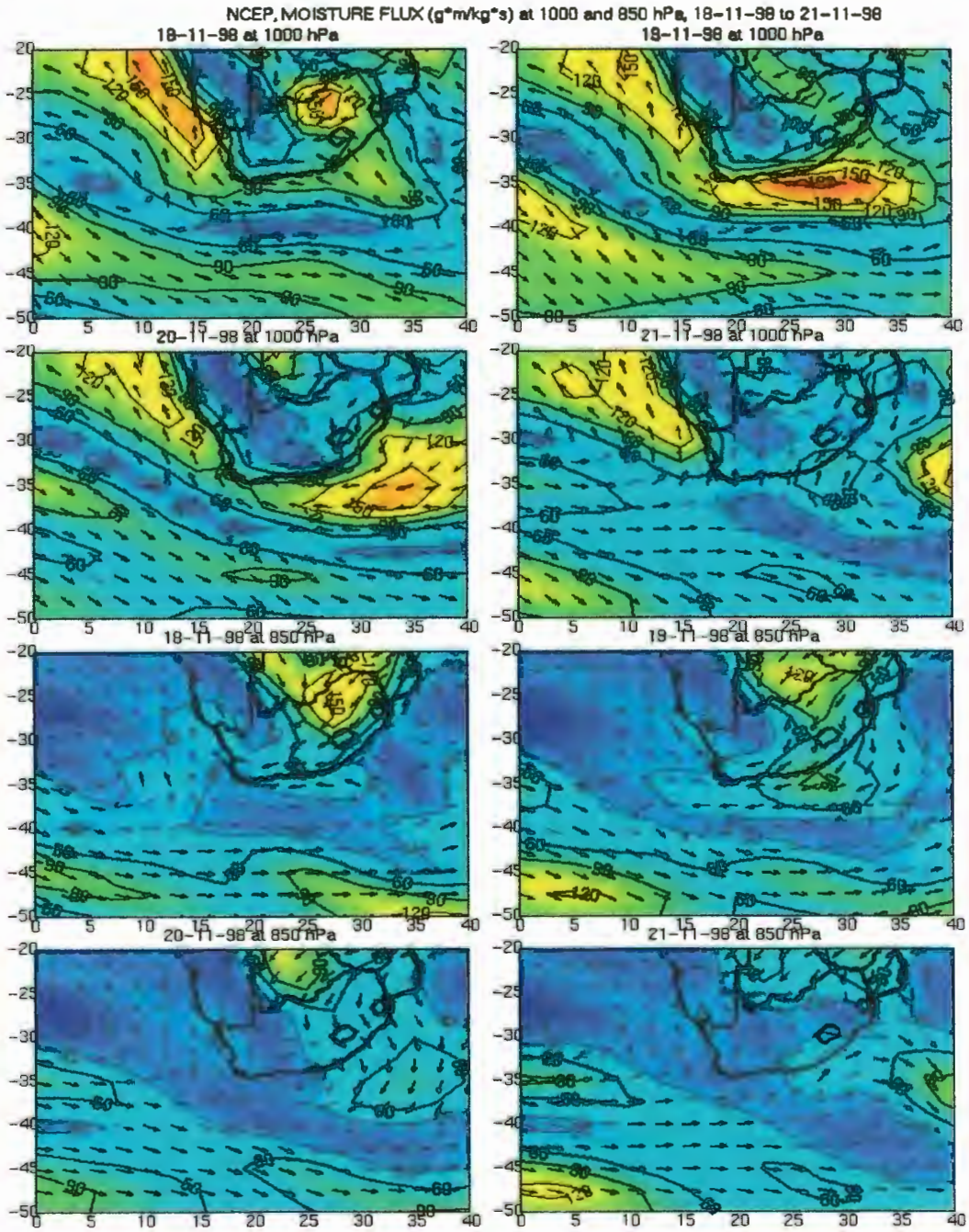


**Figure 5.29.** NCEP daily moisture flux (g·m/kg·s) values for (a) 1000- 850 h-Pa and (b) 700-500 h-Pa levels from 18 until 21 November 1998.

(b)

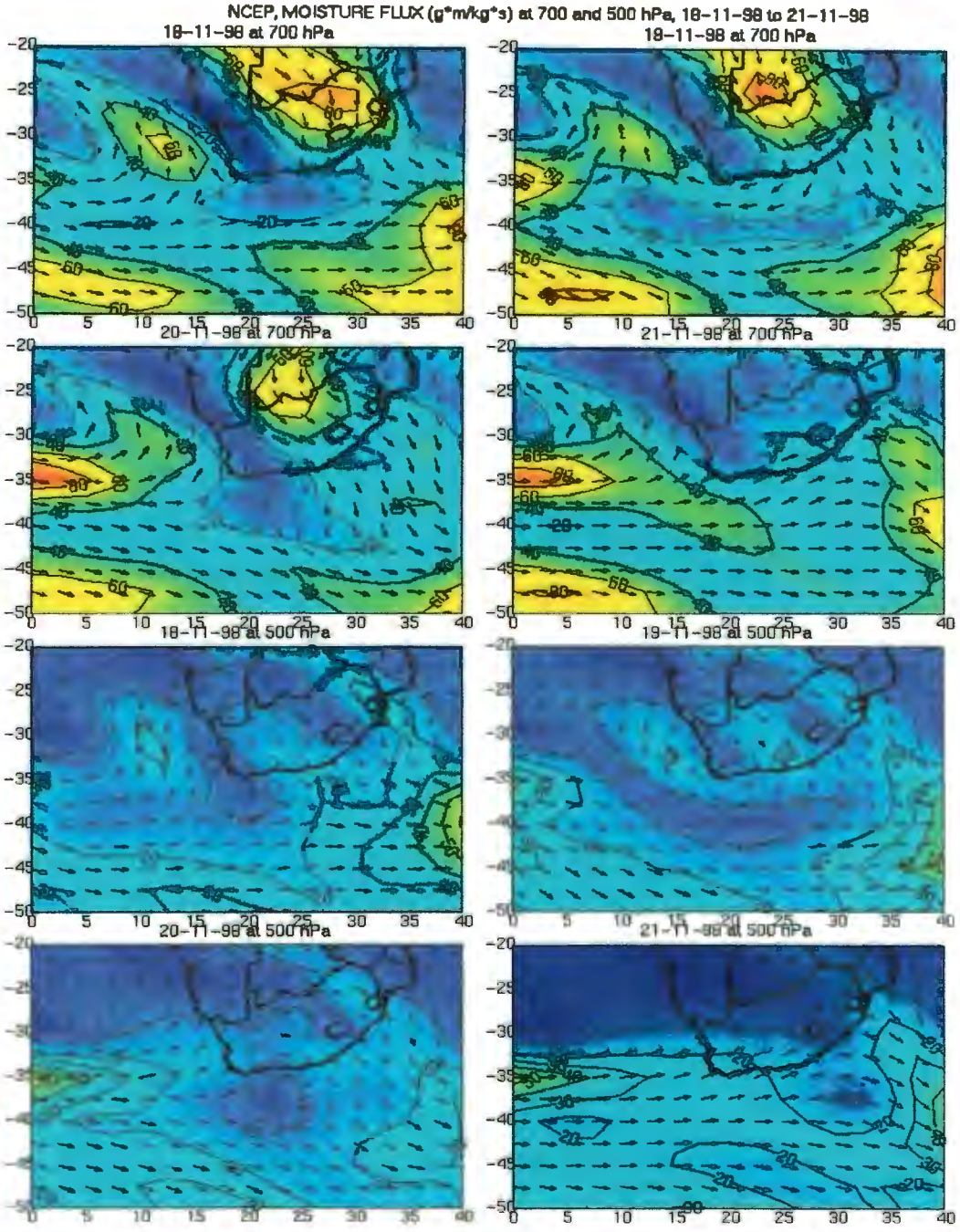


there is still moisture present but mostly above the Eastern Cape and KwaZulu-Natal provinces. As suggested in CASE DECEMBER, this presence of moisture aloft may be related to rainfall at this level in the atmosphere during intense convection. This feature can be seen in the vertical velocity fields (Figure 5.27b) as upward motion which occurs at 300 hPa and in the geopotential height fields (Figure 5.26b) as a closed low pressure system at 500 and 200 hPa on 19 November. These figures both support the contention that the moisture at 500 hPa is related to rainfall.

Looking back at the difference between the specific humidity diagrams (Figure 5.10a-b) and moisture flux diagrams (Figure 5.11a-b) from CASE DECEMBER, it is evident that although ample moisture existed in the tropics, without the wind as transport little tropical moisture reached the storm region. In CASE NOVEMBER it seems a similar situation occurred. At 1000 hPa, the anticyclone situated over the Indian Ocean resulted in strong onshore winds over the east coast (Figure 5.29a). On 19 November a maximum moisture flux of 180 g·m/kg·s moved westward from above the Agulhas Current into the storm region. This continued on 20 November, and appears to be entrained by the cyclonic motion of the wind over land. Also at 1000 hPa on 18, significant moisture flux from the tropics (150 g·m/kg·s) was advected around the surface heat low over the Northern Cape. This moisture source dissipated on 19 and 20 November, the days corresponding to heavy rainfall over the eastern coastal regions, most likely because the wind had weakened. At 850 hPa, significant moisture streamed down from the north on 18, 19 and 20 November in the northerly air flow at this level.

The 700 hPa level was a significant level for moisture transport to this storm as can seen in Figure 5.29b. A steady stream of air from the north on 18, 19 and 20 November supplied the storm region with moisture. At this point it is important to highlight that the timing and duration of moisture sources are key factors in the production of flood producing rains [Crimp and Mason 1999]. In both CASE NOVEMBER and CASE DECEMBER, moisture at the surface was obtained from the Agulhas Current one day before and during the heavy rainfall events according to the moisture flux diagrams Figure 5.11a and 5.29a. At the 850 and 700 hPa level, only CASE NOVEMBER received large amounts of moisture sourced from the tropics [Figure 5.11b and 5.29b]. This

moisture moved into the storm region the day before and during the days of the heavy rainfall event. In both cases the maximum moisture flux values were at the surface from above the Agulhas Current. This suggests that the consistent wind associated with a strong high pressure cell over the South-west Indian Ocean in conjunction with a midlevel trough tracking above a surface heat low (Figure 5.23 and Figure 5.26), is a synoptic setting

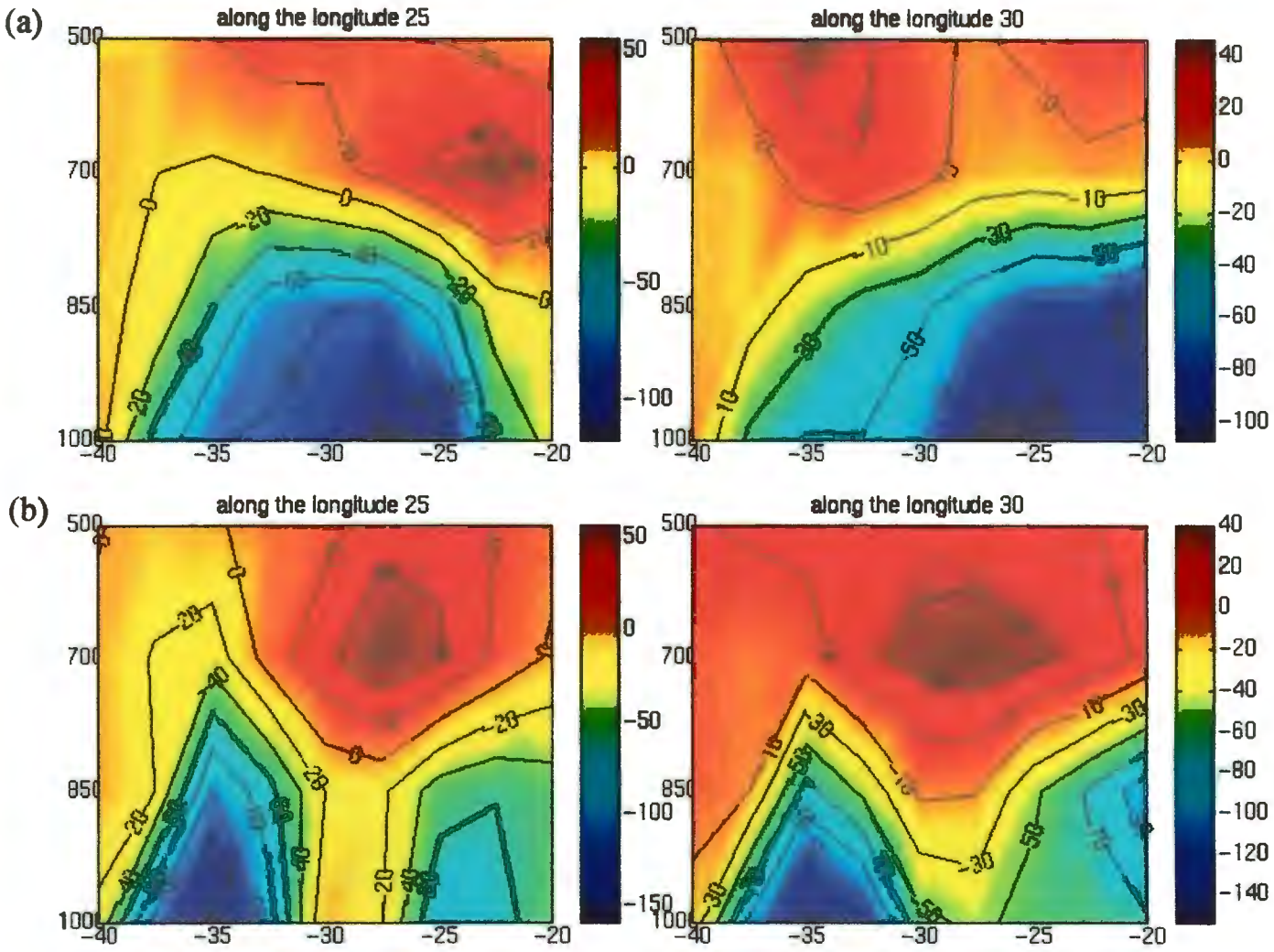


**Figure 5.30.** NCEP daily moisture flux (g·m/kg·s) values for longitudinal profiles (a) on 18 December, (b) on 19 November, (c) on 20 November and (d) on 21 November 1998 (eastward fluxes are positive; westward fluxes are negative).

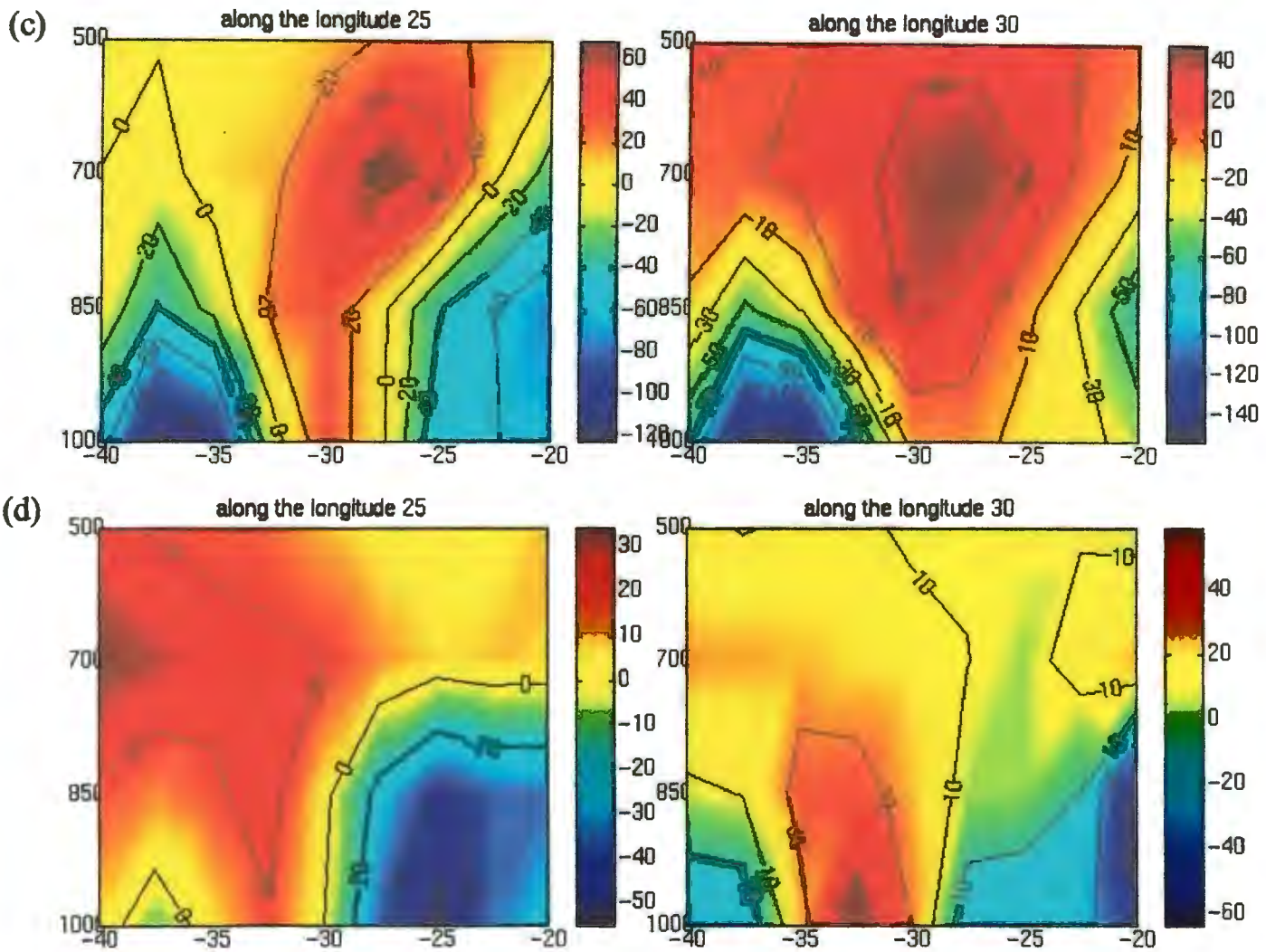


conducive to heavy rainfall over the eastern coastal regions of South Africa.

Vertical profiles of the moisture flux across the longitude 25° E on 18 November show a wide dome of surface moisture ranging from 100 down to 20 g·m/kg·s and extending up to the 800 hPa level (Figure 5.30a). This westward moving moisture is partly above the Agulhas Current (38° S to 34° S) water but also extends over land (34° S to 23° S). Above this dome of westward moving moisture (100 g·m/kg·s) is a clearly defined layer of eastward moving moisture (50 g·m/kg·s). This pattern is quite different than that found in CASE DECEMBER (Figure 5.12a). The major difference being the westward motion associated with the upper levels in Figure 5.30a does not extend to the surface over

South Africa's interior as in CASE DECEMBER. This comparison shows that for CASE NOVEMBER the vertical shear between westward and eastward flowing moisture appeared to be more important than in CASE DECEMBER where the horizontal shear was dominant.

At Longitude 30° E on 18 November (Figure 5.30a) shows a similar picture to at 25° E, however the center of the dome is not above the Agulhas Current south-east of the country (38° S to 30° S), but rather the northern reaches of South Africa (30° S to 20° S). The westward direction is still present at the surface which suggests that this moisture flux was derived from the northern Agulhas Current water east of land. Vertical shear associated with the eastward motion of moisture aloft was present at approximately the 750 hPa level.

On 19 November, the day of heavy rainfall above the Eastern Cape, a similar structure to that seen in CASE DECEMBER developed (Figure 5.12b and Figure 5.30b). A layer of minimum moisture content extended to the surface between 30° S and 28° S for longitude 25° E and 30° E. The surface westward moving moisture was still dominant in magnitude and had separated into two separate cells. From 40° S to 30° S the maximum occurs at both 25° E and 30° E over the Agulhas Current and was headed toward the storm center. This suggests that the Agulhas Current was the main source of moisture at the surface. A layer of eastward moving air with significant amounts of moisture occurred at the 700 hPa level.

A similar structure is evident for 20 November, the last day of heavy coastal rains which occurred over the KwaZulu-Natal province (Figure 5.30c). Horizontal shear now

dominated as seen in CASE DECEMBER (Figure 5.12c). The Agulhas Current moisture at the surface was still the most significant moisture contributor with values between 120 and 140 g·m/kg·s. As in CASE DECEMBER (Figure 5.12d), the day after the storm peak looked radically different. On 21 November (Figure 5.30d), the storm had moved over the ocean (Figure 5.23d and Figure 5.26a). The region which had previously shown westward moving moisture in the 40° S to 30° S latitudes, above the Agulhas Current, now showed no sign of westward moving moisture. This cell had moved over land from 30° S to 20° S and lessened from 140 g·m/kg·s to 60 g·m/kg·s.

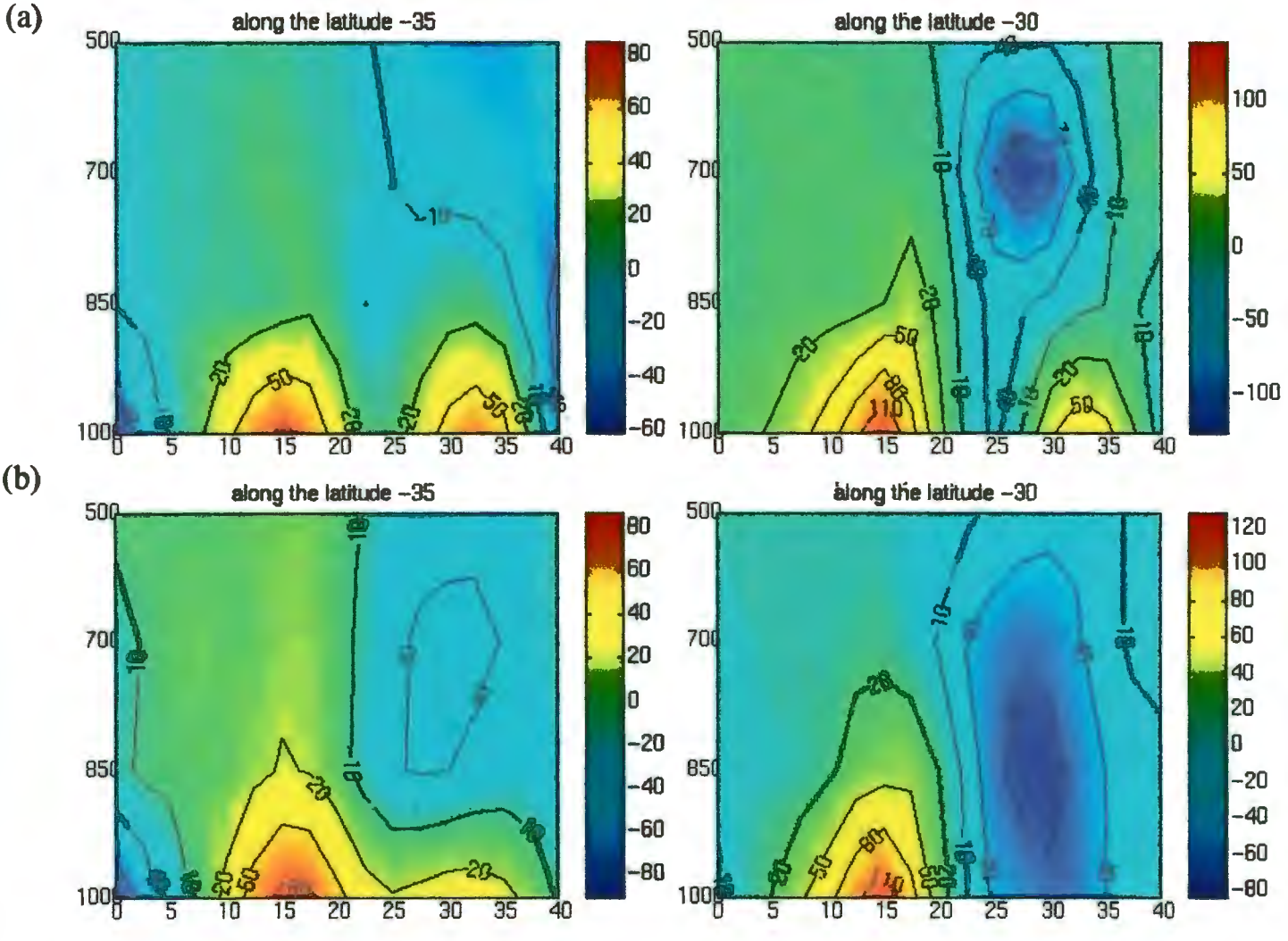


**Figure 5.31.** NCEP daily moisture flux (g·m/kg·s) values for latitudinal profiles (a) on 18 November, (b) on 19 November, (c) on 20 November and (d) on 21 November 1998 (northward fluxes are positive; southward fluxes are negative).

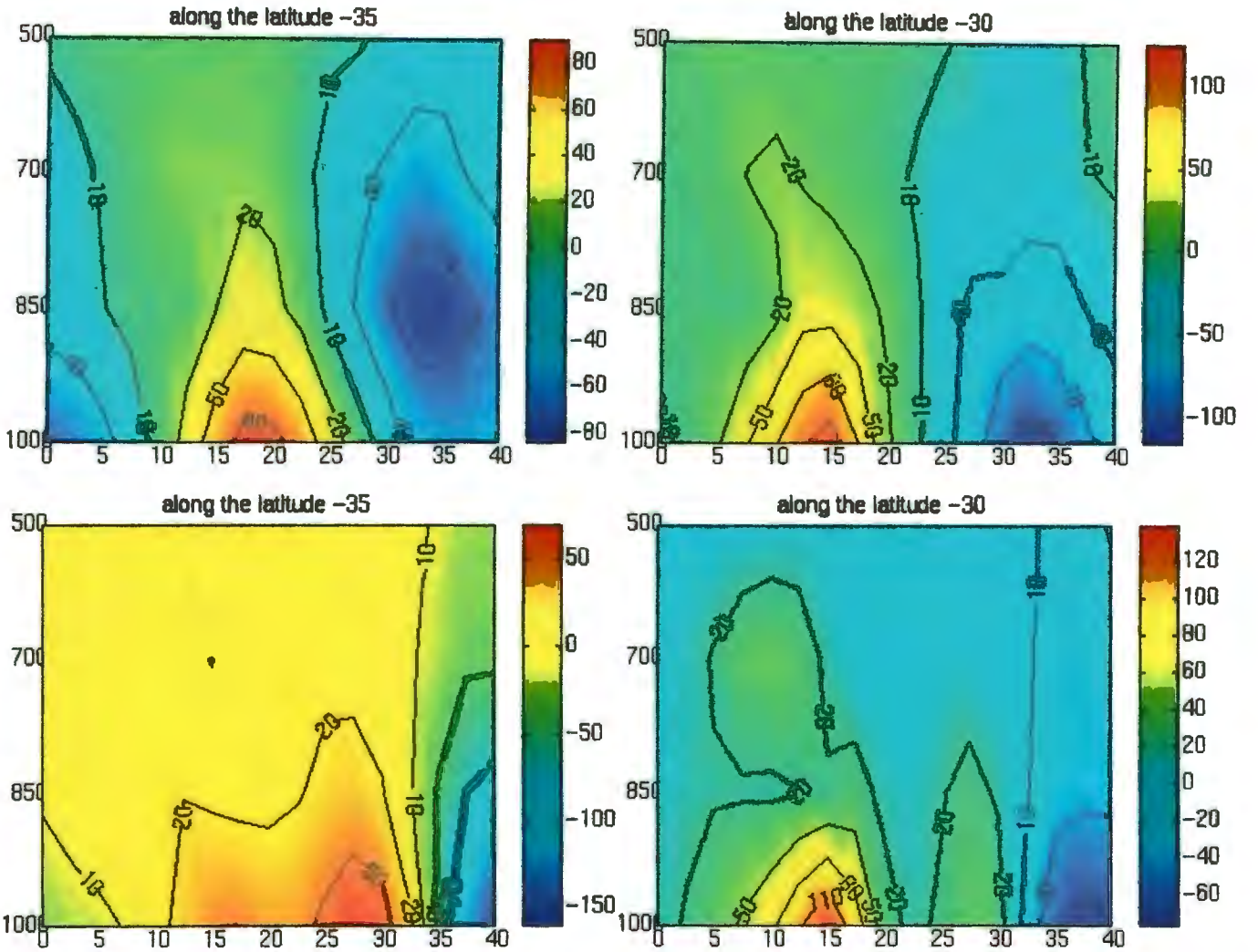


Latitudinal cross section at 35° S on 18 November shows northward moving moisture from 10° E until 35° E which covers the ocean area of the greater Agulhas Current system (Figure 5.31a). There was insignificant southward moving moisture into the storm region. A cross section at 30°S on the same day shows a cell of southward moving moisture at the 700 hPa level which was most likely of tropical origin. The cell extended to the surface but was of less magnitude in the lower levels (20°-25° E). Northward moving moisture from above the Agulhas Current can be seen moving into the storm region at the surface from 30° to 35° E. In Figure 5.31b for 19 November, the cross section at 35° S looks very similar to that of the previous day. The cross section at 30° S looks different to the previous day because the cell of northward moving moisture from

30° E to 35° E was gone. This profile appears to be completely dominated in moisture coming from the north even at the surface layers directly above the storm region. There is still the cell of northward moving moisture at the surface from 5° to 20° E but this is much farther to the west of the storm. This moisture may have been entrained by the storm on 19 November.

Figure 5.31a-d for CASE NOVEMBER is similar to Figure 5.13a-d for CASE DECEMBER in that there is a boundary which exists at roughly 20° E between northward and southward moving moisture. This boundary can be seen on 18, 19 and 20 November. As was pointed out for CASE DECEMBER, it is difficult to know the exact source of southward moving moisture as it may be coming from above the Agulhas Current as well as from the tropics. As in CASE DECEMBER, the day after the storm the winds shifted at the surface from due east to south-southwest (Figure 5.29a-b). This can be seen as an eastward shift in northward moving moisture extending to 35° E for the cross section at 35° S (Figure 5.31d).

In CASE NOVEMBER, both vertical and horizontal shear were present. This presence of horizontal and vertical shear enhances the vertical and horizontal vorticity respectively. Both vertical and horizontal vorticity are favorable for creating instability and thus convection and subsequent rainfall. Therefore, these flux diagrams show that both moisture as well as shear were significant contributors to the development of CASE NOVEMBER.

From comparing moisture profiles discussed above with the moisture flux diagram Figure 5.29, it seems that the surface moisture source is from above the Agulhas Current while at 700 hPa the moisture is of tropical origin. To distinguish whether the

southward moving moisture in Figure 5.31c on 20 November (ranging from 25° E and 40° E) is of tropical or Agulhas Current origin, backward air parcel trajectories are considered.

TRAJECTORY ANALYSIS

At the 950 hPa level on 19 November, a three day backward air parcel trajectory ending at Swellendam (34° 2' S, 20° 27' E) shows moisture was streaming into the storm center from directly above Agulhas Current water (Figure 5.32a). Figure 5.28a shows a specific humidity of 12 to 14 g/kg above the Agulhas Current comparable to the specific humidity value above the Agulhas Current in CASE DECEMBER (Figure 5.10a). At 900 hPa level on 20 November, the air parcel pathway came from the northern part of the Agulhas Current before it arrived at Durban (29° 58' S, 30° 57' E) (Figure 5.32b). This region of the Agulhas Current showed the highest temperatures in Figure 5.22. The surface level seems to be dominated by moisture from the Agulhas Current on both 19 and 20 of November.

Figure 5.32a shows that at the 700 hPa on 19, air parcels came from south-west of the continent before arriving into the storm region. This agrees well with Figure 5.31a-b which shows a northward flux of moisture extending up to the 700 hPa level. It is important to note that the magnitude of the flux at 700 hPa (20 g·m/kg·s) is much less than at the surface (80 g·m/kg·s). On 20 November at 700 hPa (Figure 5.32b), the air pathway comes streaming down from the north. This agrees well with the NCEP moisture flux Figure 5.29b.

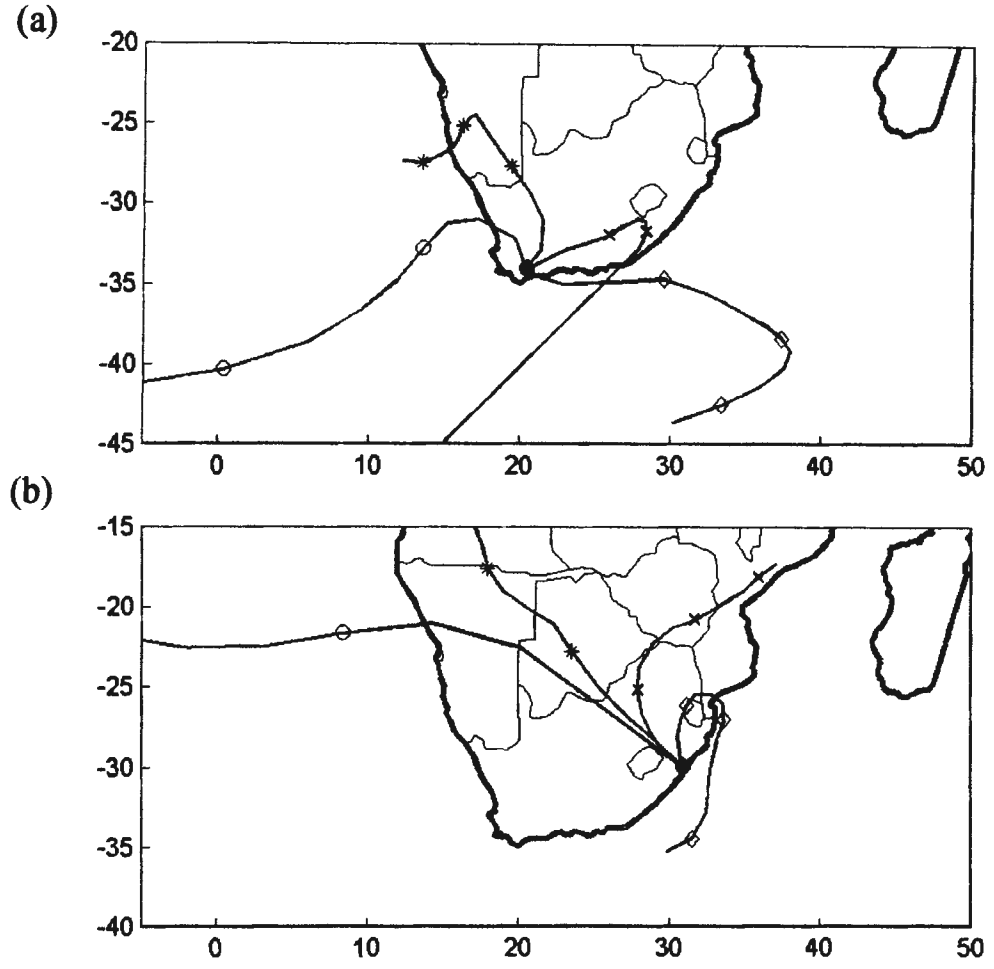


**Figure 5.32.** BADC backward trajectories for air parcels at the (a) 900 hPa (◊), 700 hPa (+), 500 hPa (*) and 200 hPa (o) 3 days prior to 19 November at 12:00 UTC and originating from the Swellendam heavy rainfall location, (b) 900 hPa (◊), 700 hPa (+), 500 hPa (*)and 200 hPa (o) 3 days prior to 20 November at 00:00 UTC originating from the Durban heavy rainfall location.

The 500 hPa level air parcel trajectory shows the air motion on 19 and 20 November may have been part of the descending branch of the westerly trough at this height (Figure 5.32a-b). The air at the 500 level is cold and dry, which further supports NCEP data which showed the cold dry air advection aloft at these heights in the atmosphere (Figure 5.29b). Cold dry air aloft and warm moist air at the surface is an atmospheric setting highly conducive to convection. At 200 hPa the air is clearly moving faster than at the lower levels on both 19 and 20 November. The air at this height is forming the descending branch of the westerly wave. That the upper air pattern at 200 hPa

shows the storm to be overlain by the descending branch of the westerly wave is evidence of surface convergence.

Regional Features

*a. TRMM analysis*

One TRMM pass on 19 and two on 20 November (Figure 5.33) provided useful imagery for this study. As in CASE DECEMBER (Figure 5.16), TRMM located most of the rainfall over the Agulhas Current. A maximum surface rainrate for the two days was measured over the Agulhas Current late on 20 November. Figure 5.34 magnifies this surface rain event and shows that the heaviest rain fell above 24° C water (Figure 5.22). The rain rate in the atmosphere (Figure 5.35) for the cross section in Figure 5.34 shows that the rain in the atmosphere stayed confined to the warm water region and remained below 8000 m. Figure 5.36 shows that the high values of latent heat in the atmosphere are also confined above the warm water.

As in CASE DECEMBER the maximum rain rates and latent heat release occurred directly above the warm water and below 4000 m above the surface. CASE DECEMBER was clearly more intense as the surface rain area and the region of most intense rainfall and latent heat release in the atmosphere were much larger (Figure 5.17, 5.18 and 5.19). Also as in CASE DECEMBER, the regional environment above the warm Agulhas water was significantly different from that above the colder ambient water. This comparison suggests that the atmosphere may be significantly modified by the Agulhas Current SSTs in terms of rainfall and latent heat release.

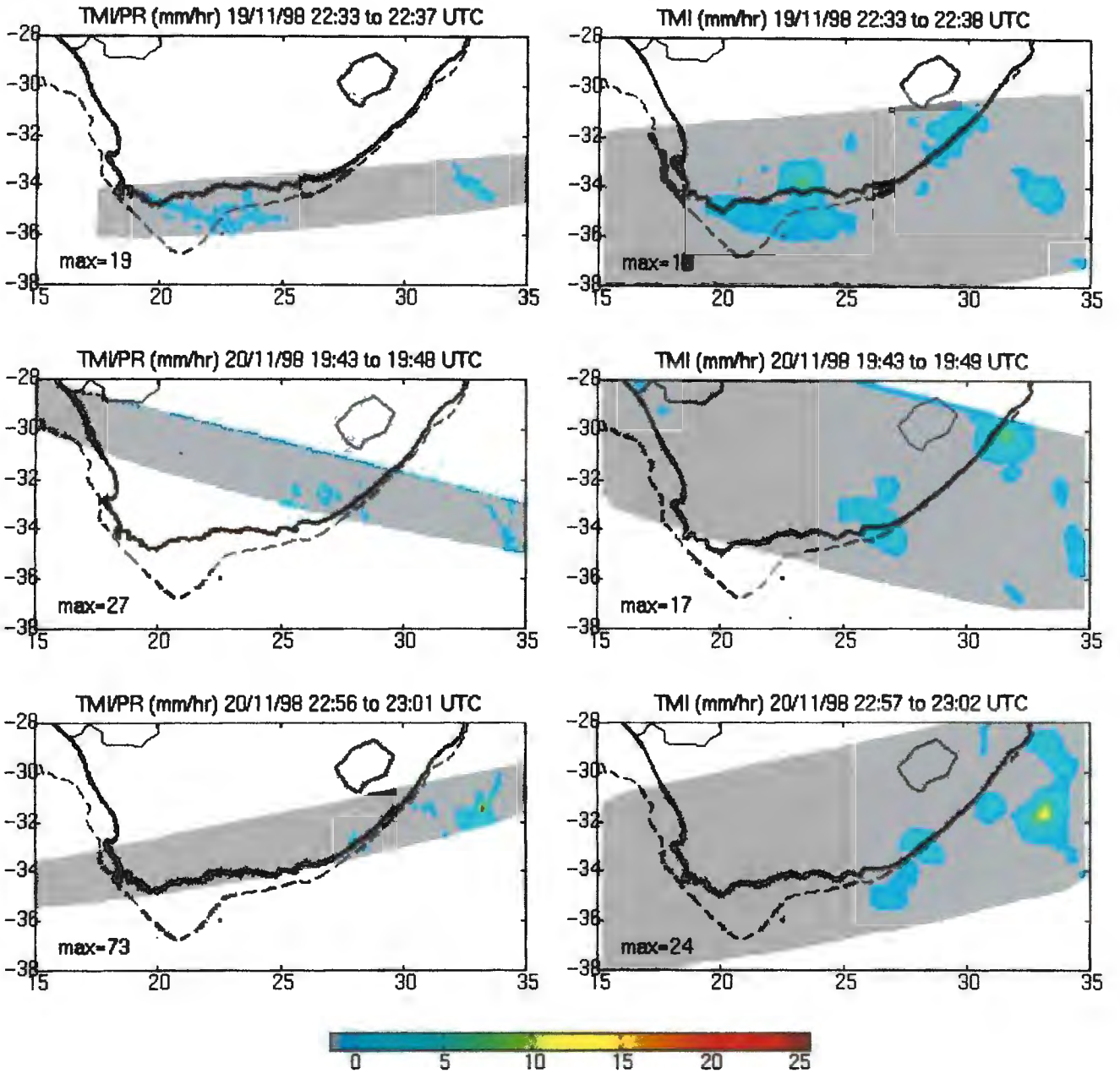


FIG. 5.33. TRMM-derived surface rain rates on 19 and 20 November 1998 for three consecutive orbit passes from TMI on the right side and from TMI/PR on the left side (mm/h).

Perhaps this rainfall and corresponding latent heat release above the current on 20 November could have been available to the storm. Latent heat in the atmosphere adds kinetic energy to the system, which enhances convection. This enhancement of convection aloft indirectly contributes to rainfall given available surface moisture is present. In this

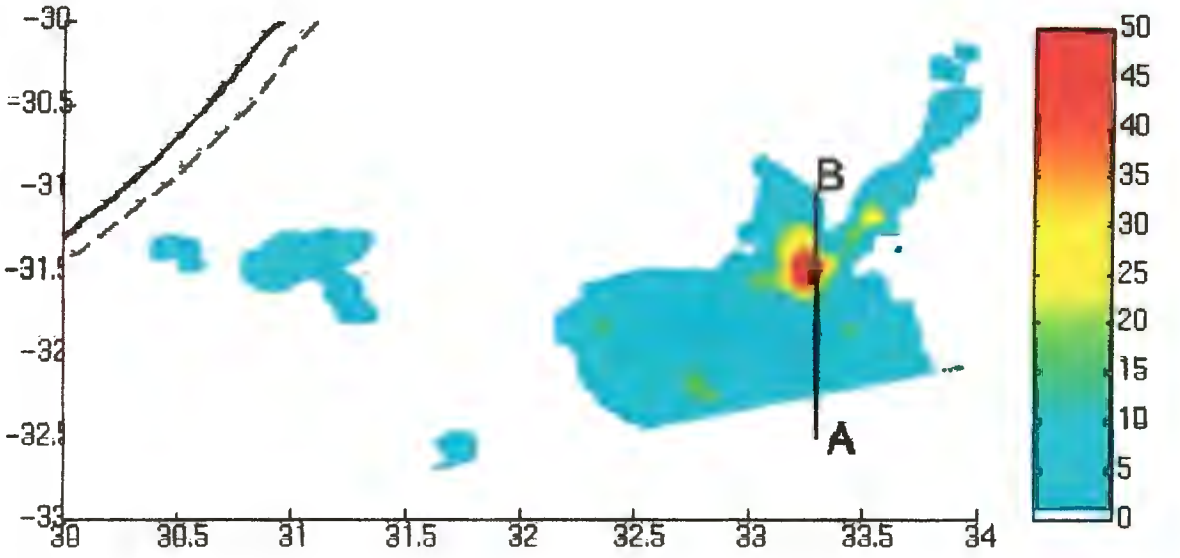


**Figure 5.34.** Zoom of the surface rain rate according to the combined PR and TMI product on board the TRMM satellite for 20 November 22:56 to 23:51 UTC over the ocean region east of Durban (Figure 5.33, bottom panel). The solid line shows the location of the coastline; the broken line the 200 m isobath that represents the edge of the continental shelf. Rain rates in mm/h are given in the color scale. The A-B line represents a longitudinal cross section across the heavy rainfall event above the Agulhas Current (later below in Figure 5.35 and 5.36).

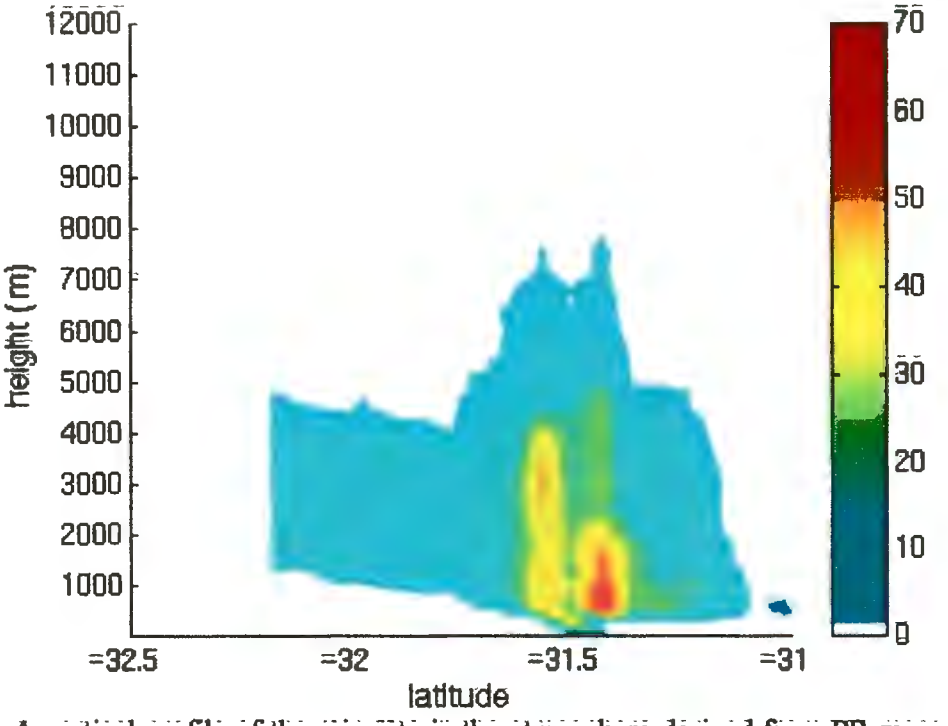


**Figure 5.35.** A vertical profile of the rain rate in the atmosphere derived from PR measurements in mm/h corresponding to the cross section B—A given in Figure 5.34 from left to right respectively.

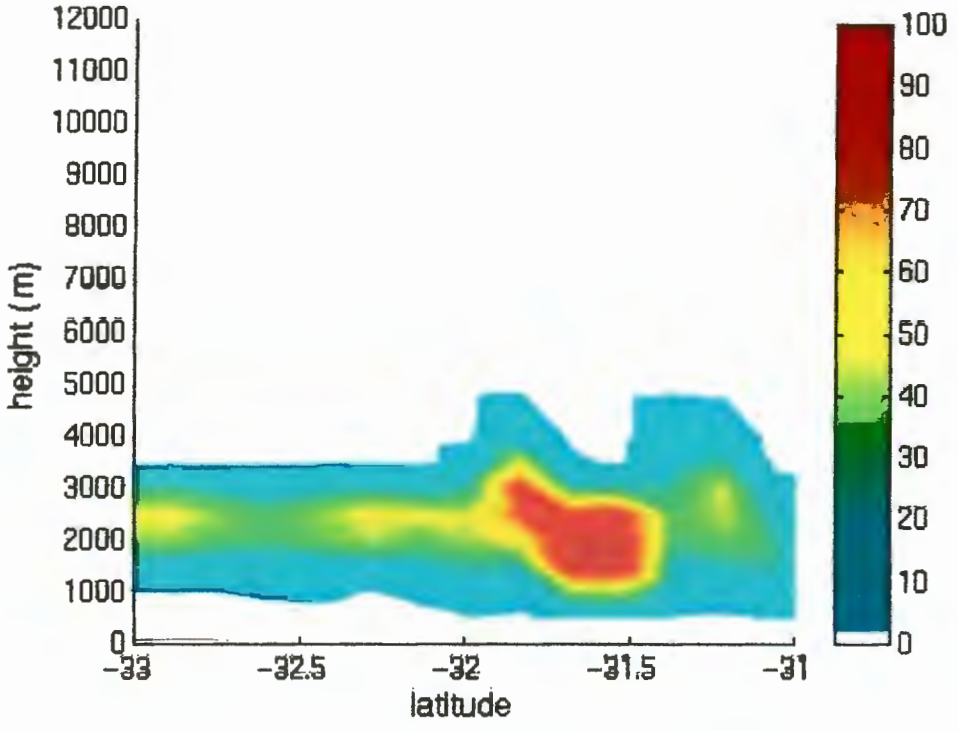


**Figure 5.36.** A vertical profile of the latent heat in the atmosphere derived from TMI measurements in °C/day corresponding to the cross section B—A given in Figure 5.34 from left to right respectively.

context, it seems plausible that the latent heat released above the Agulhas Current could have contributed to the heavy rainfall over land had the storm remained over land on 20 November and the air parcel pathway continued to be above the Agulhas Current.

# 6. CONCLUSION

This section summarizes the most important results that best address the key questions.

## What was the relative contribution of Agulhas Current moisture to CASE DECEMBER and CASE NOVEMBER?

To answer the first question moisture flux diagrams were considered. The moisture flux at the surface into the storm region was shown to be 140 g·m/kg·s from above the Agulhas Current one day prior to and during CASE DECEMBER. The tropics contributed approximately 50 g·m/kg·s at the 700 hPa level. Vertical cross sections of the moisture flux have also shown that the Agulhas Current surface input into CASE DECEMBER was approximately three times that which was coming in from the north at higher levels. Similarly, CASE NOVEMBER showed a surface moisture flux of 180 g·m/kg·s coming from above the Agulhas Current on 19 November. Roughly half this amount was shown to be coming from the tropics in the upper levels. Both CASE NOVEMBER and CASE DECEMBER therefore show that the maximum moisture flux values were at the surface from above the Agulhas Current.

Backward air parcel trajectories have clearly demonstrated that the pathway of air before arriving at CASE DECEMBER was from above the Agulhas Current at the surface

on 14 and 15 December. At the 700 hPa level, in agreement with the moisture flux diagrams, the air pathways were shown to be from the north on both days. CASE NOVEMBER shows a very similar situation. Both surface air pathways arrived at CASE NOVEMBER from above the Agulhas Current. The only difference to CASE DECEMBER is that on 19 November the 700 hPa air came from south-west of the country whereas on 20 the 700 hPa air came from the north.

Both the trajectory and the NCEP analysis therefore support the contention that moisture at the surface level in both CASE NOVEMBER and CASE DECEMBER was from above the Agulhas Current. Both cases shared a similar synoptic situation; anticyclonic flow over the South-west Indian Ocean in conjunction with a midlevel trough tracking above a surface heat low over the interior. This suggests that this is a synoptic setting that might be conducive for flooding over the eastern regions of South Africa.

The analysis so far has utilized both NCEP and ECMWF global model data sets. It is important to recognize the limitation of the coarse resolution data from both NCEP and ECMWF. Their 2.5° X 2.5° degree grids cannot take into account features such as South Africa's mountain escarpment and the Agulhas Current as well as a regional model could. In future research it would be more appropriate to use a high-resolution regional model to gain a more accurate representation of the atmospheric circulation.

## Did the regional environment above the Agulhas Current have an effect on the synoptic event's CASE DECEMBER and CASE NOVEMBER?

TRMM data above the Agulhas Current was utilized to answer the second key question. Surface rain rate plots for both cases show that the heavy rainfall events remained focused above the warm water tongue of Agulhas Current water. Significant latent heat release and rain in the atmosphere was also observed only above the warm water of the Agulhas Current. The bulk of precipitation in the atmosphere was found between 1000 and 4000 meters, consistent with latent heat release in the atmosphere. This consistent result found in all the TRMM images of surface and atmospheric rainfall directly above the high SSTs of the Agulhas Current supports the contention that the high SSTs of the Agulhas Current have a direct impact on the regional environment above the Agulhas Current.

Whether the regional environment above the Agulhas Current indirectly affects the synoptic situation over land remains unknown. To what extent the latent heat released in the atmosphere above the Agulhas Current may enhance convection over land is unanswerable with the data sources used in this study. Air parcel trajectories and NCEP parameters from global climate model data are too coarse a representation to determine whether this latent heat is transported to the storm over land. If more radiosonde data became available, it would be useful to track the signature of the latent heat released above the current in the atmosphere. This would shed more insight into the extent this latent heat modifies the synoptic events over land.

Rain rate and latent heat data have never before been observed for heavy rainfall

events above the Agulhas Current. Thus, there is no context within which these results may be compared. In future research, many synoptic scale heavy rainfall events in conjunction with regional rainfall events above the current need to be observed with TRMM to put these values into perspective. It may also be useful to look at these parameters during times of light rainfall to compare the relative amounts.

## Was the baroclinic boundary which existed between the Agulhas Current and the inland plateau during CASE DECEMBER conducive to tornado formation?

To answer this last question, observational data supplied by the South African Weather Bureau was utilized. The baroclinic boundary, which existed between the hot, dry inland plateau and the cool, moist coastal regions is shown in Figure 5.5c. The vertical vorticity at the surface, across the baroclinic boundary was calculated as $7.0 \times 10^{-5}\ s^{-1}$. This is a value comparable to that found by Rasmussen et al. [2000] considering that this calculation was made from data points 100 km apart which is 10 times farther apart than the data points in Rasmussen's research. This back of the envelope calculation demonstrated that the baroclinic boundary which existed in South Africa during CASE DECEMBER enhanced the vertical vorticity. Whether this enhancement was enough to induce tornado formation cannot be concluded from this calculation. Many more tornadoes which have formed along the eastern coastal regions need to be tracked and the data needs to be much higher in resolution to properly address whether similar values of

vertical vorticity are found.

This thesis began by emphasizing the link between South Africa's climate and weather and the surrounding ocean temperatures. Focus has since been given to the Agulhas Current due to its close proximity to the eastern coastal regions, which commonly experience heavy rainfall. The results of both CASE DECEMBER and CASE NOVEMBER have shown the Agulhas Current to be the dominant moisture source for these two extreme events. The regional environment above the current has, for the first time, been explored in terms of vertical rain rates and latent heat release. It is clear that more research utilizing the TRMM products to understand the extent to which this latent heat affects synoptic events over land should be the next step.

# REFERENCES


Bang, K. O. (1988). Floods in perspective. The Impact of the September 1987 and February/March Floods of 1988 on Agriculture. *CSIR Conference Center*, Oct 20-21, 1988, Pretoria, South Africa: various pages.

Bauer, P. , L. Schanz, R. Bennartz and P. Schlussel (1998). Outlook for combined TMI-VIRS algorithms for TRMM – lessons from the Pip and Aip projects. *Journal of the Atmospheric Sciences*, **155**: 1714-1729.

Bauer, P. and R. Bennartz (1998). Tropical Rainfall Measuring Mission microwave imaging capabilities for the observation of rain clouds. *Radio Science*, **33**: 335-349.

Carlson, T. N. (1998). Vorticity and vertical motion, in *Mid-Latitude Weather Systems*, American Meteorological Society, Boston: 27-51.

Cattle H. and C. Gordon (1990). Specification and variability of the surface forcing of the ocean, 1990, in *Climate-Ocean Interaction*, Kluwer Academic Publishers, The Netherlands: 193-210.

Charnock, H. and J. A. Businger (1991). The frontal air-sea interaction experiment in perspective. *Journal of Geophysical Research*, **96**: 8639-8642.

Crimp, S. J. and S. J. Mason (1999). The extreme precipitation event of 11 to 16 February 1996 over South Africa. *Meteorology and Atmospheric Physics*, **70**: 29-42.

D'Abreton, P. C. and J. A. Lindesay (1993). Water vapour transport over southern Africa during wet and dry early and late summer months. *International Journal of Climatology*, **13**: 151-170.

D'Abreton, P. C. and P. D. Tyson (1995). Divergent and non-divergent water vapour transport over southern Africa during wet and dry conditions. *Meteorology and Atmospheric Physics*, **55**: 47-59.

D'Abreton, P. C. and P. D. Tyson (1996). Three-dimensional kinematic trajectory modelling of water vapour transport over Southern Africa. *Water South Africa*, **22**: 297-306.

De Coning, E., G. S. Forbes and E. Poolman (1998). Heavy precipitation and flooding on 12-14 February 1996 over the summer rainfall regions of South Africa: synoptic and isentropic analysis. *National Weather Digest*, **22**: 25-36.

De Coning, E. and B. F. Adam (2000). The tornadic thunderstorm events during the 1998-1999 South African summer. *Water South Africa*, **26**: 361-376.

Doswell III, C. A. and E. N. Rasmussen (1994). The effect of neglecting the virtual temperature correction on CAPE calculations. *Weather and Forecasting*, **9**: 625-629.

Durden, S. L., Z. S. Haddad, A. Kitiyakara and F. K. Li (1998). Effects of nonuniform beam filling on rainfall retrieval for the TRMM precipitation radar. *Journal of Atmospheric and Oceanic Technology*, **15**: 635-646.

Estie, K. E. (1981). The Laingsburg flood disaster of 25 January 1981. *South African Weather Bureau Newsletter*, No. **383**: 19-32.

Fennessy, M. J. and J. Shukla (1988). Numerical simulation of the atmospheric response to the time-varying El Nino SST anomalies during May 1982 through October 1983. *Journal of Climatology*, **1**: 195-211.

Foreman, S. J. (1990). The ocean as a component of the climate system, in *Climate-Ocean Interaction*. Kluwer Academic Publishers, The Netherlands: 3-17.

Fujita, T. T. (1973). Experimental classification of tornadoes in FPP scale, in *SMRP Research Paper*, University of Chicago, Illinois: No **98**.

Gillooly, J. F. and N. D. Walker (1984). Spatial and temporal behavior of sea-surface temperatures in the South Atlantic. *South African Journal of Science*, **80**: 97-100.

Gründlingh, M. L. (1978). Drift of a satellite-tracked buoy in the southern Agulhas Current and Agulhas Return Current. *Deep-Sea Research*, **25**: 1209-1224.

Haddad, Z. S., D. A. Short, S. L. Durden, E. Im, S. Hensley, M. B. Grable and R.A. Black (1997a). A new parameterization of the rain drop size distribution. *IEEE Transactions on Geoscience and Remote Sensing*, **35**: 532-539.

Haddad, Z. S., E. A. Smith, C. D. Kummerow, T. Iguchi, M. R. Farrar, S. L. Durden, M. Alves and W. S. Olson (1997b). The TRMM `day-1' radar/radiometer combined rain-profiling algorithm. *Journal of Meteorological Society of Japan*, **75**: 799-809.

Harris, T. F. W. (1972). Sources of the Agulhas Current in the spring of 1964. *Deep-Sea Research*, **19**: 633-650.

Harrison, S. J. (1984). A generalised classification of South African summer rain-bearing synoptic systems. *Journal of Climatology*, **4**: 547-560.

Holton, J. R. (1992). *An introduction to dynamic meteorology*, Academic Press, New York: 293-294.

James, I. N. and D. L. T. Anderson (1984). The seasonal mean flow and distribution of large scale weather systems in the Southern Hemisphere: the effects of moisture transports. *Quarterly Journal of the Royal Meteorological Society*, **110**: 943-966.

Jury, M. R. (1993). A thermal front within the marine atmospheric boundary layer over the Agulhas Current south of Africa: composite aircraft observations. *Journal of Geophysical Research*, **99**: 3297-3304.

Jury, M. R. (1994). A review of the meteorology of the eastern Agulhas Bank. *South African Journal of Science*, **90**: 109-113.

Jury, M. R. and K. Levey (1993). The climatology and characteristics of drought in the Eastern Cape of South Africa. *International Journal of Climatology*, **13**: 629-641.

Jury, M. R. and N. D. Walker (1988). Marine boundary layer modification across the edge of the Agulhas Current. *Journal of Geophysical Research*, **93**: 647-654.

Jury, M. R. and S. Courtney (1991). A transition in weather over the Agulhas Current. *South African Journal of Marine Science*, **10**: 159-171.

Jury, M. R., H. R. Valentine and J. R. E. Lutjeharms (1993). Influence of the Agulhas Current on summer rainfall along the southeast coast of South Africa. *Journal of Applied Meteorology*, **32**: 1282-1287.

Jury, M. R., J. A. Lindesay and I. Wittmeyer (1990). Flood episodes in central South Africa from satellite and ECMF data. *South African Journal of Science*, **89**: 263-269.

Jury, M. R. and M. Majodina (1997). Preliminary climatology of southern Africa extreme weather: 1973-1992. *Theoretical and Applied Climatology*, **56**: 103-112.

Kalnay, E., M. Kanamitsu, M. R. Kistler, W. Collins, D. Deaven, L. Gandin, M. Iredell, S. Saha, G. White, J. Woollen, Y. Zhu, M. Chelliah, W. Ebisuzaki, W. Higgins, J. Janowiak, K. C. Mo, C. Ropelewski, J. Wang, A. Leetmaa, R. Reynolds, R. Jenne and D. Joseph (1996). The NCEP/NCAR 40-year reanalysis project. *Bulletin of the American Meteorological Society*, **77**: 437-471.

Karoly, D. J. and D. G. Vincent (1998). *Meteorology of the Southern Hemisphere*, American Meteorological Society, Boston: Code **MM49**, 410 pp.

Keen, C. S. and Tyson, P. D. (1973). Seasonality of South African rainfall: a note on its seasonal delimitation using spectral analysis. *Archiv fuer Meteorologie, Geophysik und Bioklimatologie, Serie B*, **21**: 207.

Kummerow, C. , W. Barnes, T. Kozu, J. Shiue and J. Simpson (1998). The Tropical Rainfall Measuring Mission (TRMM) sensor package. *Journal of Atmospheric and Ocean Technology*, **15**: 808-816.

Kummerow, C., S. Olson and L. Giglio (1996). A simplified scheme for obtaining precipitation and vertical hydrometeor profiles from passive microwave sensors. *IEEE Transactions on Geoscience and Remote Sensing*, **34**: 1213-1232.

Laing, A. G. and J. M. Fritsch (1993). Mesoscale Convective Complexes in Africa. *Monthly Weather Review*, **121**: 2254-2263.

Lee-Thorp, A., M. Rouault and J. R. E. Lutjeharms (1998a). Moisture uptake in the boundary layer above the Agulhas Current: a case study. *Journal of Geophysical Research*, **104**: 1423-1430.

Lee-Thorp, A., M. Rouault and J. R. E. Lutjeharms (1998b). Cumulus cloud formation above the Agulhas Current. *South African Journal Science*, **94**: 351-354.

Linacre, E. and B. Geerts (1997). *Climates and weather explained*, Routledge, London: 179 pp.

Lindesay, J. A. and M. R. Jury (1991). Atmospheric circulation controls and characteristics of a flood event in central South Africa. *International Journal of Climatology*, **11**: 609-627.

Lutjeharms, J. R. E. (1981a). Features of the southern Agulhas Current circulation from satellite remote sensing. *South African Journal of Science*, **77**: 231-236.

Lutjeharms, J. R. E. (1981b). Spatial scales and intensities of circulation in the ocean areas adjacent to South Africa. *Deep-Sea Research*, **32**: 1289-1302.

Lutjeharms, J. R. E. (2000). *The Agulhas Current*, Springer – Verlag, Berlin, in press.

Lutjeharms, J. R. E. and H. R. Valentine (1984). Southern Ocean thermal fronts south of Africa. *Deep-Sea Research*, **31**: 1461-1475.

Lutjeharms, J. R. E. and R. C. van Ballegooyen (1988a). The retroflection of the Agulhas Current. *Journal of Geophysical Research*, **93**: 1570-1583.

Lutjeharms, J. R. E. and M. Rouault (2000). Observations of cloud formation above Agulhas Current intrusions in the South-east Atlantic. *South African Journal of Science*, in press.

Lutjeharms, J. R. E., R. D. Mey and I. T. Hunter (1986). Cloud lines over the Agulhas Current. *South African Journal of Science*, **82**: 635-640.

Maddox, R. A. (1980). Mesoscale convective complexes. *Bulletin of the American Meteorological Society*, **61**: 1374-1387.

Mason, S. J. (1995). Sea-surface temperature - South African rainfall associations, 1910-1989. *International Journal of Climatology*, **15**: 119-135.

Mason, S. J., J. A. Lindesay and P. D. Tyson (1994). Simulating drought in southern Africa using sea surface temperature variations. *Water South Africa*, **20**: 15-22.

Mey, R. D. and N. D. Walker (1990). Surface heat fluxes and marine boundary layer modification in the Agulhas Retroflection Region. *Journal of Geophysical Research*, **95**: 15,997-16,015.

Norton, W. A. (1994). Breaking Rossby Waves in a model stratosphere diagnosed by a vortex-following coordinate system and a technique for advecting material contours. *Journal of the Atmospheric Sciences*, **51**: 654-673.

Olson, W., C. D. Kummerow and Y. Hong (1999). Atmospheric latent heating distributions in the tropics derived from satellite passive microwave radiometer measurements. *Journal of Applied Meteorology*, **38**: 633-664.

Pearce, A. F. (1977). Some features of the upper 500 m of the Agulhas Current. *Journal of Marine Research*, **35**: 731-751.

Preston-Whyte, R. A. and P. D. Tyson (1988). *The atmosphere and weather of southern Africa*, Oxford University Press, Cape Town: 227 pp.

Rasmussen, E. N., S. Richardson, J. M. Straka, P. M. Markowski and D. O. Blanchard (2000). The association of significant tornadoes with a baroclinic boundary on 2 June 1995. *Monthly Weather Review*, **128**: 174-128.

Reason, C. J. C. (1998). Warm and cold events in the southeast Atlantic/southwest Indian Ocean region and potential impacts on circulation and rainfall over southern Africa. *Meteorolology and Atmospheric Physics*, **69**: 49-65.

Reason, C. J. C. and H. Mulenga (1999). Relationships between South African rainfall and SST anomalies in the southwest Indian Ocean. *International Journal of Climatology*, **19**: 1651-1673.

Reynolds, R. W. and T. M. Smith (1994). Improved global sea surface temperature analyses
using optimum interpolation. *Journal of Climate*, **7**: 929-948.

Rocha, A. and I. Simmonds (1993). The influence of sea surface temperatures on summer rainfall and circulation of southern Africa. In Preprints, *4th International Conference of Southern Hemisphere Meteorology and Oceanography*, March 29 – April 2, 1993, Hobart, Australia, American Meteorological Society, Boston: 250-251.

Rouault, M., A. M. Lee-Thorp and J. R. E. Lutjeharms (2000). Observations of the atmospheric boundary layer above the Agulhas Current during alongcurrent winds. *Journal of Physical Oceanography*, **30**: 70-85.

Rouault, M., J. R. E. Lutjeharms, A. M. Lee-Thorp, M. R. Jury and M. Majodina (1998). Air-sea interaction over the Agulhas Current and implication for South African weather. Report to the Water Research Commission by the Department of Oceanography, University of Cape Town. *WRC Report*, **374/1/99**: 104 pp.

Rouault, M., A. M. Lee-Thorp, I. Ansorge and J. R. E. Lutjeharms (1995). Agulhas Current air-sea exchange experiment. *South African Journal of Science*, **91**: 493-496.

Steiner, M. and R. A. Houze (1998). Sensitivity of monthly 3-dimensional radar-echo characteristics to sampling frequency. *Journal of the Meteorological Society of Japan*, **76**: 73-95.

Streten, N. A. (1981). Southern Hemisphere sea surface temperature variability and apparent associations with Australian rainfall. *Journal of Geophysical Research*, **86**: 485-497.

Stull, R. B. (1988). *An Introduction to Boundary Layer Meteorology*, Kluwer Academic Publishers, The Netherlands: 551-553.

Taljaard, J. J. (1955). Stable stratification in the atmosphere over southern Africa. *South African Weather Bureau*, Notes **4**: 217-230.

Taljaard, J. J. (1987). The anomalous climate and weather systems over South Africa during summer 1975-1976. *South African Weather Bureau Technical Paper*, No. **16**: 153 pp.

Taljaard, J. J. (1996). Atmospheric circulations systems, synoptic climatology and weather systems of South Afrcia. Part 5: Temperature phenomena in South Africa. *South African Weather Bureau Technical Paper*, No. **31**: 42 pp.

Tennant, W. J. (1996). Influence of Indian Ocean sea-surface temperature anomalies on the general circulation of southern Africa. *South African Journal of Science*, **92**: 289-295.

Triegaardt, D. O. and W. A. Landman (1995). The influence of atmospheric long-waves on summer rainfall in the Transvaal, Orange Free State and Natal. *South African Weather Bureau Technical Paper*, No. **26**: 30 pp.

Triegaardt, D. O., D. E. Terblanche, J. Van Heerden and M. V. Laing (1988). The Natal flood of September 1987. . *South African Weather Bureau Technical Paper*, No. **19**, 62 pp.

Triegaardt, D. O., J. van Heerden and P. C. L. Steyn (1991). Anomalous precipitation and floods during February 1988. *South African Weather Bureau Technical Paper*, No. **23**, 25 pp.

Tyson, P. D., S. J. Mason and J. A. Lindesay (1993). Modelling the influence of ocean temperatures on the rainfall of southern Africa. In Preprints, *4th International Conference of Southern Hemisphere Meteorology and Oceanography*, March 29 – April 2, 1993, Hobart, Australia, American Meteorological Society, Boston: 528.

Van Heerden, J. and J. J. Taljaard (1998). Africa and surrounding waters, in *Meteorology of the Southern Hemisphere*, American Meteorological Society, Boston: Code **MM49**, 141-174.

Van Heerden, J. (1988). Floods in perspective. A season of floods over South Africa, July 1987 to June 1988. *CSIR Conference Center*, Oct 20 - 21, 1988, Pretoria, South Africa: various pages.

Van Niekerk H. and G. Sampson (1999). Hell season or par for the course: tornadoes over the Eastern Cape 1998/99. *South African Weather Bureau*, Season Internal Report Number **OB/17**: 11-24.

Walker, N. D. (1990). Links between South African summer rainfall and temperature variability of the Agulhas and Benguela Current systems. *Journal of Geophysical Research*, **95**: 3297-3319.

Walker, N. D. and J. A. Lindesay (1989). Preliminary observations of oceanic influences on the February-March 1988 floods in central South Africa. *South African Journal of Science*, **85**: 164-169.

Walker, N. D. and R. D. Mey (1988). Ocean/atmosphere heat fluxes within the Agulhas Retroflection Region. *Journal of Geophysical Research*, **93**: 15,473-15,483.

Wallace, J. M. and V. Hobbs (1977). *Atmospheric Science*, Academic Press, New York: 467 pp.

Waugh, D. W. and R. A. Plumb (1994). Contour advection with surgery - a technique for investigating finescale structure in tracer transport. *Journal of the Atmospheric Sciences*, **51**: 530-540.

Webster, P. J. (1981). Mechanisms determining the atmospheric response to sea surface temperature anomalies. *Journal of the Atmospheric Sciences*, **38**: 554-571.

Webster, P. J. and R. Lukas (1992). TOGA COARE: The coupled ocean-atmosphere response experiment. *Bulletin American Meteorological Society*, **73**: 1377-1415.

Wentz, F. J. (1996). Algorithm theoretical basis document. *Remote Sensing System Technical Report*, **12/02/96**.